The dynamic analysis of the Yme MOPUstor

MSc Thesis

Rong, Keran

Allseas

TU Delft Delft University of Technology

Title Page

Title:	The dynamic analysis of the Yme MOPUstor	
Course	OE5685-15	Problem Analysis Thesis
	OE5690-30	Thesis
Student	K.Rong, BSc (4327519)	
Supervisor	Prof. Dr. A.V. Metrikine (TU Delft) Dr.ir.Y.Yu (Allseas Engineering B.V.) Ir. P. van der Male (TU Delft)	
Contact TU Delft	TU Delft Civil Engineering and Geosciences Stevinweg 1 2628 CN Delft	
Date publication	16/06/2015	
Pages (of which appendices)	172(36)	
Words	30468	

This report has been written in fulfilment of the MSc thesis, in context of the MSc programme Offshore and Dredging engineering at the Delft University of Technology

Forewords

This thesis presents the comparative study of the three different dynamic analysis methods (quasi-static, frequency-domain, time-domain), with respect to the dynamic analysis of the Yme MOPUstor platform.

The initiation of this thesis is Allseas engineering project. As a major contractor in the oil and gas industry, Allseas group is seeking a transformation and tries to redefine herself in the platform decommissioning business. With the new built platform installation / decommissioning and pipe-lay vessel Pioneering Spirit, Allseas group is well prepared to execute her first decommissioning project, the decommissioning of the Yme MOPUstor platform. The Yme MOPUstor is a production jack up platform, located in the North Sea. It was built and installed in 2010. However, due to its obvious dynamic defects, this platform is abandoned and will be decommissioned in 2015.

After the abandon of the platform, several institutions were invited to investigate the dynamic behavior of the Yme MOPUstor. However, different conclusions are given by using different dynamic analysis methods. For the purpose of the decommissioning, it is inevitable to judge those existing studies and carry out a new dynamic analysis. Therefore, this thesis is motivated by this important and interesting challenge.

This comparative study is carried out in four aspects: the linear versus non-linear, the quasi-static versus dynamic, the stochastic versus deterministic and the efficiency. The comparative study is first demonstrated on some sample models to illustrate the fundamental differences. Then, the dynamic analyses of the Yme MOPUstor for the given sea states by using different methods are analyzed and compared.

In addition of the comparative study, a new dynamic analysis method, the higher order frequency domain method (HFD), is developed and verified. This new method is believed to significantly improve both the accuracy and the efficiency of the traditional methods. Besides, the HFD method also provides an approach to better understanding the fundamental differences between the traditional quasi-static, frequency domain and time-domain methods.

Acknowledgement

I would like to express my sincere gratefulness to my supervisors, Professor Metrkine, Dr.Yu and Mr.P. van der Male for providing me with encouragements, inspirations and supports during my thesis work. Further, I thank Mr. Van Lammeren for kindly sharing his experiences with this topic.

I also want to thank the colleagues of Allseas engineering B.V. for all the moments we shared, and Yme MOPUstor project's team for all the efforts they contributed to my thesis.

Last but not least, I would like to thank my parents for being so supportive.

Keran Rong

Delft, the Netherlands

Table of Contents

1.0 INTRODUCTION 10
1.1 Background: The Yme MOPUstor 10
1.2 Motivation 14
1.3 Objectives of the thesis 15
1.4 Conclusion 16
1.5 Structure of the thesis 16

2.0 REVIEWS OF THE TRADITIONAL DYNAMIC ANALYSIS METHODS 18
2.1 General 18
2.2 Quasi-static method (QS) 23
2.2.1 Basic idea 23
2.2.2 The maximum external force $\boldsymbol{Fmax}$ calculation 24
2.2.3 The inertia force $\boldsymbol{FI}$ calculation 24
2.3 Frequency-domain Method (FD) 27
2.3.1 Basic idea: excitation, response and transfer function 27
2.3.2 The analysis methodology on the decoupled hydro-structural model 28
2.4 Time-domain Method (TD) 32
2.4.1 Basic idea: Discretized time and status 32
2.4.2 Numerical algorithm 33
2.4.3 The analysis methodology on the decoupled hydro-structural model 34
2.5 Summary 35

3.0 HIGHER ORDER FREQUENCY DOMAIN METHOD (HFD) 36
3.1 Overview 36
3.2 The approximation of the non-linear terms 37
3.2.1 The polynomial approximation of the drag term $v|v|$ 37
3.2.2 Free surface elevation approximation 40
3.3 The application on SDOF system 44
3.4 The application on MDOF system 50
3.4.1 Step I: The calculation of the transfer functions from the fluids to the hydrodynamic forces 51
3.4.2 Step II: The calculation of the transfer funcitons from the hydrodynamic forces to the strcutural responses 56
3.5 The techniques on the improvement of the computation efficiency 63
3.5.1 The symmetry properties of the transfer functions 64
3.5.2 Pre-assessment of the transfer functions 65
3.5.3 Frequency re-discretization for the higher order transfer functions 66

4.0 THE COMPARATIVE STUDY ON SIMPLE MODELS 67
4.1 Overview 67
4.2 Nonlinear vs. linear drag term 68
4.2.1 The validation of the linearization 69
4.2.2 The validation of the linearization method 82
4.3 Varying free water surface effect 85
4.4 Dynamic versus quasi-static analysis 93

5.0 METHODOLOGY FOR THE COMPARATIVE STUDY 100
5.1 General 100
5.2 FEM model for the comparative study 102

6.0 RESULT AND ANALYSIS 106
6.1 The effect of the non-linearity 106
6.2 The dynamic versus the quasi-static 113
6.3 The deterministic versus the stochastic 114
6.4 The efficiency 118
6.5 Conclusion and practise advise 123

7.0 FURTHER STUDY 124

8.0 REFERENCE 127

I APPENDIX: THE HYDRODYNAMIC MODEL AND THE PROGRAM "HYDRO" 131
I.1 Mathematical Model of waves 131
I.1.1 Airy wave model 133
I.1.2 Stokes's wave 134
I.2 Stochastic wave theory 136
I.2.1 Wave Spectrum 136
I.2.2 Stochastic wave generation 137
I.3 Introduction to "Hydro" 138
I.4 The verification of "Hydro" 139

II APPNEDIX: POST-PROCESSING 151
II.1 The frequency domain method 151
II.2 The time domain method 155

III APPENDIX : THE STATIC LOAD CONVERSION METHOD FOR THE FREQUENCY DOMAIN METHOD 157

IV APPENDIX : THE MORISON'S EQUATION MODELLING 161
IV.1 Assumption Spectral Density of $\boldsymbol{\phi}$ 161
IV.2 The covariance of $\varphi_1(x_1,y_1,z_1,t_1)$ and $\varphi_2(x_2,y_2,z_2,t_2)$ 163
IV.3 Spectral of $\varphi_1(x_1,y_1,z_1,t_1)$ and $\varphi_2(x_2,y_2,z_2,t_2)$ 168

1.0 INTRODUCTION

This chapter provides an overview of the thesis, highlighting why, what and how the research work is presented in this thesis. It describes the background and explains the motivation for pursuing this research. In addition, it provides an overview of the thesis's objectives as well as the conclusion. Finally, the structure of the thesis is also presented in this chapter.

1.1 Background: The Yme MOPUstor

This thesis is inspired by the challenges in the Yme MOPUstor's dynamic analysis. The Yme MOPUstor is a Mobile Offshore Production Unit with a subsea storage tank, located in the Yme oil field, North Sea. [1] It was built in 2010, and will be terminated and removed in the September of 2015, due to its dynamic defects. In this section, the background and a brief description of the Yme MOPU platform are presented respectively.

To begin with, the background of the Yme MOPUstor is introduced. The Yme MOPUstor was expected to serve as a production platform for the Yme oil field [1]. The Yme field is located in the Egersund basin in the North Sea, approximately 110 km offshore in the Norwegian Continental Shelf. The Yme field was initially developed by Statoil and then abandoned due to the low oil price. In 2010, the Canadian energy giant, Talisman Energy Norge As, made an agreement with Norwegian Administration to restart the oil production of the Yme Oil field.

After being granted permission to redevelop the Yme field, Talisman Energy Norge AS has awarded a contract to Single Buoy Moorings Inc. for the development of a production unit for the Yme Project. Single Buoy Mooring Inc. proposed a MOPUstor concept as the production unit of the Yme oil field. The Yme MOPUstor is designed by SBM- GustoMSC and built in Abu Dhabi in 2010.

However, large motions occurred immediately after the installation of the Yme MOPUstor. Those large motions greatly affect the normal production activity. In July 2012, after the cracks were discovered at the grouted base of the MOPU's legs, Talisman evacuated all personnel from the facility. In March 2013, Talisman reached an agreement with Allseas engineering B.V. to terminate work on the production unit, including the decommissioning activities.

The decommissioning operation will be executed as follows. First, several bumpers and enforcement structures will be installed between the caisson and the MOPU in order to protect the caisson during the decommissioning operation. Second, an internal support platform and its associate structures will be installed at each leg as the support of a leg cutting machine. Third, within an allowed sea state, the Pioneering Spirit, Allseas's specialized decommissioning vessel will catch and hold the MOPU. Meanwhile, a cutting machine will be lifted down inside each leg to the pre-installed internal support platform to cut the legs. Finally, after all legs are cut, the cutting machines will be lifted out from the legs and the Pioneering Spirit will take the whole MOPU out from its installed location, as demonstrated in figure 1.1.

Figure 1.1 a demonstration of the decommissioning operation of the Yme MOPUstor

In addition, the structural characteristics and site condition of the Yme MOPUstor are described. A graphical representation of the Yme MOPU platform is shown in figure 1.2. According to the SBM's design report [2], the Yme MOPUstor is a platform design integrating well support, production, storage and self-installation. Overall speaking, the MOPUstor consists of two major parts: the substructure part and the jack-up production deck (or MOPU).

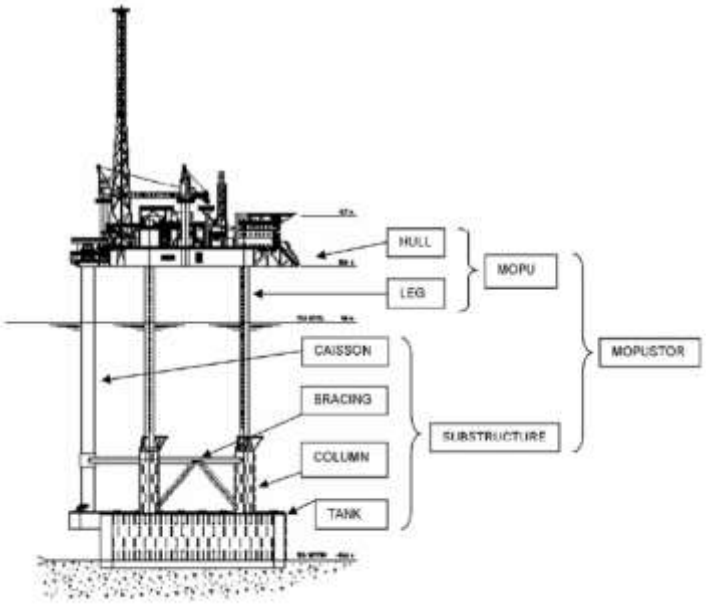

Figure 1.2 the graphical representation of the YME MOPUstor from ref [2]

The substructure part includes a subsea storage tank, a caisson (5.25m diameter) and columns and bracings that support the MOPU's legs. The storage tank is used for the oil storage and also provides the foundation for the entire platform. Well conductors including wellheads and risers are supported by a tubular caisson. The caisson protects the well conductors and risers from wave loading and provides the lateral and vertical support that is required. The caisson is designed as free-standing. After the MOPU has been installed, it provides a horizontal support to the caisson but is not fix connected.

The MOPU supports the process modules and the accommodation and provides the storage of consumables. The hull is of a typical self-floating, plated construction. As shown in Figure 1.3, The MOPU is outfitted with three circular legs (3.5m diameter), each leg is provided with a jacking system. The jacking systems lower the legs, lift the hull to the elevated position and, in the final position, lock the hull relative to the legs. The hydraulic system is not active after installation.

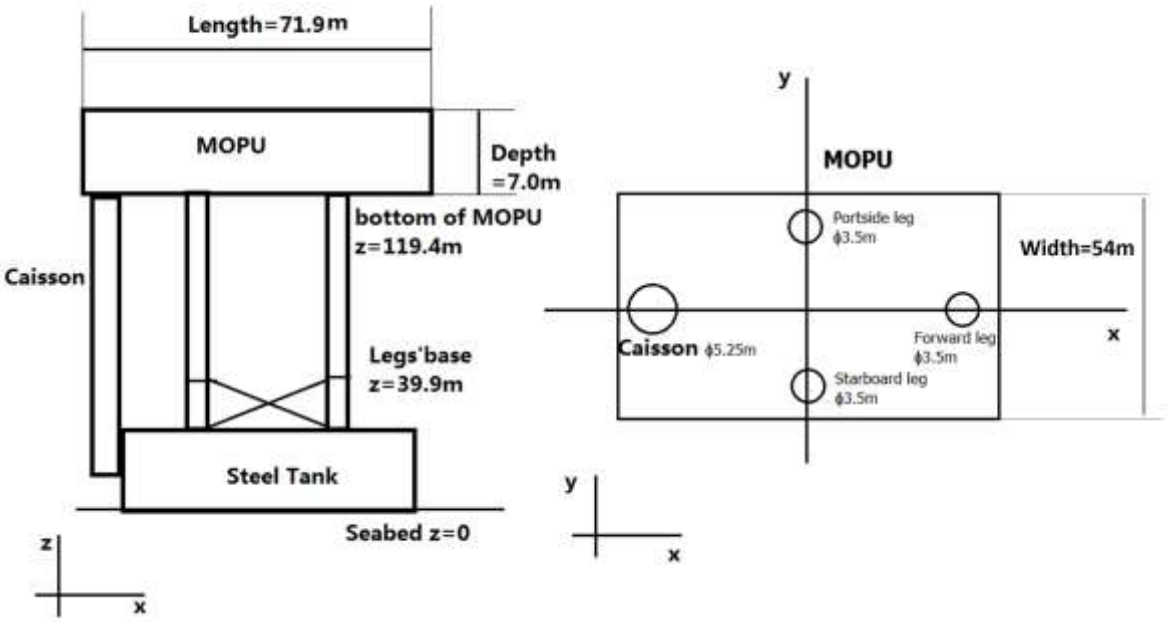

Figure 1.3 the dimensions of the Yme MOPUstor

The table 1.1 shows a summary of the structural characteristics and the site condition of the Yme MOPUstor. As listed in the table 1.1, the overall dimension of the Yme MOPUstor is 71.9m x 54m x 7.0m and the total mass of the MOPU is approximately 1.29×10^7 kg. The site's mean water depth is approximately 93.0m. The highest maximum wave within the return period of 100 years is estimated to be 27.5m.

Table 1.1 the structural characteristics and the site condition of the Yme MOPUstor

MOPU	Overall length	71.9m
	Overall Wide	54.0m
	Overall depth	7.0m
	Overall mass	1.29×10^7 kg
	Characteristics of legs	number: 3 length: 102.2 m type: plane tubular outside diameter: 3.5 m wall thickness: 75-115 mm material: NVE690 typical
Substructure	Characteristics of caisson	type: plain tubular inside diameter: 5.15 m length: 107.1 m wall thickness: 40-90 mm material: NVE40 typical
Site Condition	Water depth (MSL)	93.0 m
	Storm surge and tide (100 yr return)	1.03 m
	Airgap above MSL	24.5 m
	Max wave height (100 yr return)	27.5 m
	Associated wave period	14.0 s
	Wind velocity (1 minute, 100 yr return)	42.8 m/s
	Current velocity at surface (10 yr return)	0.90 m/s
	Current velocity at seabed (10 yr return)	0.40 m/s

1.2 Motivation

This thesis is motivated by the importance of the Yme MOPUstor's dynamic analysis, for the judgement of the existing dynamic analysis studies and its further applications in the decommissioning operation.

The dynamic analysis of the Yme MOPUstor is a challenge. The inappropriate dynamic analysis in the SBM's design report results in the abandon of the platform and a billion-dollar loss [1]. After the abandon of the platform, several institutions were invited by Talisman Energy to investigate the dynamic behaviour of the Yme MOPUstor. Their studies have shown that, the dynamic behaviour of the Yme MOPUstor is dominated by three modes, e.g. Surge, Sway and Yaw, of which natural periods are around 6-7 seconds. Those natural periods are coincident with the common periods of waves in the Yme Oil field and thus the resonance occurred. Table 1.2 shows the maximum displacement with the return period of 100 years, estimated by Atkins (UK), DNV and SBM respectively.

Table1.2 The maximum displacement within return period of 100years

Institution	Methods	The maximum displacement	Corresponding Hs	Corresponding Tp	Wave direction
DNV[3]	Time-domain	0.5m	12m	12.2sec	30deg or 150deg
Atkins[4]	Frequency-domain	1m	6.03m	7.03sec	90deg
SBM-GustoMSC [2]*	Quasi-static	0.632m	H_{max}=27.4m	T_{ass}=14.80sec	135deg

*In SBM report, the deterministic quasi-static method is adopted, hence H_{max} and T_{ass}, instead of H_s and T_p are presented

As observed from the table 1.2, there are large differences between the maximum displacement estimated by different institutions. Those differences are so critical that the different conclusions are come out on the safety aspect of the platform. Therefore, in order to judge the validation of those results, it is highly interesting and necessary to perform a comparative study of those different dynamic analysis methods for their applications on the Yme MOPUstor platform.

In addition, dynamic analysis is also critical to the decommissioning operation. First, to design all the associated components used in decommissioning operation (bumpers, internal platforms, cut machines etc), the design load case need to be determined. For example, in order to design the bumpers used in caisson's protection, the relative motion between the caisson and the MOPU need to be estimated. Second, after those associated components installed, the dynamic behaviour of the Yme MOPUstor may change and hence needs to be re-checked for the safety reason. Therefore, the dynamic analysis is inevitable for the purposes of the modification and decommissioning of the Yme MOPUstor.

Furthermore, as discussed in this thesis, all existing dynamic methods are imperfect in nature. Attempts have been made on the creation of a new possible method to improve both the accuracy and the efficiency of dynamic analysis. Besides, this new possible method may also provide us a better understanding of the traditional methods. Those attempts can be treated as a scientific study and this study may be applied in future.

In conclusion, this thesis is motivated by three questions:

(1) Previous studies have provided different result estimated by different dynamic analysis methods. How should we judge the validation and application of those results?

(2) For the purposes of the modification and decommissioning of the Yme MOPUstor, how should we perform a new dynamic analysis and what methods should we select?

(3) Could we create a new method to improve both the accuracy and the efficiency of dynamic analysis, such as non-linear frequency-domain methods? By comparison with these methods, could we have a better understanding of those traditional methods?

1.3 Objectives of the thesis

The main objective of this thesis is to perform a comparative study of quasi-static (QS), frequency-domain (FD) and time-domain (TD) dynamic analysis methods, based on their applications on the Yme MOPUstor platform. This comparative study mainly focuses on four aspects: the issue of quasi-static vs. dynamic analysis, the issue of nonlinearity, the issue of stochastic versus deterministic and the efficiency. In this comparative study, the differences between these methods are analysed both qualitatively and quantitatively.

In additions, a recommendation should be given for engineering practise. Two extreme sea cases have pre-determined by previous studies [6], representing the resonant condition and the extreme wave condition. The practise studies of the Yme MOPU's dynamic analysis will be based on these two given sea states.

Finally, an attempt should be given for the improvement of the existing method. The attempt will focus on the improvement of the traditional frequency-domain method.

1.4 Work scope and Conclusion

The comparative study is first demonstrated on some sample models to illustrate the fundamental differences, as given in Chapter 4. Then, the dynamic analyses of the Yme MOPUstor for the given sea states by using different methods are analyzed and compared. The conclusion and practise advice with respect of the dynamic analysis of the Yme MOOPUstor are given in section 6.5.

In addition of the comparative study, a new dynamic analysis method, the higher order frequency domain method (HFD), is created and verified. This new method is believed to improve both the accuracy and the efficiency of the traditional methods. Besides, the HFD method also provides an approach to better understanding the fundamental differences between the traditional QS, FD and TD methods. This method is given in Chapter 3.

1.5 Structure of the thesis

The structure of the thesis is presented in Figure 1.3.

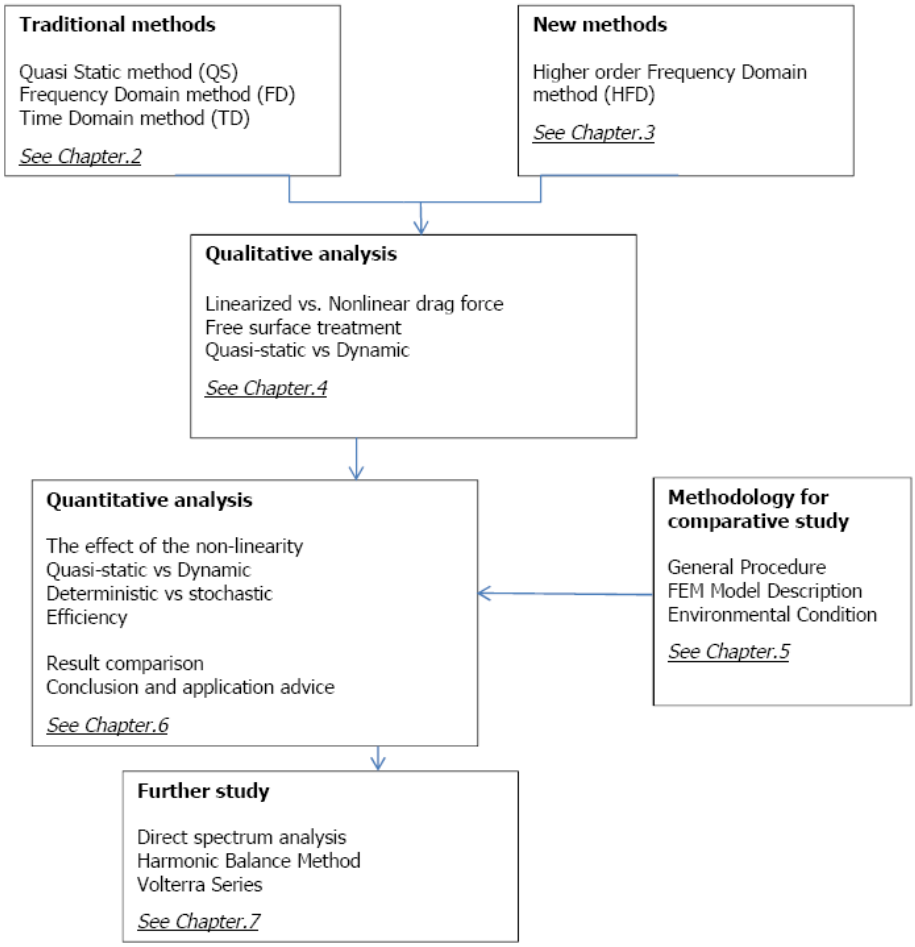

Figure 1.3 the structure of the thesis

Chapter 2 reviews the basic theoretical knowledge of the traditional dynamic analysis methods which includes the mathematical model, quasi-static (QS) method, frequency-domain (FD) and time-domain (TD) method.

In Chapter 3, the new dynamic analysis method, higher order frequency domain (HFD) method is presented. This new method has been demonstrated on both single degree of freedom (SDOF) and multi degree of freedom (MDOF) system. Besides, the techniques on the non-linear term treatment and the computation improvement are also presented in this chapter. Finally, the verifications on SDOF system are also provided.

Chapter 4 provides a comparative study on the fundamental difference between quasi-static, time-domain and time-domain methods. This analysis is mainly demonstrated on a SDOF system and focus on four aspects: quasi-static vs dynamic, linearized vs. nonlinear drag force, and free surface treatment. Compared with the new created HFD method, some fundamental differences can be well explained, especially the amplitude change and the frequency-shift caused by the non-linear terms.

Chapter 5 presents the methodology for the comparative study on the Yme MOPUstor platform, which includes the general procedures, the calibrated FEM model of the Yme MOPUstor and the environmental condition used for the comparative study.

In Chapter 6, the comparative study on the Yme MOPUstor platform is performed by using DNV Sesam^{TM} and their results have been analyzed step by step quantitatively. The conclusion and the practise advices are given in this Chapter.

Chapter 7 gives an outlook on the prospective research on the improvement of the dynamic analysis methods. Several methods are presented, which are direct spectrum conversion method, harmonic balance method and Volterra Series method.

2.0 REVIEWS OF THE TRADITIONAL DYNAMIC ANALYSIS METHODS

This chapter reviews the traditional dynamic analysis methods presented in the comparative study. The general knowledge of the physical model and the dynamic analysis is introduced first and then analysis philosophies of quasi-static, frequency-domain and time-domain methods are presented respectively. Finally, a summary is provided at the end of this chapter.

2.1 General

In this section, the general knowledge of the hydro-structural dynamic system is presented and the concepts of the coupled and decoupled hydro-structural model are introduced respectively. As mentioned later in this chapter, the decoupled hydro-structural model is adopted throughout this comparative study. In the end, the quasi-static, the frequency-domain and the time-domain methods are selected for this comparative study, with reasons.

In order to study the structural dynamic behavior quantitatively, the physical model of the Yme MOPUstor is built and spatial discretized. In this study, the MOPUstor is modelled as a linearized structure with the non-linear hydrodynamic forces. The general force equilibrium equation of such kind of model [5] can be expressed as,

In symbol form,

$$\boldsymbol{M_s}\ddot{\boldsymbol{R}} + \boldsymbol{C_s}\dot{\boldsymbol{R}} + \boldsymbol{K}\boldsymbol{R} = \boldsymbol{F_s}(t, \ddot{\boldsymbol{R}}, \dot{\boldsymbol{R}}) \tag{2.1}$$

Where,

t represents the time. n is the total number of the degrees of freedom.

$\boldsymbol{R}$ represents the global degree of freedom and the global degree of freedom component r_i represents a displacement component of one node in one direction. The r_i is located at (x_i, y_i, z_i).

$$\boldsymbol{R} = \begin{bmatrix} r_1 \\ r_2 \\ \vdots \\ r_{n-1} \\ r_n \end{bmatrix} \tag{2.2}$$

M_s represents the structural mass matrix and $m_{i,i}$ represents mass corresponding the global degree of freedom r_i from the structure.

$$M_s = \begin{bmatrix} m_{S_{1,1}} & 0 & \cdots & 0 & 0 \\ 0 & m_{S_{2,2}} & & 0 & 0 \\ \vdots & & \ddots & \vdots & \\ 0 & 0 & & m_{S_{n-1,n-1}} & 0 \\ 0 & 0 & \cdots & 0 & m_{S_{n,n}} \end{bmatrix} \tag{2.3}$$

K represents the structural stiffness matrix and $k_{i,j}$ represents the linear stiffness between the global degree of freedom i and the global degree of freedom j.

$$K = \begin{bmatrix} k_{1,1} & k_{1,2} & \cdots & k_{1,n-1} & k_{1,n} \\ k_{2,1} & k_{2,2} & & k_{2,n-1} & k_{2,n} \\ \vdots & & \ddots & \vdots & \\ k_{n-1,1} & k_{n-1,2} & \cdots & k_{n-1,n-1} & k_{n-1,n} \\ k_{n,1} & k_{n,2} & & k_{n,n-1} & k_{n,n} \end{bmatrix} \tag{2.4}$$

C_s represents the structural damping matrix, and c_{ij} represents the linear damping between the global degree of freedom I and the global degree of freedom j.

$$C_s = \begin{bmatrix} c_{s_{1,1}} & c_{s_{1,2}} & \cdots & c_{s_{1,n-1}} & c_{s_{1,n}} \\ c_{s_{2,1}} & c_{s_{2,2}} & & c_{s_{2,n-1}} & c_{s_{2,n}} \\ \vdots & & \ddots & \vdots & \\ c_{s_{n-1,1}} & c_{s_{n-1,2}} & \cdots & c_{s_{n-1,n-1}} & c_{s_{n-1,n}} \\ c_{s_{n,1}} & c_{s_{n,2}} & & c_{s_{n,n-1}} & c_{s_{n,n}} \end{bmatrix} \tag{2.5}$$

$F_s(t, \ddot{\boldsymbol{R}}, \dot{\boldsymbol{R}})$ represents the structural external force vector, and f_{s_i} represents the external force on the displacement r_i. The structural external force accounts for Weight and buoyancy, Wind forces, Hydrodynamic forces (slender member) and other loads.

$$\boldsymbol{F_s}\left(t, \ddot{\boldsymbol{R}}, \dot{\boldsymbol{R}}\right) = \begin{bmatrix} f_{s_1} \\ f_{s_2} \\ \vdots \\ f_{s_{n-1}} \\ f_{s_n} \end{bmatrix} \tag{2.6}$$

Previous studies [6] have shown that the dynamic motion is dominantly contributed by the hydrodynamic forces. Therefore, for the purpose of dynamic study, only hydrodynamic forces are considered in this thesis.

Hydrodynamic forces on slender structure can be estimated by Morison's equation [7]. The wave force d**F**, on a slender cylindrical element with diameter D and length ds is estimated as,

$$d\boldsymbol{F} = \begin{Bmatrix} df_x \\ df_y \\ df_z \end{Bmatrix} = \left\{ \frac{1}{2}\rho C_D D(v_n - r_n) \begin{bmatrix} v_{x,n} - \dot{r}_{x,n} \\ v_{y,n} - \dot{r}_{y,n} \\ v_{z,n} - \dot{r}_{z,n} \end{bmatrix} + \rho \frac{\pi}{4} D^2 C_M \begin{bmatrix} a_{x,n} - \ddot{r}_{x,n} \\ a_{y,n} - \ddot{r}_{y,n} \\ a_{z,n} - \ddot{r}_{z,n} \end{bmatrix} \right\} ds \tag{2.7}$$

Where,

$d\boldsymbol{F}$ or $\begin{Bmatrix} df_x \\ df_y \\ df_z \end{Bmatrix}$ is the wave force vector, ρ is the density of water, C_M is the mass coefficient and C_D is the drag coefficient, $\begin{bmatrix} \ddot{r}_{x,n} \\ \ddot{r}_{y,n} \\ \ddot{r}_{z,n} \end{bmatrix}$ and $\begin{bmatrix} \dot{r}_{x,n} \\ \dot{r}_{y,n} \\ \dot{r}_{z,n} \end{bmatrix}$ are the acceleration and velocity vector of the slender element, $\begin{bmatrix} a_{x,n} \\ a_{y,n} \\ a_{z,n} \end{bmatrix}$ is the water particle acceleration normal to the slender element component in each direction, and v_n or $\begin{bmatrix} v_{x,n} \\ v_{y,n} \\ v_{z,n} \end{bmatrix}$ is the water particle velocity normal to the slender element in each direction.

A graphical representation of the water particle velocity normal to the slender member is given in figure 2.1.

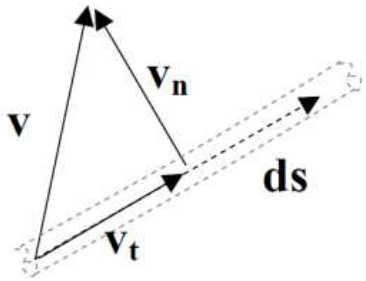

Figure 2.1 a graphical representation of water particle velocity normal to the slender element

Implement (2.7) into (2.1), the component f_{s_i} of the structural external force vector $\boldsymbol{F_s}(t, \ddot{\boldsymbol{R}}, \dot{\boldsymbol{R}})$ we obtain,

$$f_{s_i} = \alpha_{1,i}|v_n - \dot{r}_n|(v_{n_i} - \dot{r}_{n_i}) + \alpha_{2,i}(\dot{v}_{n_i} - \ddot{r}_{n_i}) \tag{2.8}$$

Where, for convenience, $\alpha_{1,i}$, and $\alpha_{2,i}$ are denoted as the drag and inertia term coefficient of the displacement i respsectively, where $\alpha_{1,i} = \frac{1}{2}\rho C_D D$ and $\alpha_{2,i} = \rho \frac{\pi}{4} D^2 C_M$

As observed from (2.9), the external force f_i depends on both the water particle's motion and the structural motion, which leads to an implicit form of the model. In

engineering practice, this coupled hydrodynamic forces' model usually is approximated as the decoupled hydrodynamic force plus two correction terms on the mass and damping matrix of the structure. In mathematics, this approximation can be expressed as,

$$f_{s_i} = \alpha_{1,i}|v_n - \dot{r}_n|(v_i - \dot{r}_i) + \alpha_{2,i}(\dot{v}_i - \ddot{r}_i) \approx \alpha_{1,i}|v_n|v_i + \alpha_{2,i}\dot{v}_i - c_{dl_i}\dot{r}_i - \alpha_{2,i}\ddot{r}_i \tag{2.9}$$

Where, the term c_{dl} is the equivalent hydrodynamic damping.

Substitute (2.9) into (2.1) and (2.2), the decoupled physical model can now be expressed in an explicit form,

$$\boldsymbol{M}\ddot{\boldsymbol{R}} + \boldsymbol{C}\dot{\boldsymbol{R}} + \boldsymbol{K}\boldsymbol{R} = \boldsymbol{F}(t) \tag{2.10}$$

Where, the terms $\boldsymbol{M}, \boldsymbol{C}$ are the mass matrix and the damping matrix including the hydrodynamic effects. Compared with $\boldsymbol{M_S}, \boldsymbol{C_s}$, $\boldsymbol{M}, \boldsymbol{C}$ includes the term $\alpha_{2,i}\ddot{r}_i$ and $c_{dl_i}\dot{r}_i$ in equation (2.9)

The DNV offshore specialized software Sesam-Genie™, is used for this comparative study. The mechanism of this software is illustrated in figure 2.2. Sesam-Genie™ adopts different packages for the hydrodynamic force and the structure calculation: Package Wajac™ is used for the hydrodynamic forces' calculations and package Sestra™ is used for structural responses' calculations.

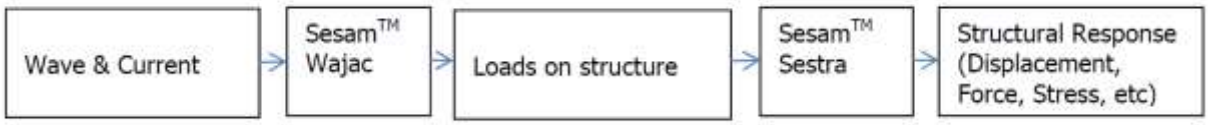

Figure 2.2 an illustration of the DNV-Genie™ analysis procedures

Due to the limitation of software used in this comparative study, the decoupled hydro-structural model (2.10), instead of the coupled model, is adopted throughout the study.

To perform a dynamic analysis on the hydro-structural model, six analysis methods are recommended by DNV [8], which are,

A: Stochastic non-linear dynamic (Time-domain methods)
B: Deterministic non-linear dynamic
C: Stochastic linear dynamic (Frequency-domain methods)
D: Deterministic non-linear static (Quasi-static methods)
E: Stochastic linear static
F: Deterministic linear static

However, none of those dynamic analysis methods is perfect in nature. Overall speaking, those methods are all facing the dilemma between the accuracy and the efficiency. A higher efficiency is compensated by the simplification of the method, which results in the sacrifice of the accuracy.

Among these methods, method A, C and D are selected in this comparative study for following reasons:

(1) The method A, C and D are the most commonly used in the dynamic analysis. The studies carried out by DNV, Atkins and SBM are performed by the method A, C and D respectively. By performing the comparative study on those three methods, the validation of the previous studies can be easily judged.

(2) The comparative study between method A, C and D are believed to be most representative. There are three major differences between these six recommended methods: stochastic vs. deterministic; non-linear vs. linear; static vs. dynamic. Those differences can be fully reflected in this comparative study.

(3) The DNV-Genie^{TM}, the software used in this comparative study is initially built based on the A, C and D methods. By adopting these three methods, the comparative study can be performed conveniently.

To sum up, the decoupled hydro-structural model is adopted in this comparative study. Three dynamic analysis methods, quasi-static method, frequency-domain method and time-domain method are selected for the comparison. In remaining part of this chapter, the analysis philosophy of QS, FD, and TD methods will be introduced respectively.

2.2 Quasi-static method (QS)

In this section, the analysis philosophy of the quasi-static method is presented, the basic idea of quasi-static method, the concepts of the external loads and the inertia loads are introduced respectively.

2.2.1 Basic idea

To understand the quasi-static method, the basic forms of the dynamic and static analysis need to be presented first. For a dynamic analysis, as demonstrated in (2.11), the system can be expressed as follow,

$$\boldsymbol{M\ddot{R} + C\dot{R} + KR = F}(t) \tag{2.10}$$

For a static analysis, no acceleration and velocity terms are involved. Hence, a static analysis only consists of two parts: the restoring force $\boldsymbol{KR}$ (represents the structural deformation) and the external load $\boldsymbol{F}$, expressed as,

$$\boldsymbol{KR_{static} = F_{static}} \tag{2.11}$$

The basic idea of quasi-static dynamic analysis methods is to estimate the dynamic motion as an extension of the static status. Through this treatment, the dynamic analysis is represented by a static analysis, and hence can be solved easier and faster. Therefore, quasi-static method is commonly used in basic design and initial dynamic estimation.

To fulfill this idea, the equation (2.11) is represented by a static analysis.

$$\boldsymbol{KR_{qs} = F_{qs}} \tag{2.12}$$

Where, the terms $\boldsymbol{R_{qs}}$ and $\boldsymbol{F_{qs}}$ are the equivalent static displacement and external force vector, which reflect the dynamic effect.

Implement (2.12) into (2.10), the equivalent external force vector $\boldsymbol{F_{qs}}$ is estimated in such way that it contains the effect of true external force $\boldsymbol{F}(t)$ and dynamic-induced terms $\boldsymbol{M\ddot{R} + C\dot{R}}$. A typical estimation of $\boldsymbol{F_{qs}}$ is given as follows [8],

$$\boldsymbol{F_{qs} = F_{max} - F_I} \tag{2.13}$$

Where, the term $\boldsymbol{F_{max}}$ is the extreme external load; the term $\boldsymbol{F_I}$ is the maximum "inertia load" which will acted on the COG of the platform. Figure 2.3 presents a demonstration of the load distribution for the quasi-static analysis.

In the remaining part of this section, the calculation procedures of $\boldsymbol{F_{max}}$ and $\boldsymbol{F_I}$ are presented separately.

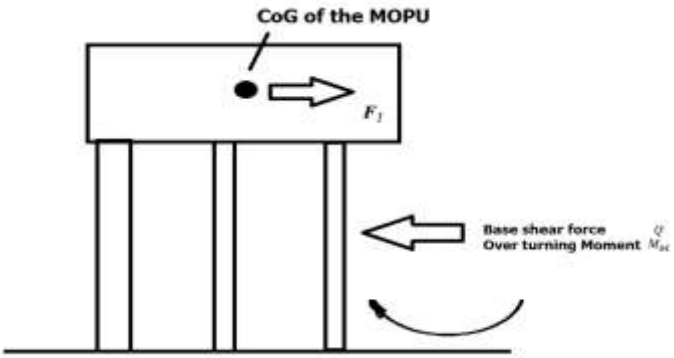

Figure 2.3 the demonstration of the load distribution of the quasi-static analysis

2.2.2 The maximum external force $\boldsymbol{F_{max}}$ calculation

For the quasi-static analysis, or deterministic non-linear static analysis according to ref [8], the calculation of the external force vector $\boldsymbol{F}(t)$ is represented by an equivalent single wave load, instead of the true stochastic wave load. A higher order wave, stokes 5th waves are recommended in this calculation and the status when the reaction force is maximum is selected. The conversion and calculation methods are widely studied and presented in Appendix I.

The characteristics of the maximum external force $\boldsymbol{F_{max}}$ calculation are highlighted as follows.

(1) Hydrodynamic nonlinearities are included in this calculation, which are the wave non-linearity, non-linear drag forces and the true free surface treatments.

(2) Because the real stochastic force calculation is represented by equivalent single wave load, thus there are deviations between true hydrodynamic loads and single wave loads.

(3) This calculation is very fast.

2.2.3 The inertia force $\boldsymbol{F_I}$ calculation

Instead of involving complex real-time dynamic calculation, quasi-static approach estimates the inertia-induced load via dynamic amplitude factor (DAF). The estimation of the inertia force $\boldsymbol{F_I}$ is given as following equation [8]

$$\boldsymbol{F_I} = Q_A(DAF - 1) \tag{2.14}$$

Where, the term Q_A is the amplitude of the base shear force Q, as demonstrated in figure 2.3

$$Q_A = \frac{1}{2}(Q_{max} - Q_{min}) \tag{2.15}$$

Where, the Q_{max} and Q_{min} are the maximum and minimum base shear force throughout the analysis.

The dynamic amplitude factor (DAF) refers to the ratio of the maximum dynamic response to the maximum static response. Several techniques can be applied to estimate the DAF's value. Among those, the simplified DAF estimation method is generally recommended [8].

The basic idea of this simplified DAF estimation method is to simplify the hydro-structural model into a SDOF system with one frequency excitation. Therefore, DAF is calculated for each natural period of the jack up structure [8]:

$$DAF = \frac{1}{\sqrt{\left[1 - \left(\frac{T_0}{T}\right)^2\right]^2 + \left(2\xi\frac{T_0}{T}\right)^2}} \tag{2.16}$$

Where
T_0= natural period
T= period of variable load
ξ=damping ratio

The simplified DAF can also be estimated with a stochastic excitation. Waves are stochastic in nature. The DAF estimation with single frequency may fail to be representative and hence it is reasonable to include the stochastic excitation into the dynamic estimation.

Holding the SDOF system assumption, the DAF is estimated as follows.

$$DAF_s = \frac{\Delta_{sig,dynamic}}{\Delta_{sig,static}} = \frac{2\sqrt{\int_0^\infty H_{dyn}^2(\omega)S(\omega)d\omega}}{2\sqrt{\int_0^\infty H_{static}^2(\omega)S(\omega)d\omega}} \tag{2.17}$$

Where:
$\Delta_{sig,dynamic}$, $\Delta_{sig,static}$ are the significant displacement from the dynamic analysis and the static analysis. $H_{dyn}(\omega)$, $H_{static}(\omega)$ are the transfer functions for the dynamic and the static analysis.

The transfer function for dynamic analysis is given as

$$H_{dyn}(\omega) = \frac{1}{\sqrt{(K - M\omega^2)^2 + \omega^2 C^2}} \tag{2.18}$$

The transfer function for static analysis is given as

$$H_{static}(\omega) = \frac{1}{K} \tag{2.19}$$

Where, the equivalent stiffness K is estimated from topside's mass M and natural period T_0, given as

$$K = M\frac{4\pi^2}{T_0^2} \tag{2.20}$$

The equivalent damping C estimated from damping ratio ξ, is given as

$$C = 2\xi\sqrt{KM} \tag{2.21}$$

In the dynamic analysis of the Yme MOPUstor, the damping ratio is estimated as 3%.

The characteristics of the inertia force $\boldsymbol{F}_I$ calculation are highlighted as follows.

(1) The calculation of the inertia force is estimated via the global performance of the platform. This calculation is quite fast and acceptable when the dynamic influence is not sensitive.

(2) For resonant condition, where inertia load is very sensitive to dynamic properties of platform, DAF estimation can be always too conservative compared with real situation.

(3) The inertia load is estimated only according to the COG of the platform. This estimation is so rough that cannot reflect the real load distribution of the inertia effect.

(4) The phase shift between inertia load and wave load is not considered in the inertia load estimation. Therefore, the inertia load may overestimate the load situation.

(5) As a "static" inertia load, this method is unsuitable for fatigue calculation.

2.3 Frequency-domain Method (FD)

In this section, the analysis philosophy of the FD method is presented, the basic idea of the FD method and its application on the decoupled hydro-structural model are introduced respectively.

2.3.1 Basic idea: excitation, response and transfer function

The basic idea of the frequency-domain methods is to separate the real motion of the displacement into a series of discretized harmonic motions. By linearizing the total system, the relation between wave and displacement can be established for each harmonic component, with respect to its amplitude and phase shifts

The objective considered in the frequency-domain methods can be identified as figure 2.4.

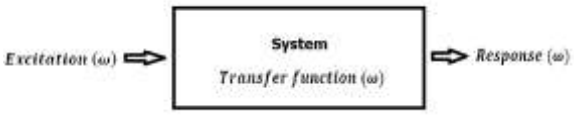

Figure 2.4 representation of a system

Where, these terminologies can be defined as follows,

(1) System: the physical and mathematical model of the interaction
(2) Excitation: the input of the system
(3) Response: the output of the system

The traditional frequency domain is defined in the field of a linear system. The characteristics of a linear system are highlighted as follows.

(1) No non-linear term can be involved in the system.
(2) The principle of superposition: the excitation component at a specific frequency only influences the response at same frequency.
(3) For the component at a specific frequency, the response amplitude is proportional to the force amplitude and the phase shift is not dependent on the force amplitude.

These dynamic characteristics can be represented as a complex transfer function $H(\omega)$. A transfer function is defined as the harmonic response due to harmonic excitation of unit excitation, e.g.

If the excitation component f at frequency ω_{ii} is given as,

$$f(t) = A_{f_{\mathrm{ii}}} \cos(\omega_{ii} t + \theta_{ii}) \tag{2.22}$$

Where $A_{f_{\mathrm{ii}}}$, ω_{ii} and θ_{ii} are the amplitude, frequency and initial phase of this excitation component.

Then, the response r will be,

$$r_i = A_{r_{ii}} \mathrm{Re}\left\{|H(\omega_{ii})| e^{i(\omega_{ii}t+\delta_{ii}+\theta_{ii})}\right\} = A_{r_{ii}} |H(\omega_{\mathrm{ii}})| \cos(\omega_{ii}t + \delta_{ii} + \theta_{ii}) \tag{2.23}$$

Where transfer function $H(\omega_{\mathrm{i}})$ is defined as
The real part of transfer function H :$H_r(\omega_{ii})$;
The imagine part of transfer function H :$H_i(\omega_{\mathrm{ii}})$;
The amplitude of transfer function H : $|H(\omega_{ii})| = \sqrt{H_r(\omega_{ii})^2 + H_i(\omega_{ii})^2}$
The phase shift of transfer function $\delta(\omega_{ii}) = atan(\frac{H_i(\omega_{ii})}{H_r(\omega_{ii})})$

2.3.2 The analysis methodology on the decoupled hydro-structural model

For the FD analysis of the Yme MOPUstor's model, the system can be identified as figure 2.5,

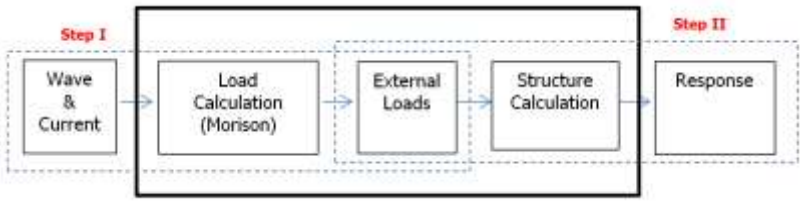

Figure 2.5 identification of the decoupled hydro-structural system in FD analysis

The discretized stochastic wave is presented as,

$$\eta = \sum_{ii=1}^{m} A_{ii} \cos(\omega_{ii}t + \theta_{ii}) \tag{2.24}$$

Where, η is the surface elevation at origin, $A_{ii}, \omega_{ii}, \theta_{ii}$ is the amplitude, frequency and initial phase angle at the frequency component ii, m is the total number of the dicretization.

The discretized external force is presented as,

$$f_i = \sum_{ii=1}^{m} A_{f_{i_{ii}}} \cos\left(\omega_{ii}t + \delta_{f_{i_{ii}}} + \theta_{ii}\right) \tag{2.25}$$

Where, f_i is the external force at displacement i, $A_{f_{i_{ii}}}, \delta_{f_{i_{ii}}}$ is the amplitude, shifted phase angle at the frequency component ii

The discretized displacement r_i is presented as,

$$r_i = \sum_{ii=1}^{m} A_{r_{i_{ii}}} \cos\left(\omega_{ii} t + \delta_{r_{i_{ii}}} + \theta_{ii}\right) \tag{2.26}$$

Where, r_i is the ith displacement, $A_{r_{i_{ii}}}, \delta_{r_{i_{ii}}}$ is the amplitude, shifted phase angle at the frequency component ii

The current-induced response is calculated separately at static analysis.

As observed in figure 2.5, the FD dynamic analysis on Yme MOPUstor can be divided into two steps.

(1) Step I: Wave η to External load f calculation, two non-linearity sources are involved in this calculation: drag force and wave-varying elevation.

(2) Step II: External load f to Structure response r_i calculation, no non-linearity source is involved in this calculation

In Step I, the hydrodynamic non-linearity needs to be linearized before the calculation. For the free surface linearization, a constant surface elevation, instead of the time-varying elevation, is assumed in this calculation. For the drag force linearization, two methods are generally proposed [8].

Method I linearized the drag term with respect to the reference wave height H_{ref} [10], expressed as,

$$\alpha_1 |v_{n_i}| \boldsymbol{v}_{n_i} \approx \alpha_1 \left|v_{n,max_i}\right| \boldsymbol{v}_{n_i} \tag{2.27}$$

Where
$\boldsymbol{v}_{n_i}$ is the undisturbed velocity of the fluid normal to the member for the displacement r_i, as discussed in section 2.1.
$\left|v_{n,max_i}\right|$ is the absolute value of the maximum velocity of the fluid normal to the member of the displacement r_i during one cycle of a wave with the reference wave height H_{ref}.

Method II linearized the drag term based on the study of Leon.E.Borgman [11], expressed as,

$$\alpha_1 |v_{n_i}| \boldsymbol{v}_{n_i} \approx \alpha_1 \sigma_u \sqrt{\frac{8}{\pi}} \boldsymbol{v}_{n_i} \tag{2.28}$$

Where σ_u is the standard deviation of the regular sinusoidal velocity.

In this comparative study, two methods will be analyzed.

In Step II, the calculation is quite straightward. The direct harmonic response method or the modal superposition methods may be used in this calculation [12].

By connecting these two steps, the transfer function $H_i(\omega_{ii})$ directly from wave to structure response is established. In practice, this transfer function is calculated with respect to a certain reference wave height H_{ref} and then applied for all the sea states.

$$H_i(\omega_{ii}) = H_{i_i}(\omega_{\mathrm{ii}}) + \boldsymbol{j} H_{i_r}(\omega_{\mathrm{ii}}) \tag{2.29}$$

Where $H_{i_i}(\omega_{\mathrm{ii}})$ and $H_{i_r}(\omega_{\mathrm{ii}})$ are defined as

$$\begin{cases} \sqrt{H_{i_r}(\omega_{\mathrm{ii}})^2 + H_{i_i}(\omega_{\mathrm{ii}})^2} = \dfrac{A_{r_{i_{ii}}}}{A_{ii}} \\ atan\left(\dfrac{H_{i_i}(\omega_{\mathrm{ii}})}{H_{i_r}(\omega_{\mathrm{ii}})}\right) = \delta_{r_{i_{ii}}}(\omega_{\mathrm{ii}}) \end{cases} \tag{2.30}$$

In hydrodynamics, the ratio of the response amplitude $A_{r_{i_{ii}}}$ to the wave amplitude A_{ii} is referred to the response amplitude operator (RAO), where RAO is a function of the wave's frequency.

$$RAO_i(\omega_{ii}) = \frac{A_{r_{i_{ii}}}}{A_{ii}} = \sqrt{H_{i_r}(\omega_{\mathrm{ii}})^2 + H_{i_i}(\omega_{\mathrm{ii}})^2} \tag{2.31}$$

By performing the spectrum and statistics analysis, the maximum value of the response within return period can be estimated. Two statistics analysis methods, the long-term statistics method and the short-term statistics method are proposed in this thesis. More details are attached in Appendix II.

The procedures of the frequency-domain calculation can be summarized in figure 2.6.

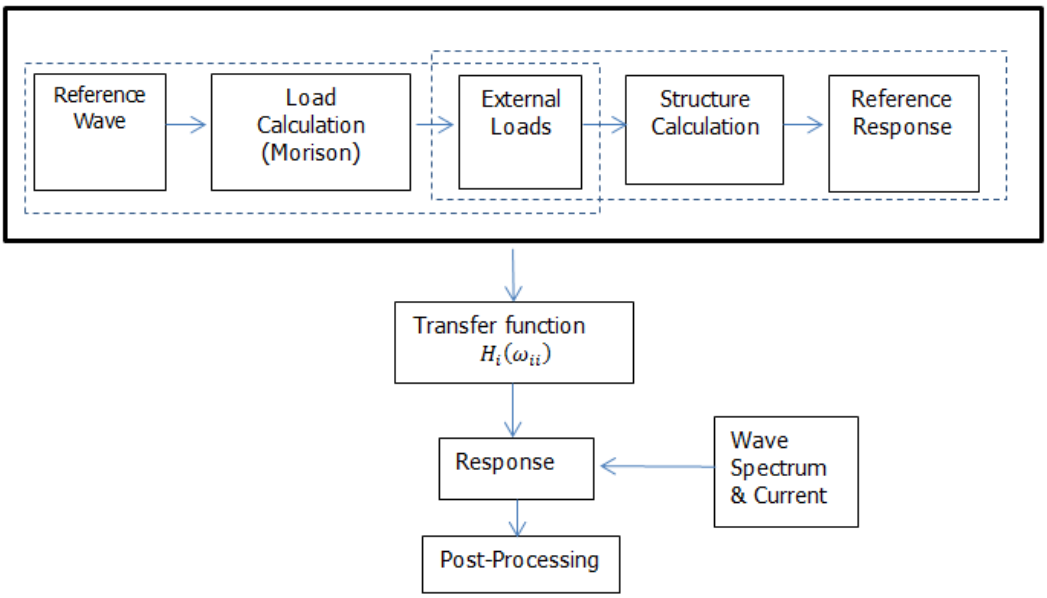

Figure 2.6 the procedures of the frequency-domain dynamic analysis method

The characteristics of the frequency-domain methods can be highlighted as follows.

(1) As a “real” dynamic analysis, the accurate load distribution can be established.

(2) Non-linear terms are linearized in this calculation, such as the free surface variation, the drag force. These linearizations induce uncertainties.

(3) The FD calculation is quite fast. Following the principle of superposition, the transfer functions only need to be calculated once, and then can be easily applied to all the sea states.

(4) Suitable for both fatigue and extreme value predication.

2.4 Time-domain Method (TD)

In this section, the analysis philosophy of the time-domain method is presented. The basic ideas of the TD method, Newmark-beta algorithm and its analysis methodology on the decoupled hydro-structural model are introduced respectively.

2.4.1 Basic idea: Discretized time and status

The idea of time-domain calculation is based on the time discretization. The first step of time-domain is to discretize the continuous motions into the status at the discretized time points. Three concepts, continuous status, time step and discretized status are denoted here.

(1) Continuous status is referred to the status (the force, wave and displacement etc.) in the continuous time history t, e.g.

$$t \rightarrow \eta(t), f_i(t), r_i(t), \dot{r}_i(t), \ddot{r}_i(t), \ldots \tag{2.32}$$

(2) Discretized status is referred to the status (the force, wave and displacement etc.) in the discretized time point t_j, e.g.

$$t_j \rightarrow \eta(t_j), f_i(t_j), r_i(t_j), \dot{r}_i(t_j), \ddot{r}_i(t_j), \ldots \tag{2.35}$$

(3) Time step is referred to the time gap between time point, e.g.

$$\Delta t_j = t_{j+1} - t_j \tag{2.36}$$

As time being discretized, the basic idea of time-domain is based on the discretized time status: the discretized status at time point t_j is calculated based on the status at previous time point t_{j-1} . Such kinds of iteration are performed for each time point till the end, and thus the motions in discretized time history are obtained.

For the time-domain calculation, fully hydrodynamic forces are calculated directly at each time point, while the structural response is calculated by using numerical algorithm.

2.4.2 Numerical algorithm

The iteration calculations are executed by applying the numerical algorithms, among which the Newmark-beta method is the most commonly used in Structural dynamics [12] [13].

The Newmark-beta method is based on the Taylor expansion of velocity and acceleration at one time step. As, shown in eqn (5.18), for one response, the status at time point t_{j+1} is approximated by its Taylor expansion at time point t_j,

$$r_{i\,j+1} = r_{i\,j} + \Delta t_j \dot{r}_{i_j} + \frac{{\Delta t_j}^2}{2}\ddot{r}_{i_j} + \frac{{\Delta t_j}^3}{6}\dddot{r}_{i_j} + O(4) \tag{2.37}$$

$$\dot{r}_{i\,j+1} = \dot{r}_{i_j} + \Delta t_j \ddot{r}_{i_j} + \frac{{\Delta t_j}^2}{2}\dddot{r}_{i_j} + O(3) \tag{2.38}$$

Where

$r_{i\,j+1}, \dot{r}_{i\,j+1}$	The displacement r_i and velocity $\dot{r}_i$ at time point t_{j+1} respectively
$r_{i\,j}, \dot{r}_{i_j}, \ddot{r}_{i_j}, \dddot{r}_{i_j}$	The displacement r_i, velocity $\dot{r}_i$, acceleration $\ddot{r}_i$ and jerk $\dddot{r}_i$ of response at t_j respectively.
$O(3), O(4)$	The term with order higher than 3,4

Among those, the higher order term effects are estimated as a weight of the jerk term, as shown below,

$$r_{i\,j+1} = r_{i\,j} + \Delta t_j \dot{r}_{i_j} + \frac{{\Delta t_j}^2}{2}\ddot{r}_{i_j} + \frac{{\Delta t_j}^3}{6}\dddot{r}_{i_j} + O(4) \approx r_{i\,j} + \Delta t_j \dot{r}_{i_j} + \frac{{\Delta t_j}^2}{2}\ddot{r}_{i_j} + \beta\frac{{\Delta t_j}^3}{6}\dddot{r}_{i_j} \tag{2.39}$$

$$\dot{r}_{i\,j+1} = \dot{r}_{i_j} + \Delta t_j \ddot{r}_{i_j} + \frac{{\Delta t_j}^2}{2}\dddot{r}_{i_j} + O(3) \approx \dot{r}_{i_j} + \Delta t_j \ddot{r}_{i_j} + \frac{{\Delta t_j}^2}{2}\gamma\dddot{r}_{i_j} \tag{2.40}$$

Where the jerk term is estimated as,

$$\dddot{r}_{i_j} = \frac{\ddot{r}_{i_{j+1}} - \ddot{r}_{i_j}}{\Delta t_j} \tag{2.40}$$

Table 2.1 shows the possible combinations of the γ and β values. Among those, the linear acceleration method is adopted in this comparative study.

Table 2.1. the possible values of γ and β		
Method	γ	β
Central difference method	0.5	0
Fox-Goodwin method	0.5	1/12
Linear acceleration method	0.5	1/6
Constant average acceleration method	0.5	1/4

Furthermore, the selection of time step is important. The time step needs to be set small enough to reflect the motion at certain frequency [14]. It is recommended to be 1/25 of the interesting frequency [14].

2.4.3 The analysis methodology on the decoupled hydro-structural model

Similar to the frequency-domain calculation, the TD analysis of the decoupled hydro-structural model is divided into three steps.

(1) Step I: discretized external load calculations (Fully non-linear Morison's equation)

(2) Step II: discretized structural response calculations (Newmark-beta method)

(3) Step III: post-processing

Step I and Step II have been well explained in the previous section, while step III is analyzed statistically. A study has been carried out on the goodness of fit of several possible statistics methods in extreme value predication [14]. In this study, the generalized extreme distribution model is adopted and explained in Appendix II.

To sum up, the characteristics of the time-domain methods can be highlighted as follows.

(1) Most accurate method in principle: involved all the non-linearity and dynamic effect.

(2) Most time-consuming

(3) Complicated post-processing, may be sensitive to the selected time-step

(4) Facing the convergence problem and may effected by the transition motion

2.5 Summary

In this chapter, the decoupled hydro-structural model is introduced and adopted as the reference model in the comparative study

$$\boldsymbol{M\ddot{R} + C\dot{R} + KR = F}(t)$$

Three general accepted methods are selected in this comparative study
(1) Stochastic non-linear dynamic (Time-domain methods)
(2) Stochastic linear dynamic (Frequency-domain methods)
(3) Deterministic non-linear static (Quasi-static methods)

Quasi-static method is a common method used for the determination of the extreme response. So-called quasi-static, as its name, treats the dynamic analysis as an extension of the static analysis. The inertia-induced load is estimated as the static load via so-called dynamic amplitude factor or DAF. DAF is the ratio of the maximum dynamic response to the maximum static response. Several techniques can be applied to estimate DAF, such simplified DAF method.

Frequency-domain (FD) approach is another commonly used method in the dynamic analysis regarding its advantages. Instead of considering the motions as a quasi-static status or in time-history, FD approach treats the motions as a series of harmonic motions. The conventional “frequency-domain” or frequency-domain method for linearized system, each component of the excitations has only one corresponding response with the same frequency, following the principle of superposition. Frequency-domain is generally used in fatigue limit state analysis and may be applied in ultimate analysis.

Time-domain approach is the most accurate and most complex method in structural dynamic calculation. The mechanism of time-domain is based on the iteration over time steps, e.g. status (excitations and their corresponding response) at the current time point is calculated based on the status at the previous time point. Such iterations is performed numerically till the end. Time-domain is the most widely applied but most time consumed.

The details of the post-processing are attached in Appendix II.

A brief summary of the characteristics of those three methods is presented in table 2.2.

Table 2.2 the characterizes of quasi-static, frequency-domain and time-domain methods

Method	External Force			Dynamic	Post Processing	Time Consuming
	drag force	inertia Force	free surface treatment			
Quasi-static	Non-linear	Accurate	Non-linear	Estimated	No need	Very fast
Frequency-domain	linearized	Accurate	Linearized	Accurate	Rayleigh distribution	fast
Time-domain	Non-linear	Accurate	Non-linear	Numerical	Generalized extreme value distribution	Very slow

3.0 HIGHER ORDER FREQUENCY DOMAIN METHOD (HFD)

This chapter presents, a new dynamic analysis method, the higher order frequency domain (HFD) method. It is begun with the polynomial approximation of the non-linear term and then the applications on both SDOF and MDOF system. The techniques on the computation improvement are also provided in this chapter. This new method has been applied on both SDOF and MDOF system.

3.1 Overview

As discussed in Chapter 2, all of the traditional dynamic analysis methods are imperfect in nature, facing the dilemma between the accuracy and the efficiency. In this study, the investigations have been carried out on the improvement of the traditional methods, especially the frequency domain method. For this reason, the higher order frequency domain (HFD) method is created.

The basic idea of the higher order frequency domain (HFD) method is to approximate the non-linear terms as the higher order polynomial functions, and calculate those higher order terms by using the higher order transfer functions.

Taking an example of a cubic excitation, if we have a harmonic input f with the amplitude of A and the frequency of ω, the cubic excitation f^3 can be treated as a linear summation of four complex terms. Then the non-linear problem is converted into a linear problem.

$$f^3 = \left(A\cos(\omega t)\right)^3 = A^3\left(\frac{e^{j\omega t} + e^{-j\omega t}}{2}\right)^3 = \frac{A^3}{8}\left(e^{j3\omega t} + e^{-j3\omega t} + 3e^{j\omega t} + 3e^{-j\omega t}\right)$$

Non-linear ⇨ linear

Three characteristics of the higher order frequency domain method are highlighted as follows. With those characteristics, the HFD method may be served as another dynamic analysis option in the future.

(1) The analysis of the HFD method is limited to the decoupled hydro-structural model.

(2) The drag-forces and the free surface elevations are approximated as the higher order polynomial functions.

(3) The phenomenon of the frequency-shifts can be predicted in the HFD method.

In additions, some differences between the traditional dynamic analysis methods can be explained by the HFD methods qualitatively and quantitatively, especially the influence of linearization in the traditional frequency-domain method. Those differences will be discussed in Chapter 4 and Chapter 6.

3.2 The approximation of the non-linear terms

To begin with, the issue of non-linear terms' approximation is discussed.

The core of the HFD method is the non-linear terms' approximation. As mentioned in previous section, the non-linear terms, the drag-forces and the free surface elevation, are approximated as some polynomial functions. Hence, the results from the HFD method are valid only if those polynomial functions' approximation are representative. Therefore, those approximations are significantly important and need to be discussed first.

In this section, the polynomial approximation of the drag term and the free surface elevation effect are discussed respectively.

3.2.1 The polynomial approximation of the drag term $v|v|$

As presented in the Chapter 2, the decoupled hydrodynamic force on each element can be expressed as follow,

$$d\boldsymbol{F} = \alpha_1 |v_n| \boldsymbol{v}_n + \alpha_2 \dot{\boldsymbol{v}}_n \tag{3.1}$$

Where the $d\boldsymbol{F}$ is the external force vector in x,y,z, direction, $\boldsymbol{v}_n$ is the fluid's velocity vector normal to the element in x,y,z direction. α_1 and α_2 are the simplified drag and inertia coefficients respectively, as indicated in equation (2.9).

As observed from (3.1), the non-linearity of the hydrodynamic forces comes from the quadratic drag term in the Morison's equation. Although the drag term is normally called "quadratic", the drag term is actually the influence by those infinite higher order terms, due to the presents of the absolute value operation.

For the purpose of the approximation, the drag term is approximated as a polynomial function with finite order terms, as shown in equation (3.2) and equation (3.3). Here, due to the symmetry of the absolute terms, only odd terms exist in this approximation.

$$d\boldsymbol{F} \approx \alpha_1 (p_1 + p_3 v_n^2 + p_5 v_n^4 + p_7 v_n^6 + \cdots) \boldsymbol{v}_n + \alpha_2 \dot{\boldsymbol{v}}_n \tag{3.2}$$

Or

$$|v_n| v_n = (\boldsymbol{v}_n \cdot \boldsymbol{v}_n) v_n \approx (p_1 + p_3 v_n^2 + p_5 v_n^4 + p_7 v_n^6 + \cdots) v_n \tag{3.3}$$

This approximation is carried out in such way: The values of the absolute term $|v_n|$ are discretized by the step of 0.001m/s, within a certain range. The polynomial functions with a certain order accuracy are adopted to fit those discretized value. Those curve fittings are performed by using Matlab™ curve fitting toolbox with the maximum likelihood function method (MLE).

Table.3.1 shows the accuracy of the curve fittings with different fitting ranges and different fitting orders. As observed from the table 3.1, both the fitting range and the fitting order affect the accuracy. The validation of a longer fitting range is compensated by the reduction of the overall accuracy. Besides, the resolution of the fitting for a certain range is improved by the increase of the fitting order.

Table3.1.Root mean squared error (RMSE) for different fitting ranges and different fitting orders

Order\Range	+/-5m/s	+/-10m/s	+/-15m/s	+/-20m/s	+/-25m/s
1st order fitting	1.4463	2.8896	4.3333	5.7764	7.2198
3rd order fitting	0.3618	0.7226	1.0836	1.4443	1.8051
5th order fitting	0.1811	0.3615	0.542	0.7224	0.9027
7th order fitting	0.1133	0.226	0.3388	0.4516	0.5643

The 3rd order fitting within +/-20m/s fitting range is recommended with reasons. First, the typical range of the fluid's velocity in hydrodynamic calculation is within +/- 20 m/s. Second, as observed in table 3.1, compared with the 1st order fitting (linearized drag force), the 3rd order fitting improves the accuracy of 75%, the 5th order fitting improves the accuracy of 87.5%. The amount of computation increased significantly from 3rd order fitting to 5th order fitting. Therefore, the 3rd order fitting is recommended.

For the 3rd order fitting within +/-20m/s fitting range, the coefficients of this approximation are estimated as, (within 95% confidence)

$$p_1 = 6.25\ (6.234, 6.266)$$

$$p_3 = 0.03646\ (0.0364, 0.03652) \tag{3.4}$$

Or

$$|v_n|v_n \approx 6.25v_n + 0.03646v_n^3 \tag{3.5}$$

Figure 3.1 shows the plot of the $|v_n|v_n$, the 1st order approximation, and the 3rd order approximation. From the plot, it is observed that the 3rd order approximation significantly improves the accuracy of the curve fitting compared with linear fitting. The 3rd order approximation is believed to be accurate enough for the engineering applications.

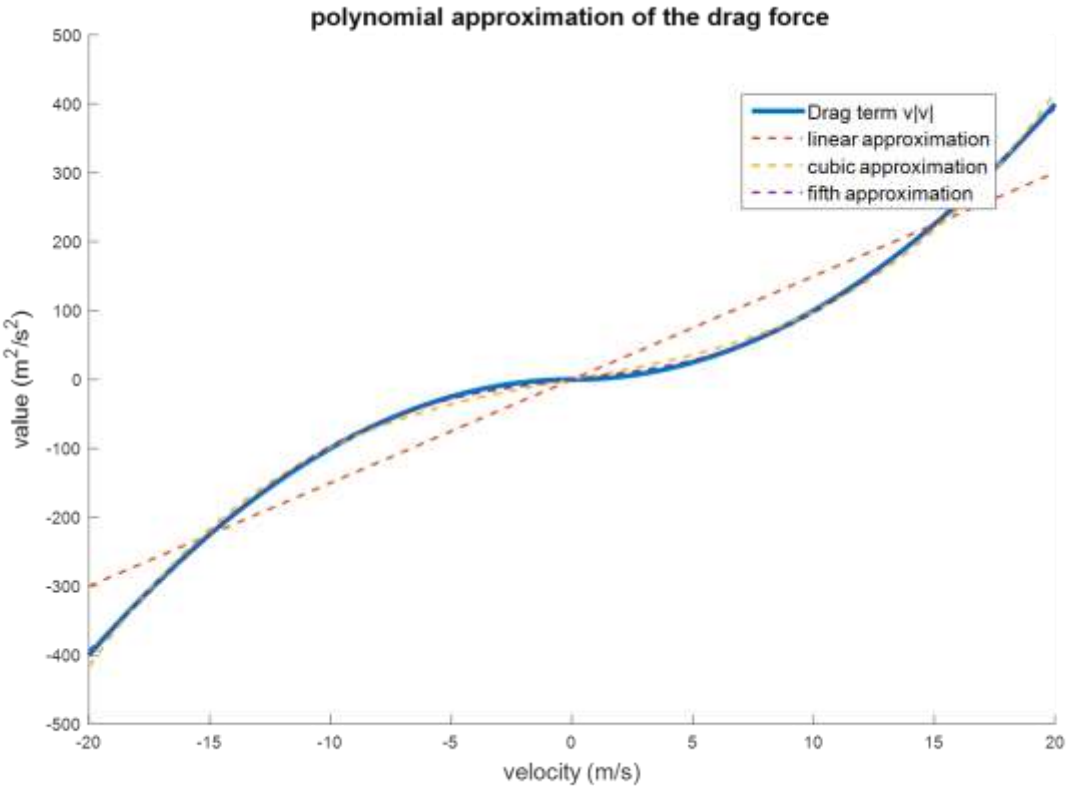

Figure 3.1 the plot of the $|v_n|v_n$, linear, cubic and fifth approximation.

To sum up, the total Morison's force within +/- 20m/s can be approximated as a linear term plus a cubic term, expressed as,

$$d\boldsymbol{F} \approx \alpha_1(6.25 + 0.03646v_n^2)\boldsymbol{v}_n + \alpha_2\dot{\boldsymbol{v}}_n = (6.25\alpha_1\boldsymbol{v}_n + \alpha_2\dot{\boldsymbol{v}}_n) + 0.03646\alpha_1(\boldsymbol{v}_n \cdot \boldsymbol{v}_n)\boldsymbol{v}_n \tag{3.6}$$

$$d\boldsymbol{F} \approx d\boldsymbol{F}^{(1)} + d\boldsymbol{F}^{(3)} \tag{3.7}$$

Where $d\boldsymbol{F}^{(1)}$refers to the linear part of the force, $d\boldsymbol{F}^{(3)}$ refers to the cubic part of the force.

Previous studies has shown some similar approaches [15]. However, this approximation is developed independently in this study and is different from the other methods, in principle.

3.2.2 Free surface elevation approximation

The approximation of the free surface elevation effect is difficult. First, the nodes effects by the free surface elevation are varying stochastically due to the stochastics wave loads. Second, the magnitude of the free surface-induced wave loads is difficult to be expressed. Therefore, the effect of the free surface elevation can only be roughly estimated.

The studies by X.Y.Zheng and C.Y.Liaw [15] propose a quadratic approximation of free surface elevation. By using the knowledge of Taylor series expansion, the inundation force due to varying free surface elevation can be represented by a 'concentrated load', acting on the structure at the mean water level. Their studies focus on the legs along the vertical direction and the directing spectrum calculation, instead of the higher order transfer function.

In this approximation, the z=0 is set at the mean water level for convenience. The inundation force due to varying free surface elevation is expanded into 3D-frame and can be expressed as,

$$\boldsymbol{F_{ei}} = \int_0^{s_\eta} \boldsymbol{f}(s)ds = \int_0^{\eta} \boldsymbol{f}\left(\frac{1}{p_z}z\right)\frac{1}{p_z}dz \tag{3.8}$$

Where F_{ei} is the inundation force vector, s_η and η are the surface elevation along the member direction and z-direction respectively, $\boldsymbol{f}$ is the Morison's force, p_z is the projection of member length s into z-axis. E.g

$$z = p_z s \tag{3.9}$$

Applying the Taylor expansion into (3.8) at z=0, we have

$$\boldsymbol{F_{ei}} = \int_0^{\eta} \boldsymbol{f}\left(\frac{1}{p_z}z\right)\frac{1}{p_z}dz \approx 0 + \boldsymbol{f}(0)\frac{1}{p_z}\eta + \frac{\partial \boldsymbol{f}(0)}{\partial z}\frac{1}{p_z}\frac{\eta^2}{2} + \cdots \tag{3.10}$$

As observed in equation (3.8), the effect of the inundation force is approximated as a polynomial 'concentrated' load acted on the mean water level. However, the study by X.Y.Zheng and C.Y.Liaw [15] , only gives the correction on the total force, without consideration of the load distribution. Therefore, besides this concentrated force, a correction term on moment also needs to be applied at same location, as shown in figure 3.2.

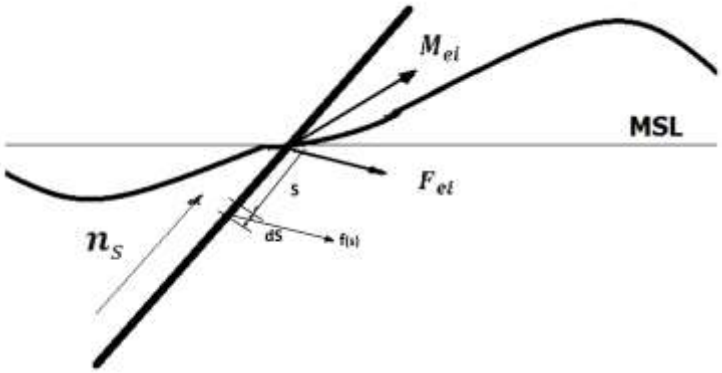

Figure 3.2 the graphic representation of the approximation of the free surface effect

The moment effect of the inundation forces about the mean water level can be presented as,

$$\boldsymbol{M_{ei}} = \int_0^{s_\eta} \boldsymbol{f}(s) \times \boldsymbol{n}_s s \, ds = \int_0^{\eta} \boldsymbol{f}\left(\frac{1}{p_z} z\right) \times \boldsymbol{n}_s \frac{z}{{p_z}^2} dz \tag{3.11}$$

Where, the term $\boldsymbol{M_{ei}}$ is the moment of the inundation force about the mean water level, $\boldsymbol{n}_s$ is the unit direction along the member element.

Applying the Taylor expansion into (3.11) at z=0, we have

$$\boldsymbol{M_{ei}} = \int_0^{\eta} \boldsymbol{f}\left(\frac{1}{p_z} z\right) \times \boldsymbol{n}_s \frac{z}{{p_z}^2} dz \approx 0 + 0 + \boldsymbol{f}(0) \times \boldsymbol{n}_s \frac{\eta^2}{2{p_z}^2} + \cdots \tag{3.12}$$

As discussed in section 3.2.1, the Morison force can be approximated as a linear term $\boldsymbol{f^1}(s)$ plus a cubic term $\boldsymbol{f^3}(s)$, express as

$$\boldsymbol{f}(s) \approx \boldsymbol{f^{(1)}}(s) + \boldsymbol{f^{(3)}}(s) \tag{3.13}$$

Based on the study in previous section, the cubic effect inside the drag term is far more smaller than the linear effect inside the drag term. Therefore, the interaction between and cubic part in drag force and the higher order part in the free surface effect are in a level higher than 5th order and hence can be ignored.

Substitute (3.9) into (3.11) and (3.12), ignoring the term higher than 3rd order, we have

$$\begin{aligned}\boldsymbol{F_{ei}} &\approx \left(\boldsymbol{f^{(1)}}(0)+\boldsymbol{f^{(3)}}(0)\right)\frac{1}{p_z}\eta+\frac{\partial}{\partial z}\left(\boldsymbol{f^{(1)}}(0)+\boldsymbol{f^{(3)}}(0)\right)\frac{1}{p_z}\frac{\eta^2}{2}+\cdots \\ &\approx \boldsymbol{f^{(1)}}(0)\frac{1}{p_z}\eta+\frac{\partial \boldsymbol{f^{(1)}}(0)}{\partial z}\frac{1}{p_z}\frac{\eta^2}{2}\end{aligned} \tag{3.14}$$

$$\boldsymbol{M_{ei}} \approx 0+0+(\boldsymbol{f^{(1)}}(0)+\boldsymbol{f^{(3)}}(0))\times \boldsymbol{n}_s\frac{\eta^2}{2{p_z}^2}+\cdots \approx \boldsymbol{f^{(1)}}(0)\times \boldsymbol{n}_s\frac{\eta^2}{2{p_z}^2} \tag{3.15}$$

The term "$\frac{\partial \boldsymbol{f^{1}}(0)}{\partial z}\frac{1}{p_z}\frac{\eta^2}{2}$" in equation (3.14) is debatable for the 1st order stochastic wave. The 1st order stochastic wave, as used in this study is based on the superposition of the Airy waves, in which there is no definition for the waves above the mean water level. Therefore, the term "$\frac{\partial \boldsymbol{f^{1}}(0)}{\partial z}$", in principle, cannot be defined within the 1st order accuracy. The higher order wave theory, such as the 2nd order stochastic wave model, can induce the expression of this derivation. In this study, this derivation term will not be introduced, and hence the estimation of those inundation effects is limited to the 2nd order accuracy.

To handle the discontinuity of the velocity's profile, the wheeler wave treatment may be adopted here. As introduced in Appendix I, the wheeler stretched treatment [7] calculates wave kinematics at the mean water level at the true surface and its corresponding distribution down to the seabed is stretched accordingly. Therefore, there is no discontinuity occurs between the velocity above and below the MSL.

Assume a vertical pipe is fixed at seabed and extended into a level far beyond the mean water level. Then the hydrodynamic load on it can be expressed as,

$$F=\int_{-d}^{\eta} f\left(\frac{z-\eta}{1+\frac{\eta}{d}}\right)dz=\int_{-d}^{0} f\left(\frac{z-\eta}{1+\frac{\eta}{d}}\right)dz+\int_{0}^{\eta} f\left(\frac{z-\eta}{1+\frac{\eta}{d}}\right)dz \tag{3.16}$$

For application in offshore industry, the wave elevation η is relative small to the water depth d. Therefore, the Taylor expansion is applied to approximate the term "$\frac{z-\eta}{1+\frac{\eta}{d}}$", expressed as,

$$\frac{z-\eta}{1+\frac{\eta}{d}} = (z-\eta)\frac{1}{1+\frac{\eta}{d}} \approx (z-\eta)(1-\frac{\eta}{d}+\left(\frac{\eta}{d}\right)^2-\left(\frac{\eta}{d}\right)^3+\cdots) \tag{3.17}$$

With the Taylor expansion at z=0, then the equation (3.16) can be rewritten as,

$$\begin{aligned} F = \int_{-d}^{\eta} f\left(\frac{z-\eta}{1+\frac{\eta}{d}}\right)dz \\ \approx \int_{-d}^{0} f\left((z-\eta)(1-\frac{\eta}{d}+\left(\frac{\eta}{d}\right)^2-\left(\frac{\eta}{d}\right)^3+\cdots)\right)dz \\ + f\left((0-\eta)(1-\frac{\eta}{d}+\left(\frac{\eta}{d}\right)^2-\left(\frac{\eta}{d}\right)^3+\cdots)\right)\eta \end{aligned} \tag{3.18}$$

The verifications of the free surface elevation's approximation are difficult. A 3D model needs to be built and a serious sensitivity study needs to be carried out. A simple verification are given in chapter 4.

To sum up, the effect of the free surface elevation can be approximated as a concentrated force and a concentrated moment at the mean water level. Combining the cubic approximation of the drag term, the concentrated force and the moments are given as,

$$\boldsymbol{F_{ei}} \approx \boldsymbol{f}^{(1)}(0)\frac{1}{p_z}\eta + 0(2) \rightarrow \boldsymbol{F_{ei}}^{(2)} \tag{3.19}$$

$$\boldsymbol{M_{ei}} = \boldsymbol{f}^{(1)}(0) \times \boldsymbol{n}_s\frac{\eta^2}{2{p_z}^2} + 0(4) \rightarrow \boldsymbol{0} \tag{3.20}$$

3.3 The application on SDOF system

In this section, the application of the HFD method on the single degree of freedom (SDOF) system is presented. In this application, the effect of the drag term is presented in this system, while the effect of the free surface elevation is not considered.

For the better understanding, the following situation is assumed. As presented in figure 3.3, a pipe with a total mass of m_0 is horizontally fixed on a frame inside the water and perpendicular to the 2D wave. The interaction between pipe and frame can be represented by an equivalent stiffness k and an equivalent dampingc_0. The spectrum of the waves is assumed to be $S_{\eta\eta}(\omega)$ and the velocity profile of the current is $u_c(z)$, with same direction of the waves. The coordinate of the system is fixed at sea bed, aligned perpendicular to the pipe. The mean sea level is z=d. The location of pipe is $z = z_p, x = x_p$

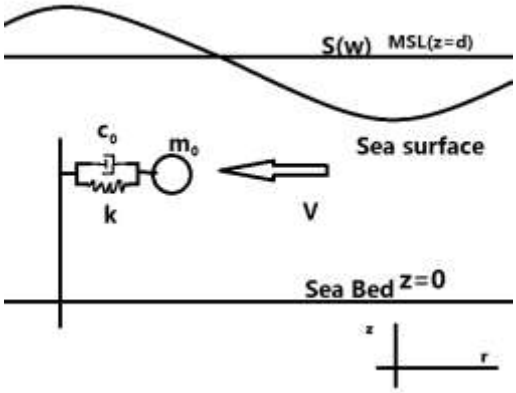

Figure 3.3 the graphic representation of the assumed SDOF system

The problem described above can be indentified as a SDOF system, expressed as

$$m_0\ddot{x} + c_0\dot{x} + kx = \alpha_1|v - \dot{x}|(v - \dot{x}) + \alpha_2(\dot{v} - \ddot{x})$$

$$\downarrow$$

$$m\ddot{x} + c\dot{x} + kx = \alpha_1|v|v + \alpha_2\dot{v} \tag{3.21}$$

Where $\ddot{r}, \dot{r}$ and r is the acceleration, velocity and displacement of the pipe in x direction. α_1 and α_2 are the coefficients for the drag and inertia force, which are assumed to be constant. v and $\dot{v}$ are the horizontal velocity and acceleration of the incoming water at (x_p, z_p).

With the decoupled hydro-structural model being established, the next action is to convert the fluid information $S_{\eta\eta}(\omega)$ and $u_c(z)$ into the fluid's velocity v.

For the 1st order stochastic wave [8], the horizontal velocity v at pipe location (x_p, z_p) is modelled as

$$v = \sum_{ii=1}^{m} A_{a,ii}\omega_{ii}\frac{\cosh k_{ii}z_p}{\sinh k_{ii}d}\cos\left(\omega_i t - k_{ii}x_p + \phi_{ii}\right) \tag{3.22}$$

Where,

$A_{a,ii}$ The amplitude of the wave component ii, e.g. $A_{a,ii}=\sqrt{2S_{\eta\eta}(\omega_i)\Delta\omega_i}$

ω_{ii} The angular frequency of the wave component ii

k_{ii} The wave number of the wave component ii, e.g.

$$\omega_{ii}{}^2 = gk_{ii}tanh(k_{ii}d)$$

ϕ_{ii} Random phase, uniformly distributed between 0 and 2π

$\Delta\omega_i$ frequency band width associated with ω ii, i.e. $\Delta\omega_i = (\omega_{i+1} - \omega_i)$

m The total number of the discretized frequencies

Convert (3.22) into the complex form, we have

$$\begin{aligned} v(t) &= \sum_{ii=1}^{m}\frac{A_{a,ii}}{2}\omega_{ii}\frac{\cosh k_{ii}z_p}{\sinh k_{ii}d}\left(e^{\boldsymbol{j}(\omega_i t - k_{ii}x_p + \phi_{ii})} + e^{-\boldsymbol{j}(\omega_i t - k_{ii}x_p + \phi_{ii})}\right) \\ &= \sum_{ii=1}^{m}\frac{A_{a,ii}}{2}\omega_{ii}\frac{\cosh k_{ii}z_p}{\sinh k_{ii}d}e^{-\boldsymbol{j}k_{ii}x_p}e^{\boldsymbol{j}(\omega_i t + \phi_{ii})} \\ &\quad + \sum_{ii=1}^{m}\frac{A_{a,ii}}{2}(-\omega_{ii})\frac{\cosh(-k_{ii}z_p)}{\sinh(-k_{ii}d)}e^{-\boldsymbol{j}(-k_{ii})x_p}e^{\boldsymbol{j}((-\omega_i)t + (-\phi_{ii}))} \end{aligned} \tag{3.23}$$

From the knowledge of ocean waves, we know the surface elevation η at origin (0, d) is

$$\eta = \sum_{ii=1}^{m} A_{a,ii}\cos(\omega_i t + \phi_{ii}) = \sum_{ii=1}^{m}\frac{A_{a,ii}}{2}\mathrm{e}^{\boldsymbol{j}(\omega_i t + \phi_{ii})} + \sum_{ii=1}^{m}\frac{A_{a,ii}}{2}\mathrm{e}^{\boldsymbol{j}(-\omega_i t - \phi_{ii})} \tag{3.24}$$

As observed from equation (3.23) (3.24), the transfer function from the wave elevation to the fluid's velocity component, $H_w(\omega, x, z)$, can be defined for non-zero frequency component, expressed as

$$H_w(\omega, x, z) = \omega\frac{\cosh kz}{\sinh kd}e^{-\boldsymbol{j}k_{ii}x}, \omega \neq 0 \tag{3.25}$$

Then (3.23) can be rewritten as ,

$$v(t) = \sum_{ii=1}^{m} H_w(\omega_{ii}, x_p, z_p) \frac{A_{a,ii}}{2} e^{\boldsymbol{j}(\omega_i t + \phi_{ii})} + \sum_{ii=1}^{m} H_w(-\omega_{ii}, x_p, z_p) \frac{A_{a,ii}}{2} e^{\boldsymbol{j}((-\omega_i)t + (-\phi_{ii}))} \tag{3.26}$$

Hence, for each harmonic component η_{ii} of wave elevation, the corresponding horizontal velocity at pipe's location will be,

$$v_{ii}(t) = V_{ii} e^{\boldsymbol{j}\omega_{ii}t} = H_{w,p}(\omega_{ii}) A_{ii} e^{\boldsymbol{j}\omega_{ii}t} \tag{3.27}$$

Where $H_{w,p}(\omega_{ii}) = H_w(\omega_{ii}, x_p, z_p) \rightarrow$ the transfer function from the wave to the velocity at pipe' s location, $A_{ii} = \frac{A_{a,ii}}{2} e^{\boldsymbol{j}\phi_{ii}}$

$v_{ii}(t)$ is the ii[th] component of total velocity at pipe with amplitude V_{ii} and frequency ω_{ii}, e.g.

$$v(t) = \sum_{ii=0}^{2m} V_{ii} e^{\boldsymbol{j}\omega_{ii}t} = \sum_{ii=0}^{2m} H_{w,p}(\omega_{ii}) A_{ii} e^{\boldsymbol{j}\omega_{ii}t} \tag{3.28}$$

The index of frequencies ω_{ii} have been modified to involve the negative frequencies' component and the current profile. Thus, the total number of frequencies are doubled. The current's velocity can be treated as a harmonic input with a zero-frequency,e.g.

$$u_c(z_p) = V_0 e^{\boldsymbol{j}0t} \tag{3.29}$$

Where $u_c(z)$ is the velocity of current at pipe. Thus, $H_w(\omega, x, z)$ at $\omega = 0$ is defined based on the profile of the current.

$$H_w(0, x, z) = \frac{u_c(z)}{u_c(z = d)} \tag{3.30}$$

$$A_0 = u_c(z = d) \tag{3.31}$$

With the fluid's velocity defined, its corresponding fluid's acceleration can also be defined as,

$$\dot{\mathrm{v}}(\mathrm{t}) = \sum_{ii=0}^{2m} \boldsymbol{j}\omega_{ii} V_{ii} e^{\boldsymbol{j}\omega_{ii}t} = \sum_{ii=0}^{2m} \boldsymbol{j}\omega_{ii} H_{w,p}(\omega_{ii}) A_{ii} e^{\boldsymbol{j}\omega_{ii}t} \tag{3.32}$$

Thus the decoupled SDOF governing equation (3.21) can be rewritten as,

$$m\ddot{r} + c\dot{r} + kr = \alpha_1 \left| \sum_{ii=0}^{2m} V_{ii} e^{\boldsymbol{j}\omega_{ii}t} \right| \left(\sum_{ii=0}^{2m} V_{ii} e^{\boldsymbol{j}\omega_{ii}t} \right) + \alpha_2 \left(\sum_{ii=0}^{2m} \boldsymbol{j}\omega_{ii} V_{ii} e^{\boldsymbol{j}\omega_{ii}t} \right) \tag{3.33}$$

Or

$$\begin{aligned} m\ddot{r} + c\dot{r} + kr = \alpha_1 & \left| \sum_{ii=0}^{2m} H_{w,p}(\omega_{ii}) A_{ii} e^{\boldsymbol{j}\omega_{ii}t} \right| \left(\sum_{ii=0}^{2m} H_{w,p}(\omega_{ii}) A_{ii} e^{\boldsymbol{j}\omega_{ii}t} \right) \\ & + \alpha_2 \left(\sum_{ii=0}^{2m} \boldsymbol{j}\omega_{ii} H_{w,p}(\omega_{ii}) A_{ii} e^{\boldsymbol{j}\omega_{ii}t} \right) \end{aligned} \tag{3.34}$$

Substitute the drag term's approximaton(3.5) into (3.33), the equation (3.33) can be rewritten as

$$m\ddot{r} + c\dot{r} + kr = \alpha_1 \left[p_1 \sum_{ii=0}^{2m} V_{ii} e^{\boldsymbol{j}\omega_{ii}t} + p_3 \left(\sum_{ii=0}^{2m} V_{ii} e^{\boldsymbol{j}\omega_{ii}t} \right)^3 \right] + \alpha_2 \left(\sum_{ii=0}^{2m} \boldsymbol{j}\omega_{ii} V_{ii} e^{\boldsymbol{j}\omega_{ii}t} \right) \tag{3.35}$$

Expand 3rd order term in right hand side of (3.35), we obtain the system, which consists of the linear and cubic excitations,

$$m\ddot{r} + c\dot{r} + kr = \sum_{ii=0}^{2m} (\alpha_1 p_1 + \boldsymbol{j}\omega_{ii}\alpha_2) V_{ii} e^{\boldsymbol{j}\omega_{ii}t} + \alpha_1 p_3 \sum_{ii=0}^{2m} \sum_{jj=0}^{2m} \sum_{kk=0}^{2m} V_{ii} V_{jj} V_{kk} e^{\boldsymbol{j}(\omega_{ii}+\omega_{jj}+\omega_{kk})t} \tag{3.36}$$

The structure is assumed to be linear, thus the dynamic response of the structural follows the principle of the superpoistion. Therefore, the total response $r(t)$ can be treated as superposition of two parts: the resposne component due the linear part of the external force and the response component due the cubic part of the external force.

$$r(t) = r_1(t) + r_2(t) \tag{3.37}$$

Where, $r(t)$ is the total response, $r_1(t)$ is the response due to the linear part of the exitation, $r_2(t)$ is the respone due to the cubic part of the exciation.

The response component $r_1(t)$ is calculated form the linear part of the excitation,

$$r_1(t) = \sum_{ii=0}^{2m} (\alpha_1 p_1 + \boldsymbol{j}\omega_{ii}\alpha_2) H_s(\omega_{ii}) V_{ii} e^{\boldsymbol{j}\omega_{ii}t} \tag{3.38}$$

Or

$$r_1(t) = \sum_{ii=0}^{2m} (\alpha_1 p_1 + \boldsymbol{j}\omega_{ii}\alpha_2) H_s(\omega_{ii}) \left(H_{w,p}(\omega_{ii}) A_{ii} e^{\boldsymbol{j}\omega_{ii}t}\right) \tag{3.39}$$

Where $H_s(\omega_{ii})$ is the structural transfer function of the SDOF system, well known as

$$H_s(\omega_{ii}) = \frac{1}{(k - m{\omega_{ii}}^2) + \boldsymbol{j}\omega_{ii} c} \tag{3.40}$$

For this system, the 1st order transfer function $H_1(\omega_{ii})$ from the wave to the structural responses can be defined as,

$$H_1(\omega_{ii}) = (\alpha_1 p_1 + \boldsymbol{j}\omega_{ii}\alpha_2) H_s(\omega_{ii}) H_{w,p}(\omega_{ii}) \tag{3.41}$$

$$r_1(t) = \sum_{ii=1}^{2m} H_1(\omega_{ii}) A_{ii} e^{\boldsymbol{j}\omega_{ii}t} \tag{3.42}$$

The response component $r_2(t)$ is calculated from the cubic excitations. Each component of the cubic excitation $V_{ii}V_{jj}V_{kk}e^{\boldsymbol{j}(\omega_{ii}+\omega_{jj}+\omega_{kk})t}$ can be treated as a linear excitation with the amplitude of $(V_{ii}V_{jj}V_{kk})$ and the frequency of $(\omega_{ii} + \omega_{jj} + \omega_{kk})$. The relations between the excitation and the response thus can be calculated via the traditional frequency domain knowledge, expressed as

$$r_2(t) = \sum_{ii=0}^{2m} \alpha_1 p_3 H_s(\omega_{ii} + \omega_{jj} + \omega_{kk}) V_{ii}V_{jj}V_{kk} e^{\boldsymbol{j}(\omega_{ii}+\omega_{jj}+\omega_{kk})t} \tag{3.43}$$

Or

$$r_2(t) = \sum_{ii=0}^{2m}\sum_{jj=0}^{2m}\sum_{kk=0}^{2m} \alpha_1 p_3 H_s(\omega_{ii} + \omega_{jj} + \omega_{kk}) H_{w,p}(\omega_{ii}) H_{w,p}\left(\omega_{jj}\right) H_{w,p}(\omega_{kk}) (A_{ii} A_{jj} A_{kk} e^{\boldsymbol{j}(\omega_{ii}+\omega_{jj}+\omega_{kk})t}) \tag{3.44}$$

In (3.44), the relations between the fluids and structural responses are estalished for the cubic excitaton. Here, the 3rd transfer function $H_3(\omega_{ii}, \omega_{jj}, \omega_{kk})$ can be defined as

$$H_3\left(\omega_{ii}, \omega_{jj}, \omega_{kk}\right) = \alpha_1 p_3 H_s\left(\omega_{ii} + \omega_{jj} + \omega_{kk}\right) H_{w,p}(\omega_{ii}) H_{w,p}\left(\omega_{jj}\right) H_{w,p}(\omega_{kk}) \tag{3.45}$$

Thus,

$$r_2(t) = \sum_{ii=0}^{2m}\sum_{jj=0}^{2m}\sum_{kk=0}^{2m} H_3\left(\omega_{ii}, \omega_{jj}, \omega_{kk}\right)\left(A_{ii} A_{jj} A_{kk} e^{\boldsymbol{j}(\omega_{ii}+\omega_{jj}+\omega_{kk})t}\right) \tag{3.46}$$

As observed from (3.46), the arrangement of $\omega_{ii}, \omega_{jj}, \omega_{kk}$ doesn't affect the value of $H_3\left(\omega_{ii}, \omega_{jj}, \omega_{kk}\right)$.

To sum up, the total response $r(t)$ is given as ,

$$\begin{aligned} r(t) &= r_1(t) + r_2(t) \\ &= \sum_{ii=1}^{2m} H_1(\omega_{ii}) A_{ii} e^{\boldsymbol{j}\omega_{ii}t} \\ &\quad + \sum_{ii=0}^{2m}\sum_{jj=0}^{2m}\sum_{kk=0}^{2m} H_3\left(\omega_{ii}, \omega_{jj}, \omega_{kk}\right)(A_{ii} A_{jj} A_{kk} e^{\boldsymbol{j}(\omega_{ii}+\omega_{jj}+\omega_{kk})t}) \end{aligned} \tag{3.47}$$

3.4 The application on MDOF system

In this section, the application of the HFD method is exteneded to the multidegree of system in 3D space. In this application, the effects of the non-linear drag force and the free surface elevation are included in this application.

As introduced in Chapter 2, the 3D decoupled hydro-structural model is presented as follow,

$$\begin{bmatrix} m_{1,1} & 0 & \cdots & 0 & 0 \\ 0 & m_{2,2} & & 0 & 0 \\ \vdots & & \ddots & \vdots & \\ 0 & 0 & & m_{n-1,n-1} & 0 \\ 0 & 0 & \cdots & 0 & m_{n,n} \end{bmatrix} \begin{bmatrix} \ddot{r}_1 \\ \ddot{r}_2 \\ \vdots \\ \ddot{r}_{n-1} \\ \ddot{r}_n \end{bmatrix} + \begin{bmatrix} c_{1,1} & c_{1,2} & \cdots & c_{1,n-1} & c_{1,n} \\ c_{2,1} & c_{2,2} & & c_{2,n-1} & c_{2,n} \\ \vdots & & \ddots & \vdots & \\ c_{n-1,1} & c_{n-1,2} & \cdots & c_{n-1,n-1} & c_{n-1,n} \\ c_{n,1} & c_{n,2} & & c_{n,n-1} & c_{n,n} \end{bmatrix} \begin{bmatrix} \dot{r}_1 \\ \dot{r}_2 \\ \vdots \\ \dot{r}_{n-1} \\ \dot{r}_n \end{bmatrix}$$
$$+ \begin{bmatrix} k_{1,1} & k_{1,2} & \cdots & k_{1,n-1} & k_{1,n} \\ k_{2,1} & k_{2,2} & & k_{2,n-1} & k_{2,n} \\ \vdots & & \ddots & \vdots & \\ k_{n-1,1} & k_{n-1,2} & \cdots & k_{n-1,n-1} & k_{n-1,n} \\ k_{n,1} & k_{n,2} & & k_{n,n-1} & k_{n,n} \end{bmatrix} \begin{bmatrix} r_1 \\ r_2 \\ \vdots \\ r_{n-1} \\ r_n \end{bmatrix} = \begin{bmatrix} f_1 \\ f_2 \\ \vdots \\ f_{n-1} \\ f_n \end{bmatrix} \tag{3.48}$$

Where the relevant symbols have been defined in Chapter 2.

Similar to the SDOF's applcation, the calculaton procedure consists of two steps.

(1) Step I: The calculation of the transfer functions from the fluids to the hydrodynamic forces

(2) Step II: The calculation of the transfer funcitons from the hydrodynamic forces to the strcutural responses.

3.4.1 Step I: The calculation of the transfer functions from the fluids to the hydrodynamic forces

The transfer functions from the fluids to the hydrodynamic forces consist of two parts: the transfer functions of these Morison's forces and the transfer functions of these varying surface induced forces. These calculations will be demonstrated respectively.

To begin with, the fluids properties need to be studied. For a structure in the 3D frame [16], the potential function $\phi_{ii}(x,y,z,t)$ of a harmonic incoming wave $A_{ii}e^{\boldsymbol{j}\omega_{ii}t}$can be expressed as follow,

$$\phi_{ii}(x,y,z,t) = \Phi(\omega_{ii},x,y,z)A_{ii}e^{\boldsymbol{j}\omega_{ii}t} \tag{3.49}$$

Where, including the current profile as the zero-frequency component, expressed as

$$\Phi(\omega,x,y,z) = -\boldsymbol{j}\frac{g}{2\omega}\frac{\cosh kz}{\cosh kd}e^{-\boldsymbol{j}k(xcos\theta_w+ysin\theta_w)}, \qquad \omega \neq 0 \tag{3.50}$$

$$\Phi(0,x,y,z) = (\frac{u_c(z)}{u_c(z=d)}\cos\theta_c\, x + \frac{u_c(z)}{u_c(z=d)}\sin\theta_c\, y), \qquad \omega = 0 \tag{3.51}$$

Where, θ_w is the direction of the incoming wave with respect to the x-coordinate. θ_c is the direction of the current with respect to the x-coordinate. Hence, the velocity at point (x,y,z) is

$$\begin{cases} u_{x,ii} = \dfrac{\partial\phi_{ii}}{\partial x} = \dfrac{\partial\Phi}{\partial x}(\omega_{ii})A_{ii}e^{\boldsymbol{j}\omega_{ii}t} \\ u_{y,ii} = \dfrac{\partial\phi_{ii}}{\partial y} = \dfrac{\partial\Phi}{\partial x}(\omega_{ii})A_{ii}e^{\boldsymbol{j}\omega_{ii}t} \\ u_{z,ii} = \dfrac{\partial\phi_{ii}}{\partial z} == \dfrac{\partial\Phi}{\partial z}(\omega_{ii})A_{ii}e^{\boldsymbol{j}\omega_{ii}t} \end{cases} \tag{3.52}$$

Combining the velocity at each frequency, the total velocity in 3D frame can be expressed as,

$$\begin{cases} u_x = \sum_{ii=0}^{2m} \frac{\partial \phi_{ii}}{\partial x} = \sum_{ii=0}^{2m} \frac{\partial \Phi}{\partial x}(\omega_{ii}) A_{ii} e^{j\omega_{ii}t}, \\ u_y = \sum_{ii=0}^{2m} \frac{\partial \phi_{ii}}{\partial y} = \sum_{ii=0}^{2m} \frac{\partial \Phi}{\partial y}(\omega_{ii}) A_{ii} e^{j\omega_{ii}t}, \\ u_z = \sum_{ii=0}^{2m} \frac{\partial \phi_{ii}}{\partial z} = \sum_{ii=0}^{2m} \frac{\partial \Phi}{\partial z}(\omega_{ii}) A_{ii} e^{j\omega_{ii}t} \end{cases} \tag{3.53}$$

With the velocity being defined, the 3D Morison's force in frequency-domain needs to be determined. As presented in figure 3.4, for a structural beam member with segment ($dx\boldsymbol{i} + dy\boldsymbol{j} + dz\boldsymbol{k}$), its normal direction $\boldsymbol{n}_s$ is

$$\boldsymbol{n}_s = \frac{dx\boldsymbol{i} + dy\boldsymbol{j} + dz\boldsymbol{k}}{ds} \tag{3.54}$$

Where

$$d\boldsymbol{s} = (dx\ dy, dz)$$

$$ds = \sqrt{dx^2 + dy^2 + dz^2}$$

$$\boldsymbol{v} = (u_x\ u_y, u_z) \tag{3.55}$$

The velocity component $\boldsymbol{v}_t$ in tangential direction is expressed as follow,

$$\boldsymbol{v_t} = \frac{\boldsymbol{v} * \boldsymbol{ds}}{ds^2}(dx\boldsymbol{i} + dy\boldsymbol{j} + dz\boldsymbol{k}) = \frac{u_x dx + u_y dy + u_z dz}{ds^2}(dx\boldsymbol{i} + dy\boldsymbol{j} + dz\boldsymbol{k}) \tag{3.56}$$

Thus, the velocity component v_n in normal direction is

$$\boldsymbol{v_n} = \boldsymbol{v} - \boldsymbol{v_t} \tag{3.57}$$

Substitute (3.50), (3.51) into (3.52), we have

$$\begin{aligned} \boldsymbol{v_n} &= u_x\boldsymbol{i} + u_y\boldsymbol{j} + u_z\boldsymbol{k} - \frac{u_x dx + u_y dy + u_z dz}{ds^2}(dx\boldsymbol{i} + dy\boldsymbol{j} + dz\boldsymbol{k}) \\ &= \left(u_x - \frac{u_x dx + u_y dy + u_z dz}{ds^2} dx\right)\boldsymbol{i} + \left(u_y - \frac{u_x dx + u_y dy + u_z dz}{ds^2} dy\right)\boldsymbol{j} \\ &+ \left(u_z - \frac{u_x dx + u_y dy + u_z dz}{ds^2} dz\right)\boldsymbol{k} \end{aligned} \tag{3.58}$$

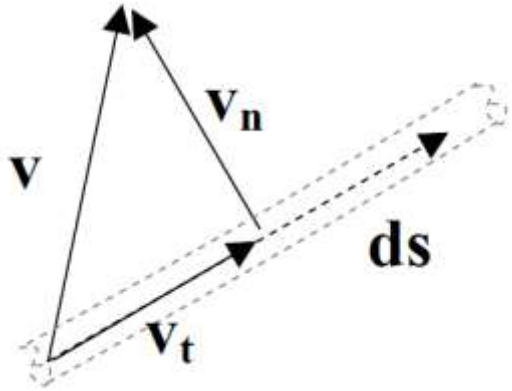

Figure 3.4 a graphical representation of the water particle velocity normal to the slender element

Substitute (3.52) into (3.58), we have

$$\boldsymbol{v_n(t)} = \sum_{\boldsymbol{ii=0}}^{\boldsymbol{2m}} \left(\left(\frac{\partial \Phi}{\partial x}(\omega_{ii}) - \frac{\frac{\partial \Phi}{\partial x}(\omega_{ii})dx + \frac{\partial \Phi}{\partial x}(\omega_{ii})dy + \frac{\partial \Phi}{\partial x}(\omega_{ii})dz}{ds^2} dx \right) \boldsymbol{i} + \left(\frac{\partial \Phi}{\partial y}(\omega_{ii}) - \frac{\frac{\partial \Phi}{\partial x}(\omega_{ii})dx + \frac{\partial \Phi}{\partial x}(\omega_{ii})dy + \frac{\partial \Phi}{\partial x}(\omega_{ii})dz}{ds^2} dy \right) \boldsymbol{j} + \left(\frac{\partial \Phi}{\partial z}(\omega_{ii}) - \frac{\frac{\partial \Phi}{\partial x}(\omega_{ii})dx + \frac{\partial \Phi}{\partial x}(\omega_{ii})dy + \frac{\partial \Phi}{\partial x}(\omega_{ii})dz}{ds^2} dz \right) \boldsymbol{k} \right) A_{ii} e^{j\omega_{ii}t} \tag{3.59}$$

Rewritten (3.59) via the transfer function from the fluids into velocities, we have

$$\boldsymbol{v_n(t)} = \sum_{\boldsymbol{ii=0}}^{\boldsymbol{2m}} \left(H_{v_n,x}(\omega_{ii})\boldsymbol{i} + H_{v_n,y}(\omega_{ii})\boldsymbol{j} + H_{v_n,z}(\omega_{ii})\boldsymbol{k} \right) A_{ii} e^{j\omega_{ii}t} \tag{3.60}$$

Where, the transfer functions are defined as

$$H_{v_n,x}(\omega_{ii}) = \frac{\partial \Phi}{\partial x}(\omega_{ii}) - \frac{\frac{\partial \Phi}{\partial x}(\omega_{ii})dx + \frac{\partial \Phi}{\partial x}(\omega_{ii})dy + \frac{\partial \Phi}{\partial x}(\omega_{ii})dz}{ds^2} dx$$

$$H_{v_n,y}(\omega_{ii}) = \frac{\partial \Phi}{\partial y}(\omega_{ii}) - \frac{\frac{\partial \Phi}{\partial x}(\omega_{ii})dx + \frac{\partial \Phi}{\partial x}(\omega_{ii})dy + \frac{\partial \Phi}{\partial x}(\omega_{ii})dz}{ds^2} dy$$

$$H_{v_n,z}(\omega_{ii}) = \frac{\partial \Phi}{\partial z}(\omega_{ii}) - \frac{\frac{\partial \Phi}{\partial x}(\omega_{ii})dx + \frac{\partial \Phi}{\partial x}(\omega_{ii})dy + \frac{\partial \Phi}{\partial x}(\omega_{ii})dz}{ds^2} dz \tag{3.61}$$

As the normal velocity being defined, the cubic approximation of the Morison's force can be rewritten as

$$\begin{aligned}\boldsymbol{f_s} &= \alpha_{1,s}|\boldsymbol{v_n}|\boldsymbol{v_n} + \alpha_{2,s}\dot{\boldsymbol{v}}_{\boldsymbol{n}} \approx \alpha_{1,s}p_3(\boldsymbol{v_n}\cdot\boldsymbol{v_n})\cdot\boldsymbol{v_n} + \left(\alpha_{1,s}p_1 + j\omega_{ii}\alpha_{2,s}\right)\dot{\boldsymbol{v}}_{\boldsymbol{n}} \\ &\approx \alpha_{1,s}p_3\sum_{ii=0}^{2m}\sum_{jj=0}^{2m}\Big(H_{v_n,x}(\omega_{ii})H_{v_n,x}(\omega_{jj}) + H_{v_n,y}(\omega_{ii})H_{v_n,y}(\omega_{jj}) \\ &+ H_{v_n,z}(\omega_{ii})H_{v_n,z}(\omega_{jj})\Big)A_{ii}A_{jj}e^{\boldsymbol{j}(\omega_{ii}+\omega_{jj})t})\sum_{\boldsymbol{ii=0}}^{\boldsymbol{2m}}\big(H_{v_n,x}(\omega_{kk})\boldsymbol{i} + H_{v_n,y}(\omega_{kk})\boldsymbol{j} \\ &+ H_{v_n,z}(\omega_{kk})\boldsymbol{k}\big)A_{kk}e^{j\omega_{kk}t} \\ &+ \sum_{\boldsymbol{ii=0}}^{\boldsymbol{2m}}\big(\alpha_{1,s}p_1 + j\omega_{ii}\alpha_{2,s}\big)\big(H_{v_n,x}(\omega_{ii})\boldsymbol{i} + H_{v_n,y}(\omega_{ii})\boldsymbol{j} + H_{v_n,z}(\omega_{ii})\boldsymbol{k}\big)A_{ii}e^{j\omega_{ii}t}\end{aligned}$$

(3.62)

Or in the form of the components in each direction,

$$\begin{aligned}\boldsymbol{f_{s,x}} &= \alpha_{1,s}p_3\sum_{ii=0}^{2m}\sum_{jj=0}^{2m}H_{v_n}(\omega_{ii},\omega_{jj})A_{ii}A_{jj}e^{\boldsymbol{j}(\omega_{ii}+\omega_{jj})t}\sum_{kk=0}^{2m}H_{v_n,x}(\omega_{kk})A_{kk}e^{j\omega_{kk}t} \\ &+ \sum_{ii=0}^{2m}\big(\alpha_{1,s}p_1 + \boldsymbol{j}\omega_{ii}\alpha_{2,s}\big)H_{v_n,x}(\omega_{ii})\,A_{ii}e^{j\omega_{ii}t} \\ \boldsymbol{f_{s,y}} &= \alpha_{1,s}p_3\sum_{ii=0}^{2m}\sum_{jj=0}^{2m}H_{v_n}(\omega_{ii},\omega_{jj})A_{ii}A_{jj}e^{\boldsymbol{j}(\omega_{ii}+\omega_{jj})t}\sum_{kk=0}^{2m}H_{v_n,y}(\omega_{kk})A_{kk}e^{j\omega_{kk}t} \\ &+ \sum_{ii=0}^{2m}\big(\alpha_{1,s}p_1 + \boldsymbol{j}\omega_{ii}\alpha_{2,s}\big)H_{v_n,y}(\omega_{ii})\,A_{ii}e^{j\omega_{ii}t} \\ \boldsymbol{f_{s,z}} &= \alpha_{1,s}p_3\sum_{ii=0}^{2m}\sum_{jj=0}^{2m}H_{v_n}(\omega_{ii},\omega_{jj})A_{ii}A_{jj}e^{\boldsymbol{j}(\omega_{ii}+\omega_{jj})t}\sum_{kk=0}^{2m}H_{v_n,z}(\omega_{kk})A_{kk}e^{j\omega_{kk}t} \\ &+ \sum_{ii=0}^{2m}\big(\alpha_{1,s}p_1 + \boldsymbol{j}\omega_{ii}\alpha_{2,s}\big)H_{v_n,z}(\omega_{ii})\,A_{ii}e^{j\omega_{ii}t}\end{aligned}$$

(3.63)

Where, $H_{v_n}(\omega_{ii}, \omega_{jj})$ is defined as,

$$H_{v_n}(\omega_{ii}, \omega_{jj}) = H_{v_n,x}(\omega_{ii})H_{v_n,x}(\omega_{jj}) + H_{v_n,y}(\omega_{ii})H_{v_n,y}(\omega_{jj}) + H_{v_n,z}(\omega_{ii})H_{v_n,z}(\omega_{jj})$$

(3.64)

Substitute equation (3.63) into the decoupled hydro-structural model, we have the components of the external force vector.

$$\begin{aligned} f_{s,i} = \alpha_{1,i}p_3 \sum_{ii=0}^{2m}\sum_{jj=0}^{2m} H_{v_n,i}(\omega_{ii}, \omega_{jj})A_{ii}A_{jj}e^{j(\omega_{ii}+\omega_{jj})t} \sum_{kk=0}^{2m} H_{v_n,i}(\omega_{kk})A_{kk}e^{j\omega_{kk}t} \\ + \sum_{ii=0}^{2m}(\alpha_{1,i}p_1 + \boldsymbol{j}\omega_{ii}\alpha_{2,i})H_{v_n,i}(\omega_{ii})\,A_{ii}e^{j\omega_{ii}t} \\ = \alpha_{1,i}p_3 \sum_{ii=0}^{2m}\sum_{jj=0}^{2m}\sum_{kk=0}^{2m} H_{v_n,i}(\omega_{ii}, \omega_{jj})H_{v_n,i}(\omega_{kk})A_{ii}A_{jj}e^{j(\omega_{ii}+\omega_{jj})t}A_{kk}e^{j\omega_{kk}t} \\ + \sum_{ii=0}^{2m}(\alpha_{1,i}p_1 + \boldsymbol{j}\omega_{ii}\alpha_{2,i})H_{v_n,i}(\omega_{ii})\,A_{ii}e^{j\omega_{ii}t} \end{aligned}$$

(3.65)

In addition of the Morison's equation, the equivalent concentrated force of the varying free surface correction for the 1st order stochastic wave are calculated as

$$F_{ei_{i_0}} = \sum_{ii=0}^{2m}(\alpha_{1,i_0}p_1 + j\omega_{ii}\alpha_{2,i_0})H_{v_n,i_0}(\omega_{ii})\,A_{ii}e^{j\omega_{ii}t}\frac{1}{p_{z_{i_0}}}\eta_{i_0}$$

(3.66)

Where $\boldsymbol{i_0}$ refer to the nodes which is located at mean water level,

$p_{z_{i_0}}$ is the projection coefficient, the η_{i_0} is the surface elevation at node i_0, where $\boldsymbol{\eta_{i_0}}$ can be expressed as,

$$\eta = \sum_{ii=1}^{m} A_{a,ii}\cos(\omega_{ii}t + \phi_{ii} - k_{ii}(x_0 cos\theta_w + y_0 sin\theta_w)) = \sum_{ii=0}^{2m} H_{\eta_{i_0}}(x_0, y_0, \omega_{ii})A_{ii}e^{j\omega_{ii}t}$$

(3.67)

Where x_0, y_0 refers to the coordinate of the node i_0, where the location transfer function $H_{\eta_{i_0}}(x_0, y_0, \omega_{ii})$ is defined as

$$H_{\eta_{i_0}}(x_0, y_0, \omega_{ii}) = e^{-\boldsymbol{j}k_{ii}(xcos\theta_w + ysin\theta_w)}, \qquad for\ \omega_{ii} \neq 0 \tag{3.68}$$

$$H_{\eta_{i_0}}(x_0, y_0, \omega_{ii}) = 0, \qquad for\ \omega_{ii} = 0 \tag{3.69}$$

To, sum up, the $F_{ei_{i_0}}$ at node i_0 can be expressed as,

$$\begin{aligned} F_{ei_{i_0}} &= \sum_{ii=0}^{2m} \left(\alpha_{1,i_0} p_1 + j\omega_{ii}\alpha_{2,i_0}\right) H_{v_n,i_0}(\omega_{ii})\, A_{ii} e^{j\omega_{ii}t} \frac{1}{p_{z_{i_0}}} \sum_{ii=0}^{2m} H_{\eta_{i_0}}(x_0, y_0, \omega_{ii}) A_{ii} e^{j\omega_{ii}t} \\ &= \sum_{ii=0}^{2m}\sum_{ii=0}^{2m} \left(\alpha_{1,i_0} p_1 \right. \\ &\quad \left. + j\omega_{ii}\alpha_{2,i_0}\right) H_{v_n,i_0}(\omega_{ii}) H_{\eta_{i_0}}\left(x_0, y_0, \omega_{jj}\right) \frac{1}{p_{z_{i_0}}} A_{ii} e^{j\omega_{ii}t} A_{jj} e^{j\omega_{jj}t} \end{aligned} \tag{3.70}$$

Till now, the transfer functions from the fluids to the hydrodynamic forces have been well defined.

3.4.2 Step II: The calculation of the transfer funcitons from the hydrodynamic forces to the strcutural responses

Similarly to the SDOF system, now the structural response of the MDOF system can be divided into three parts: the responses due to the linear excitation, the responses due to the quadratic excitation and the responses due to the cubic excitation.

$$\boldsymbol{R}(t) = \boldsymbol{R}^{(1)}(t) + \boldsymbol{R}^{(2)}(t) + \boldsymbol{R}^{(3)}(t) \tag{3.71}$$

Where,

The term $\boldsymbol{R}^{(1)}$ refers to the structural responses due to the linear excitations. These linear excitations are mainly contributed by the inertia forces and the linear part of the drag force's cubic approximations.

The term $\boldsymbol{R}^{(2)}$ refers to the structural responses due to the quadratic excitations. These quadratic excitations are mainly contributed by the quadratic approximation of varying surface-induced forces.

The term $\boldsymbol{R}^{(3)}$ refers to the structural responses due to the cubic excitations. Those cubic excitations are mainly contributed by the cubic part of the drag force's cubic approximations.
In the remaining part of this section, the calculation of the structural responses $R_1 \; and \; R_3$ will be presented first. Then the calculation of R_2 is provided.

For the structural responses due to the linear excitations $\boldsymbol{R}^{(1)}$,

$$M\ddot{\boldsymbol{R}}^{(1)} + C\dot{\boldsymbol{R}}^{(1)} + K\boldsymbol{R}^{(1)} = \boldsymbol{F}^{(1)} = \sum_{ii=0}^{2m} \begin{bmatrix} H_{v_n,1}(\omega_{ii})\left[\alpha_{1,1}p_1 + \boldsymbol{j}\omega_{ii}\alpha_{2,1}\right] \\ H_{v_n,2}(\omega_{ii})\left[\alpha_{1,2}p_1 + \boldsymbol{j}\omega_{ii}\alpha_{2,2}\right] \\ \vdots \\ H_{v_n,n}(\omega_{ii})\left[\alpha_{1,n}p_1 + \boldsymbol{j}\omega_{ii}\alpha_{2,n}\right] \end{bmatrix} A_{ii}\, e^{\boldsymbol{j}\omega_{ii}t}$$

(3.72)

For the structural responses due to the cubic excitations $\boldsymbol{R}^{(3)}$,

$$M\ddot{\boldsymbol{R}}^{(3)} + C\dot{\boldsymbol{R}}^{(3)} + K\boldsymbol{R}^{(3)} = \boldsymbol{F}^{(3)}$$
$$= \sum_{ii=0}^{2m}\sum_{jj=0}^{2m}\sum_{kk=0}^{2m} \begin{bmatrix} H_{v_n,1}(\omega_{ii},\omega_{jj})H_{v_n,1}(\omega_{kk})\left[\alpha_{1,1}p_3\right] \\ H_{v_n2}(\omega_{ii},\omega_{jj})H_{v_n,2}(\omega_{kk})\left[\alpha_{1,2}p_3\right] \\ \vdots \\ H_{v_nn}(\omega_{ii},\omega_{jj})H_{v_n,n}(\omega_{kk})\left[\alpha_{1,n}p_3\right] \end{bmatrix} A_{ii}A_{jj}A_{kk}e^{\boldsymbol{j}(\omega_{ii}+\omega_{jj}+\omega_{kk})t}$$

(3.73)

The left hand side of those equations represents the linear structure. It is well known that, the structural responses of the linear structure follow the principle of superposition. For the structural responses due to the linear excitations $\boldsymbol{R}^{(1)}$ with frequency ω_{ii}, we have

$$M\ddot{\boldsymbol{R}}^{(1)} + C\dot{\boldsymbol{R}}^{(1)} + K\boldsymbol{R}^{(1)} = (-M{\omega_{ii}}^2 + \boldsymbol{j}\omega_{ii}C + K)\begin{bmatrix} {R^{(1)}}_{1,ii} \\ {R^{(1)}}_{2,ii} \\ \vdots \\ {R^{(1)}}_{n-1,ii} \\ {R^{(1)}}_{n,ii} \end{bmatrix} e^{\boldsymbol{j}\omega_{ii}t}$$

(3.74)

Where the term ${R^{(1)}}_{n-1,ii}$ represents the amplitude of the displacement r_i under the excitation's frequency ω_{ii}.

$\mathrm{S}(\omega_{ii})$ is denoted as

$$-M{\omega_{ii}}^2 + \boldsymbol{j}\omega_{ii}C + K = \mathrm{S}(\omega_{ii})$$

(3.75)

Thus, for each excitation's frequency ω_{ii}, the structural responses due to the linear excitations R_1 can be rewritten as,

$$\mathrm{S}(\omega_{ii})\begin{bmatrix} {R^{(1)}}_{1,ii} \\ {R^{(1)}}_{2,ii} \\ \vdots \\ {R^{(1)}}_{n-1,ii} \\ {R^{(1)}}_{n,ii} \end{bmatrix} e^{\boldsymbol{j}\omega_{ii}t} = \begin{bmatrix} H_{v_n,1}(\omega_{ii},\omega_{jj})H_{v_n,1}(\omega_{kk})[\alpha_{1,1}p_1 + \boldsymbol{j}\omega_{ii}\alpha_{2,1}] \\ H_{v_n2}(\omega_{ii},\omega_{jj})H_{v_n,2}(\omega_{kk})[\alpha_{1,1}p_1 + \boldsymbol{j}\omega_{ii}\alpha_{2,1}] \\ \vdots \\ H_{v_nn}(\omega_{ii},\omega_{jj})H_{v_n,n}(\omega_{kk})[\alpha_{1,1}p_1 + \boldsymbol{j}\omega_{ii}\alpha_{2,1}] \end{bmatrix} A_{ii}\, e^{\boldsymbol{j}\omega_{ii}t}$$

(3.76)

Hence, the explicit form of the $\boldsymbol{R}^{(1)}$ can be obtained,

$$\begin{bmatrix} {R^{(1)}}_{1,ii} \\ {R^{(1)}}_{2,ii} \\ \vdots \\ {R^{(1)}}_{n-1,ii} \\ {R^{(1)}}_{n,ii} \end{bmatrix} = \mathrm{S}^{-1}(\omega_{ii}) \begin{bmatrix} H_{v_n,1}(\omega_{ii},\omega_{jj})H_{v_n,1}(\omega_{kk})[\alpha_{1,1}p_1 + \boldsymbol{j}\omega_{ii}\alpha_{2,1}] \\ H_{v_n2}(\omega_{ii},\omega_{jj})H_{v_n,2}(\omega_{kk})[\alpha_{1,1}p_1 + \boldsymbol{j}\omega_{ii}\alpha_{2,1}] \\ \vdots \\ H_{v_nn}(\omega_{ii},\omega_{jj})H_{v_n,n}(\omega_{kk})[\alpha_{1,1}p_1 + \boldsymbol{j}\omega_{ii}\alpha_{2,1}] \end{bmatrix} A_{ii}$$

(3.77)

To sum up, the 1st order transfer function $H_{1,i}(\omega_{ii})$ from the fluids to the structural responses for each displacement i can be defined as

$$\begin{bmatrix} H_{1,1}(\omega_{ii}) \\ H_{1,2}(\omega_{ii}) \\ \vdots \\ H_{1,n}(\omega_{ii}) \end{bmatrix} = \mathrm{S}^{-1}(\omega_{ii}) \begin{bmatrix} H_{v_n,1}(\omega_{ii},\omega_{jj})H_{v_n,1}(\omega_{kk})[\alpha_{1,1}p_1 + \boldsymbol{j}\omega_{ii}\alpha_{2,1}] \\ H_{v_n2}(\omega_{ii},\omega_{jj})H_{v_n,2}(\omega_{kk})[\alpha_{1,1}p_1 + \boldsymbol{j}\omega_{ii}\alpha_{2,1}] \\ \vdots \\ H_{v_nn}(\omega_{ii},\omega_{jj})H_{v_n,n}(\omega_{kk})[\alpha_{1,1}p_1 + \boldsymbol{j}\omega_{ii}\alpha_{2,1}] \end{bmatrix}$$

(3.78)

For the structural responses due to the cubic excitations $\boldsymbol{R}^{(3)}$, for each frequency combination$\omega_{ii}, \omega_{jj}, \omega_{kk}$,

$$\begin{aligned} \mathrm{S}(\omega_{ii} + \omega_{jj} + \omega_{kk}) &\begin{bmatrix} {R^{(3)}}_{1,ii,jj,kk} \\ {R^{(3)}}_{2,ii,jj,kk} \\ \vdots \\ {R^{(3)}}_{n,ii,jj,kk} \\ {R^{(3)}}_{n-1,ii,jj,kk} \end{bmatrix} e^{\boldsymbol{j}(\omega_{ii}+\omega_{jj}+\omega_{kk})t} \\ &= \begin{bmatrix} H_{v_n,1}(\omega_{ii},\omega_{jj})H_{v_n,1}(\omega_{kk})[\alpha_{1,1}p_3] \\ H_{v_n2}(\omega_{ii},\omega_{jj})H_{v_n,2}(\omega_{kk})[\alpha_{1,2}p_3] \\ \vdots \\ H_{v_nn}(\omega_{ii},\omega_{jj})H_{v_n,n}(\omega_{kk})[\alpha_{1,s}p_3] \end{bmatrix} A_{ii}\, A_{jj} A_{kk} e^{\boldsymbol{j}(\omega_{ii}+\omega_{jj}+\omega_{kk})t} \end{aligned}$$

(3.79)

Hence, the explicit form of the $\boldsymbol{R}^{(3)}$ can be obtained,

$$\begin{bmatrix} R^{(3)}{}_{1,ii,jj,kk} \\ R^{(3)}{}_{2,ii,jj,kk} \\ \vdots \\ R^{(3)}{}_{n,ii,jj,kk} \\ R^{(3)}{}_{n-1,ii,jj,kk} \end{bmatrix} = \mathrm{S}^{-1}(\omega_{ii}+\omega_{jj}+\omega_{kk}) \begin{bmatrix} H_{v_n,1}(\omega_{ii},\omega_{jj})H_{v_n,1}(\omega_{kk})[\alpha_{1,1}p_3] \\ H_{v_n2}(\omega_{ii},\omega_{jj})H_{v_n,2}(\omega_{kk})[\alpha_{1,2}p_3] \\ \vdots \\ H_{v_nn}(\omega_{ii},\omega_{jj})H_{v_n,n}(\omega_{kk})[\alpha_{1,s}p_3] \end{bmatrix} A_{ii}\, A_{jj} A_{kk}$$

(3.80)

To sum up, the 3rd order transfer function $H_{3,i}(\omega_{ii},\omega_{jj},\omega_{kk})$ from the fluids to the structural responses for each displacement i can be defined as

$$\begin{bmatrix} H_{3,1}(\omega_{ii},\omega_{jj},\omega_{kk}) \\ H_{3,2}(\omega_{ii},\omega_{jj},\omega_{kk}) \\ \vdots \\ H_{3,n}(\omega_{ii},\omega_{jj},\omega_{kk}) \end{bmatrix} = \mathrm{S}^{-1}(\omega_{ii}+\omega_{jj}+\omega_{kk}) \begin{bmatrix} H_{v_n,1}(\omega_{ii},\omega_{jj})H_{v_n,1}(\omega_{kk})[\alpha_{1,1}p_3] \\ H_{v_n2}(\omega_{ii},\omega_{jj})H_{v_n,2}(\omega_{kk})[\alpha_{1,2}p_3] \\ \vdots \\ H_{v_nn}(\omega_{ii},\omega_{jj})H_{v_n,n}(\omega_{kk})[\alpha_{1,s}p_3] \end{bmatrix}$$

(3.81)

Modal analysis techniques can be applied to improve the computing efficiency of $\mathrm{S}^{-1}(\omega)$. Denote the eigenvectors $[\Phi]$ and corresponding eigenvalues $[\lambda^2]$, we have

$$[\boldsymbol{\Phi}]^{\boldsymbol{T}}[\boldsymbol{M}][\boldsymbol{\Phi}] = [\boldsymbol{I}]$$

$$[\boldsymbol{\Phi}]^{\boldsymbol{T}}[\boldsymbol{K}][\boldsymbol{\Phi}] = [\boldsymbol{\lambda^2}]$$

$$[\mathbf{R}] = [\boldsymbol{\Phi}][\boldsymbol{R}^*]$$

(3.82)

Where $[\boldsymbol{R}^*]$ are the response in the model coordinate.

The damping matrix $[\boldsymbol{C}]$ is assumed to be Rayleigh damping, the damping term thus can be treated as additional part of mass and stiffness matrix.

$$[\boldsymbol{C}] = \beta_1[\boldsymbol{M}] + \beta_2[\boldsymbol{K}]$$

(3.83)

Thus, the model for the responses due to the linear excitations $\boldsymbol{R}^{(1)}$, can be rewritten as

$$[\Phi]^{\mathrm{T}}\left[-\omega^2(1+\beta_1)[\mathrm{M}]+(1+\beta_2)[\mathrm{K}]\right][\Phi]\begin{bmatrix} {R^{(1)^*}}_{1,ii} \\ {R^{(1)^*}}_{2,ii} \\ \vdots \\ {R^{(1)^*}}_{n-1,ii} \\ {R^{(1)^*}}_{n,ii} \end{bmatrix} = [\Phi]^{\mathrm{T}}\begin{bmatrix} H_{v_n,1}(\omega_{ii})\left[\alpha_{1,1}p_1+\boldsymbol{j}\omega_{ii}\alpha_{2,1}\right] \\ H_{v_n,2}(\omega_{ii})\left[\alpha_{1,2}p_1+\boldsymbol{j}\omega_{ii}\alpha_{2,2}\right] \\ \vdots \\ H_{v_n,n}(\omega_{ii})\left[\alpha_{1,n}p_1+\boldsymbol{j}\omega_{ii}\alpha_{2,n}\right] \end{bmatrix} A_{ii}$$

(3.84)

$$\left[-\omega^2(1+\beta_1)[\mathrm{I}]+(1+\beta_2)[\lambda^2]\right]\begin{bmatrix} {R^{(1)^*}}_{1,ii} \\ {R^{(1)^*}}_{2,ii} \\ \vdots \\ {R^{(1)^*}}_{n-1,ii} \\ {R^{(1)^*}}_{n,ii} \end{bmatrix} = [\Phi]^{\mathrm{T}}\begin{bmatrix} H_{v_n,1}(\omega_{ii})\left[\alpha_{1,1}p_1+\boldsymbol{j}\omega_{ii}\alpha_{2,1}\right] \\ H_{v_n,2}(\omega_{ii})\left[\alpha_{1,2}p_1+\boldsymbol{j}\omega_{ii}\alpha_{2,2}\right] \\ \vdots \\ H_{v_n,n}(\omega_{ii})\left[\alpha_{1,n}p_1+\boldsymbol{j}\omega_{ii}\alpha_{2,n}\right] \end{bmatrix} A_{ii}$$

(3.85)

Hence, the explicit form of the $\boldsymbol{R}^{(1)^*}$ can be obtained,

$$\begin{bmatrix} R_{1,ii} \\ R_{2,ii} \\ \vdots \\ R_{n-1,ii} \\ R_{n,ii} \end{bmatrix} = [\Phi]\left[-\omega^2\left(1+\beta_1\right)[\mathrm{I}]+\left(1+\beta_2\right)\left[\lambda^2\right]\right]^{-1}[\Phi]^{\mathrm{T}}\begin{bmatrix} H_{v_n,1}(\omega_{ii})\left[\alpha_{1,1}p_1+\boldsymbol{j}\omega_{ii}\alpha_{2,1}\right] \\ H_{v_n,2}(\omega_{ii})\left[\alpha_{1,2}p_1+\boldsymbol{j}\omega_{ii}\alpha_{2,2}\right] \\ \vdots \\ H_{v_n,n}(\omega_{ii})\left[\alpha_{1,n}p_1+\boldsymbol{j}\omega_{ii}\alpha_{2,n}\right] \end{bmatrix} A_{ii}$$

(3.86)

In expanded form,

$$\begin{bmatrix} {R^*}_{1,ii} \\ {R^*}_{2,ii} \\ \vdots \\ {R^*}_{n-1,ii} \\ {R^*}_{n,ii} \end{bmatrix} = [\Phi]\begin{bmatrix} \frac{1}{-\omega^2(1+\beta_1)+(1+\beta_2){\lambda_1}^2} & 0 & 0 & 0 \\ 0 & \frac{1}{-\omega^2(1+\beta_1)+(1+\beta_2){\lambda_2}^2} & 0 & 0 \\ 0 & 0 & \ddots & 0 \\ 0 & 0 & 0 & \frac{1}{-\omega^2(1+\beta_1)+(1+\beta_2){\lambda_n}^2} \end{bmatrix}[\Phi]^{\mathrm{T}}\begin{bmatrix} H_{v_n,1}(\omega_{ii})\left[\alpha_{1,1}p_1+\boldsymbol{j}\omega_{ii}\alpha_{2,1}\right] \\ H_{v_n,2}(\omega_{ii})\left[\alpha_{1,2}p_1+\boldsymbol{j}\omega_{ii}\alpha_{2,2}\right] \\ \vdots \\ H_{v_n,n}(\omega_{ii})\left[\alpha_{1,n}p_1+\boldsymbol{j}\omega_{ii}\alpha_{2,n}\right] \end{bmatrix} A_{ii}$$

(3.87)

Thus the 1st order frequency response function can be rewritten as

$$\begin{bmatrix} H_{1,1}(\omega_{ii}) \\ H_{1,2}(\omega_{ii}) \\ \vdots \\ H_{1,n}(\omega_{ii}) \end{bmatrix} = [\Phi] \begin{bmatrix} \frac{1}{-\omega^2(1+\beta_1)+(1+\beta_2)\lambda_1{}^2} & 0 & 0 & 0 \\ 0 & \frac{1}{-\omega^2(1+\beta_1)+(1+\beta_2)\lambda_2{}^2} & 0 & 0 \\ 0 & 0 & \ddots & 0 \\ 0 & 0 & 0 & \frac{1}{-\omega^2(1+\beta_1)+(1+\beta_2)\lambda_n{}^2} \end{bmatrix} [\Phi]^{\mathrm{T}} \begin{bmatrix} H_{v_n,1}(\omega_{ii})[\alpha_{1,1}p_1 + \boldsymbol{j}\omega_{ii}\alpha_{2,1}] \\ H_{v_n,2}(\omega_{ii})[\alpha_{1,2}p_1 + \boldsymbol{j}\omega_{ii}\alpha_{2,2}] \\ \vdots \\ H_{v_n,n}(\omega_{ii})[\alpha_{1,n}p_1 + \boldsymbol{j}\omega_{ii}\alpha_{2,n}] \end{bmatrix}$$

(3.88)

Similarly, the 3rd order frequency response function can be rewritten as

$$\begin{bmatrix} H_{3,1}(\omega_{ii},\omega_{jj},\omega_{kk}) \\ H_{3,2}(\omega_{ii},\omega_{jj},\omega_{kk}) \\ \vdots \\ H_{3,n}(\omega_{ii},\omega_{jj},\omega_{kk}) \end{bmatrix} = [\Phi] \begin{bmatrix} \frac{1}{-(\omega_{ii}+\omega_{jj}+\omega_{kk})^2(1+\beta_1)+(1+\beta_2)\lambda_1{}^2} & 0 & 0 & 0 \\ 0 & \frac{1}{-(\omega_{ii}+\omega_{jj}+\omega_{kk})^2(1+\beta_1)+(1+\beta_2)\lambda_2{}^2} & 0 & 0 \\ 0 & 0 & \ddots & 0 \\ 0 & 0 & 0 & \frac{1}{-(\omega_{ii}+\omega_{jj}+\omega_{kk})^2(1+\beta_1)+(1+\beta_2)\lambda_n{}^2} \end{bmatrix} [\Phi]^{\mathrm{T}} \begin{bmatrix} H_{v_n,1}(\omega_{ii},\omega_{jj})H_{v_n,1}(\omega_{kk})[\alpha_{1,1}p_3] \\ H_{v_n2}(\omega_{ii},\omega_{jj})H_{v_n,2}(\omega_{kk})[\alpha_{1,2}p_3] \\ \vdots \\ H_{v_n n}(\omega_{ii},\omega_{jj})H_{v_n,n}(\omega_{kk})[\alpha_{1,s}p_3] \end{bmatrix}$$

(3.89)

To now, the 1st order and 3rd order transfer function are obtained.

For the 2nd transfer function, the nodes at the mean water level need to be identified before the calculation. This identification process can be represented an operator (i) ,

$$\delta(i) = \begin{cases} 1, & if\ displacement\ i\ is\ located\ at\ mean\ water\ level \\ 0, & if\ displacement\ i\ is\ not\ located\ at\ mean\ water\ level \end{cases}$$

(3.90)

Then the structural responses due to the quadratic excitations $\boldsymbol{R}^{(2)}$ are expressed as,

$$M\ddot{\boldsymbol{R}}^{(2)} + C\dot{\boldsymbol{R}}^{(2)} + K\boldsymbol{R}^{(2)} = \boldsymbol{F}^{(2)}$$

$$= \sum_{ii=0}^{2m}\sum_{jj=0}^{2m} \begin{bmatrix} \delta(1)\left(\alpha_{1,i_0}p_1 + j\omega_{ii}\alpha_{2,i_0}\right)H_{v_n,i_0}(\omega_{ii})H_{\eta_{i_0}}(x_0,y_0,\omega_{jj})\dfrac{1}{p_{z_{i_0}}} \\ \delta(2)\left(\alpha_{1,i_0}p_1 + j\omega_{ii}\alpha_{2,i_0}\right)H_{v_n,i_0}(\omega_{ii})H_{\eta_{i_0}}(x_0,y_0,\omega_{jj})\dfrac{1}{p_{z_{i_0}}} \\ \vdots \\ \delta(n)\left(\alpha_{1,i_0}p_1 + j\omega_{ii}\alpha_{2,i_0}\right)H_{v_n,i_0}(\omega_{ii})H_{\eta_{i_0}}(x_0,y_0,\omega_{jj})\dfrac{1}{p_{z_{i_0}}} \end{bmatrix} A_{ii}A_{jj}\, e^{\boldsymbol{j}(\omega_{ii}+\omega_{jj})t}$$

(3.91)

Similar to the calculation of the 1st order and 3rd order transfer functions, the 2nd transfer function for those selected displacements can be expressed as,

$$\begin{bmatrix} H_{2,1}(\omega_{ii},\omega_{jj}) \\ H_{2,2}(\omega_{ii},\omega_{jj}) \\ \vdots \\ H_{2,n}(\omega_{ii},\omega_{jj}) \end{bmatrix} = S^{-1}(\omega_{ii}+\omega_{jj} + \omega_{kk}) \begin{bmatrix} \delta(1)(\alpha_{1,i_0}p_1 + j\omega_{ii}\alpha_{2,i_0})H_{v_n,i_0}(\omega_{ii})H_{\eta_{i_0}}(x_0,y_0,\omega_{jj})\dfrac{1}{p_{z_{i_0}}} \\ \delta(2)(\alpha_{1,i_0}p_1 + j\omega_{ii}\alpha_{2,i_0})H_{v_n,i_0}(\omega_{ii})H_{\eta_{i_0}}(x_0,y_0,\omega_{jj})\dfrac{1}{p_{z_{i_0}}} \\ \vdots \\ \delta(3)(\alpha_{1,i_0}p_1 + j\omega_{ii}\alpha_{2,i_0})H_{v_n,i_0}(\omega_{ii})H_{\eta_{i_0}}(x_0,y_0,\omega_{jj})\dfrac{1}{p_{z_{i_0}}} \end{bmatrix} \tag{3.92}$$

$$\begin{bmatrix} H_{2,1}(\omega_{ii},\omega_{jj}) \\ H_{2,2}(\omega_{ii},\omega_{jj}) \\ \vdots \\ H_{2,n}(\omega_{ii},\omega_{jj}) \end{bmatrix} = [\Phi] \begin{bmatrix} \dfrac{1}{-(\omega_{ii}+\omega_{jj}+\omega_{kk})^2(1+\beta_1)+(1+\beta_2)\lambda_1{}^2} & 0 & 0 & 0 \\ 0 & \dfrac{1}{-(\omega_{ii}+\omega_{jj}+\omega_{kk})^2(1+\beta_1)+(1+\beta_2)\lambda_2{}^2} & 0 & 0 \\ 0 & 0 & \ddots & 0 \\ 0 & 0 & 0 & \dfrac{1}{-(\omega_{ii}+\omega_{jj}+\omega_{kk})^2(1+\beta_1)+(1+\beta_2)\lambda_n{}^2} \end{bmatrix} [\Phi]^{\mathrm{T}} \begin{bmatrix} \delta(1)(\alpha_{1,i_0}p_1 + j\omega_{ii}\alpha_{2,i_0})H_{v_n,i_0}(\omega_{ii})H_{\eta_{i_0}}(x_0,y_0,\omega_{jj})\dfrac{1}{p_{z_{i_0}}} \\ \delta(2)(\alpha_{1,i_0}p_1 + j\omega_{ii}\alpha_{2,i_0})H_{v_n,i_0}(\omega_{ii})H_{\eta_{i_0}}(x_0,y_0,\omega_{jj})\dfrac{1}{p_{z_{i_0}}} \\ \vdots \\ \delta(3)(\alpha_{1,i_0}p_1 + j\omega_{ii}\alpha_{2,i_0})H_{v_n,i_0}(\omega_{ii})H_{\eta_{i_0}}(x_0,y_0,\omega_{jj})\dfrac{1}{p_{z_{i_0}}} \end{bmatrix} \tag{3.93}$$

Till now the 2nd order transfer function is defined.

To sum up, in this section, the 1st order, 2nd order and 3rd order transfer function from the fluids to the structural responses are derived for the multi degree of freedom system. The total procedure consists of two steps.

The step I is the transformation from the wave and current information to the hydrodynamic loads. This step includes the 3D potential functions of the fluid's accelerations and velocities, Morison's force conversion and free surface-induced force.

The step II is the calculation from external force vector to the structural displacement vector. This step includes the calculation of the 1st order transfer functions (induced by the inertia and linear part of the drag force), the 2nd order transfer functions (induced by free surface induced force) and the 3rd order transfer functions (induced by the cubic part of the drag force).

3.5 The techniques on the improvement of the computation efficiency

The orders of the transfer function greatly affect the efficiency of the computation. Taking the 3rd order transfer function as an example, the number of the 3rd order transfer functions need to be calculated depends on the number of discrete frequencies. However, a large number of discrete frequencies may result in an extremely large amount of the 3rd order transfer functions.

To estimate the computation time, first, the properties of the 3rd order transfer function need to be studied. The total number of the 3rd transfer function need to be calculated for m discretized frequencies are,

$$N_3 = (2m+1) * (2m+1) * (2m+1) \tag{3.94}$$

As observed from (3.94), the total number of the 3rd transfer function may become incredible large with a fine discretization of the wave spectrum. Taking 60 discretized frequencies as an example, then the N3 will equal 1,771,561 (assuming 30s for each calculation, then the total time will be 2years!), which is totally unacceptable for computer calculation.

Therefore, three techniques are proposed to improve the calculation efficiency, which are

(1) The symmetry properties of the transfer functions
(2) Pre-assessment of the transfer functions
(3) Frequency re-discretization for the higher order transfer functions

These techniques will be presented respectively.

3.5.1 The symmetry properties of the transfer functions

From the equations (3.63) (3.79), it is clear that the 3rd transfer functions have the following property.

$$H_3(\omega_{ii}, \omega_{jj}, \omega_{kk}) = H_3(\omega_{jj}, \omega_{ii}, \omega_{kk}) \tag{3.95}$$

In addition, the response will be in real space if the excitation is in real space. Then the transfer function set with negative and positive of same frequency value $\omega_{ii} + \omega_{jj} + \omega_{kk}$, will be,

$$\begin{aligned} H_3(\omega_{ii}, \omega_{jj}, \omega_{kk}) A_{ii} A_{jj} A_{kk} e^{j(\omega_{ii}+\omega_{jj}+\omega_{kk})t} \\ + H_3(-\omega_{ii}, -\omega_{jj}, -\omega_{kk}) A_{ii} A_{jj} A_{kk} e^{-j(\omega_{ii}+\omega_{jj}+\omega_{kk})t} \\ \rightarrow |H_3(\omega_{ii}, \omega_{jj}, \omega_{kk})| A_{ii} A_{jj} A_{kk} \cos\left[(\omega_{ii} + \omega_{jj} + \omega_{kk})t \right. \\ \left. + angle\left(H_3(\omega_{ii}, \omega_{jj}, \omega_{kk})\right)\right] \end{aligned} \tag{3.96}$$

In imagine part,

$$\begin{aligned} Im\Big[H_3(\omega_{ii}, \omega_{jj}, \omega_{kk}) A_{ii} A_{jj} A_{kk} e^{j(\omega_{ii}+\omega_{jj}+\omega_{kk})t} \\ + H_3(-\omega_{ii}, -\omega_{jj}, -\omega_{kk}) A_{ii} A_{jj} A_{kk} e^{-j(\omega_{ii}+\omega_{jj}+\omega_{kk})t}\Big] = 0 \end{aligned} \tag{3.97}$$

To sum up,

$$H_3(\omega_{ii}, \omega_{jj}, \omega_{kk}) = H_3(-\omega_{ii}, -\omega_{jj}, -\omega_{kk}) \tag{3.98}$$

Thus, if N discrete frequencies are adopted for FD calculation, the total number N_3 of the 3rd order transfer function need to be calculated will be reduced to

$$N_3 = \frac{[(C_{2n}^2 + C_{2n}^1)C_{2n}^1]}{2} = 2n^3 + n^2 \tag{3.99}$$

If n=60, then the N_3 will be,

$$N_3 = 435{,}600$$

The amount of the computation has reduced 75.4% (2years to 30days).

3.5.2 Pre-assessment of the transfer functions

The properties of the symmetry still cannot reduce the amount of the computation to a satisfied level and hence the technique of the pre-assessment is proposed.

The basic idea of the pre-assessment technique is to judge the priorities of the 3rd order transfer function before the massive calculation. By only selecting these transfer functions, which are the most important for the result, the total amount of the computation can be greatly reduced.

As observed from the equation (3.80), the complex amplitude of the responses due to the cubic excitation are given as,

$$\begin{bmatrix} R^{(3)}{}_{1,ii,jj,kk} \\ R^{(3)}{}_{2,ii,jj,kk} \\ \vdots \\ R^{(3)}{}_{n,ii,jj,kk} \\ R^{(3)}{}_{n-1,ii,jj,kk} \end{bmatrix} = S^{-1}(\omega_{ii}+\omega_{jj}+\omega_{kk}) \begin{bmatrix} H_{v_n,1}(\omega_{ii},\omega_{jj})H_{v_n,1}(\omega_{kk})[\alpha_{1,1}p_3] \\ H_{v_n2}(\omega_{ii},\omega_{jj})H_{v_n,2}(\omega_{kk})[\alpha_{1,2}p_3] \\ \vdots \\ H_{v_nn}(\omega_{ii},\omega_{jj})H_{v_n,n}(\omega_{kk})[\alpha_{1,s}p_3] \end{bmatrix} A_{ii}\, A_{jj} A_{kk} \tag{3.100}$$

As observed, those responses' amplitudes are dominated by two factors which are,

(1) Dynamic effect, which is represented by the structural part of the (3.100).

$$S^{-1}(\omega_{ii}+\omega_{jj}+\omega_{kk}) \tag{3.101}$$

The dynamic effect will be significant around the dominated natural periods

(2) The external excitation part, which is represented by the hydrodynamic part of the (3.100)

$$\begin{bmatrix} H_{v_n,1}(\omega_{ii},\omega_{jj})H_{v_n,1}(\omega_{kk})[\alpha_{1,1}p_3] \\ H_{v_n2}(\omega_{ii},\omega_{jj})H_{v_n,2}(\omega_{kk})[\alpha_{1,2}p_3] \\ \vdots \\ H_{v_nn}(\omega_{ii},\omega_{jj})H_{v_n,n}(\omega_{kk})[\alpha_{1,s}p_3] \end{bmatrix} A_{ii}\, A_{jj} A_{kk} \tag{3.102}$$

This part will be significant only around the highest amplitudes.

Therefore, based on those two factors, the properties of the 3rd order transfer functions can be determined.

In practice, the amplitudes $A_{ii}A_{jj}A_{kk}$ and the frequencies $\omega_{ii}+\omega_{jj}+\omega_{kk}$ of all of the 3rd order transfer functions are pre-calculated. Then these transfer functions with the highest priorities can be selected, based on two criteria,

(1) For the responses of which the frequency $\omega_{ii}+\omega_{jj}+\omega_{kk}$ are within the certain range around the natural periods.

(2) For the responses of which the amplitude $A_{ii}A_{jj}A_{kk}$ are above a certain value.

By performing this selection, the amount of the computation can be significantly reduced, while the accuracy of the results can be guaranteed.

3.5.3 Frequency re-discretization for the higher order transfer functions

These discretized frequencies used for the 3rd order transfer functions can be different from the frequencies used for these 1st order and 2nd order transfer functions' calculations. As indicated in equation (3.65), the total structural responses can be divided into the responses due to the linear, quadratic and cubic part of the approximation. According to the principle of superposition, the response calculations of these three parts are independent to each other. Because of this property, the calculation of the 3rd order transfer functions can be isolated from the other transfer functions. Therefore, a new frequency discretization may be applied for the higher order transfer function calculations.

An analysis strategy can be that, a fine frequency discretization may be applied for these linear transfer function calculations, while a rough frequency discretization may be applied for these cubic transfer function calculations.

Still taking the example of n=60, the number of new discretization may be reduced to 20, and thus the total number of the 3rd order transfer function need to be calculated will be

$$N_3=\frac{[(C_{2n}^2+C_{2n}^1)C_{2n}^1]}{2}=2n^3+n^2=16{,}400 \tag{3.103}$$

The amount of the computation has reduced 96.3% (30 days to 1.13 days).

Till now, these three techniques for the improvement of the computation speed are introduced. These techniques may be combined to reduce the total computation time to a quite short time, which makes the higher order frequency domain method be very competitive, compared with those traditional dynamic analysis methods.

4.0 THE COMPARATIVE STUDY ON SIMPLE MODELS

This chapter presents the qualitative study of the differences between the quasi-static, frequency-domain and time-domain methods. The study mainly focus on three aspects (linearized vs nonlinear drag force, free surface treatment and the dynamic vs quasi-static) and these studies are demonstrated on some simple models. For the purpose of better understanding, the differences in these three aspects will be enlarged and analyzed by comparing with the HFD method qualitatively and quantitatively.

4.1 Overview

As mentioned in section 2.1, the traditional dynamic analysis methods presented in this study can be cataloged as,

(1) Time-domain method (Stochastic non-linear dynamic)
(2) Frequency-domain method (Stochastic linear dynamic)
(3) Quasi-static method (Deterministic non-linear static)

The major considerations [8] between these methods can be identified as,

- dynamic versus (quasi) static analysis
- stochastic versus deterministic analysis
- non-linear versus linear analysis

The issue of the dynamic versus (quasi) static analysis refers to the treatment of the dynamic effect in the analysis. As discussed in Chapter 2, for the ultimate limit state analysis, the dynamic status may be represented by a static status, which is more convenient for the analysis. Hence, the study on this aspect mainly focuses on the fluids and the validation of the static representation.

The issue of the stochastic versus deterministic analysis refers to the treatment of the real stochastic effect in the analysis. The real excitations of the fluids are stochastic in nature. For practice, those stochastic excitations may be represented by a single-frequency excitation. Hence, the study on this aspect mainly focuses on the validation of this simplification.

The issue of the non-linear versus linear analysis refers to the validation of the linearization of the non-linear terms in the analysis. The study on this aspect consists of two major parts: the linearization of the drag term and the free surface treatment. The analysis of those two parts will be demonstrated respectively.

In addition of those aspects, for engineering practice, the efficiency of the dynamic analysis is also a critical issue. The efficiency constraints the applications of the dynamic analysis in engineering practice. For example, the time-domain is the most accurate method in principle. However, its large time-computation, may result in the

delay of those urgent projects. The study on the issue of the efficiency focuses on the comparison between the accuracy and the time consuming.
Among those aspects, the issue of the stochastic versus deterministic analysis and the efficiency is not presented in this simple analysis and will be analysis quantitatively in Chapter 7. The issues of dynamic versus quasi-static, linearization of the drag force are demonstrated on a SDOF system. The issue of the free surface treatment will be demonstrated on a single vertical beam, with the self –code "hydro" program.

In summary, the simple comparative analysis on four aspects are presented in this study,

(1) Linear versus non-linear drag force
(2) Free surface treatment
(3) Dynamic versus quasi-static analysis

Throughout this study, the time-domain method is assumed to be the reference method, because it is the most accurate methods in principle. The studies on these four aspects are based on this assumption and presented respectively. Besides, the HFD method is served as an analytical approach to explain the differences between different methods.

4.2 Nonlinear vs. linear drag term

As mentioned by DNV, the linearization of the drag term introduces uncertainties [8]. However, DNV doesn't mention what kinds of these uncertainties are. The purpose of the study in this section is to identify and analysis these "uncertainties" in order to have a deeper understanding of the effect of the linearization. In summary, two issues are checked in this study,

(1) The validation of the linearization
(2) The validation of the methods for the linearization

To begin with, the system for study is carried out. A simple single degree of system is capable of reflecting the effect of drag-term and thus is adopted as the model. This SDOF system for study is assumed, and presented as follows.

$$m\ddot{r} + c\dot{r} + kr = \alpha_1 |v| v \tag{4.1}$$

Where, m represents the mass of the system, c represents the damping coefficient of the system and k represents the stiffness of the system. α_1 represents the drag coefficient. (Inertia term is irrelevant to this study and thus not presented here)

The term v represents the velocity of the fluids. The velocity of the fluids, instead of the wave elevations and current's profile is controlled as the excitation of the system.

The dynamic analysis of this SDOF system is given in three methods: the time-domain method, the traditional frequency-domain method and the higher order frequency-domain method. The time-domain method is the most accurate method in principle and hence it is carried out as the reference. The traditional frequency-domain linearized the drag-term, and thus can be used for investigating the linearization's effect. Finally, the analysis by the higher order frequency domain method is provided to explain the underlying causes of the deviation by using the drags' linearization. The expressions for these three models are,

The model for the time domain method

$$m\ddot{r} + c\dot{r} + kr = \alpha_1 |v| v \tag{4.2}$$

The model for the traditional frequency domain method

$$m\ddot{r} + c\dot{r} + kr = \alpha_1 C_{linear} v \tag{4.3}$$

Where C_{linear} is the coefficient of linearization.

The model for the higher order frequency domain method

$$m\ddot{r} + c\dot{r} + kr = \alpha_1 (p_1 v + p_3 v^3) \tag{4.4}$$

Where p_1 and p_3 are the linear and cubic coefficients.

4.2.1 The validation of the linearization

The studies of the validation of the linearization are carried out in three situations, with reasons:

(1) A single sinusoidal excitation (single wave)
(2) A single sinusoidal excitation plus a constant current (wave-current interaction)
(3) Multi- sinusoidal excitation (multi-wave interaction)

These studies are carried out respectively

For a single sinusoidal excitation, the velocity is assumed as follow,

$$v = V_0 \cos(\omega t) \tag{4.5}$$

Where V_0 and ω are the amplitude and frequency of this excitation.

Substitute (4.5) into (4.3) (4.4), the model for the time-domain, the frequency-domain and the higher order frequency-domain methods are expressed as,

The model for the time domain method (Newmark-beta method)

$$m\ddot{r} + c\dot{r} + kr = \alpha_1 |V_0 \cos(\omega t)| V_0 \cos(\omega t) \tag{4.6}$$

The model for the traditional frequency domain method

$$m\ddot{r} + c\dot{r} + kr = \alpha_1 C_{linear} V_0 \, cos(\omega t) \tag{4.7}$$

The model for the higher order frequency domain method

$$m\ddot{r} + c\dot{r} + kr = \alpha_1 (p_1 V_0 \, cos(\omega t) + p_3 (V_0 \, cos(\omega t))^3) \tag{4.8}$$

Expand (4.8), we have,

$$m\ddot{r} + c\dot{r} + kr = \alpha_1 p_1 V_0 \, cos(\omega t) + \alpha_1 p_3 V_0^3 \left(\frac{1}{4}\cos(3\omega t) + \frac{3}{4}\cos(\omega t)\right)$$

$$m\ddot{r} + c\dot{r} + kr = \left(\alpha_1 p_1 V_0 + \frac{3}{4}\alpha_1 p_3 V_0^3\right)\cos(\omega t) + \frac{1}{4}\alpha_1 p_3 V_0^3 \cos(3\omega t) \tag{4.9}$$

Compare the (4.9) with (4.7), two distinctions are observed.

(1) The force component at the original frequency ω is not linearly proportional to the amplitude of the excitation V_0, due to the present of the term V_0^3.

(2) Besides, the force at the original frequency ω. The force component $\frac{1}{4}\alpha_1 p_3 V_0^3 \cos(3\omega t)$ at a new frequency 3ω is also generated by these excitations.

The first distinction announces the feasibility's limitation of the traditional frequency-domain method. As mentioned in Chapter 2, the common procedure used in the traditional frequency-domain method is to calculate the transfer functions with a reference wave height, and then apply these transfer functions to all the sea states for the dynamic analysis. However, as shown in the figure 4.1, due to the present of the cubic order term $\frac{3}{4}\alpha_1 p_3 V_0^3$, the accuracy of this method may be significantly reduced, with the increase of the V_0. When the V_0 increases from 0m/s to the 10m/s, the $\frac{3}{4}\alpha_1 p_3 V_0^3$ approximately increased 100 units. For the range of V_0 from 15m/s to 25m/s, the $\frac{3}{4}\alpha_1 p_3 V_0^3$ approximately increased 400 units, 400 % of those from 0m/s to 10m/s. Therefore, a single set of the transfer functions for multi sea states' calculation may fail to be representative.

This defect can be somehow partly compensated by the iteration of the linearization. As proposed in ref [19], the drag-term in one loop may be linearized based on the standard deviation of the velocity calculated from the previous loop. By using these iteration procedures, the transfer functions for each sea state are optimized and thus a reasonable result may be obtained [19]. This linearization method will be further discussed in the section 4.2.2.

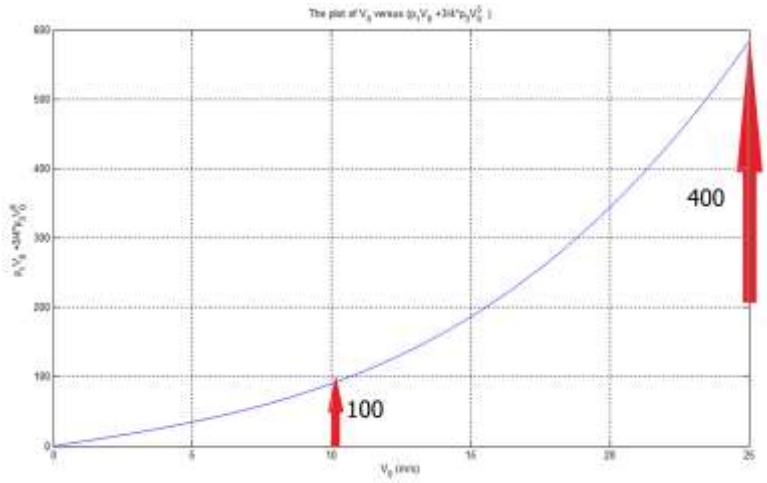

Figure 4.1 the plot of V_0 versus $p_1V_0 + \frac{3}{4}p_3V_0^3$ (p_1, p_2 are optimized for +-20m/s range)

The second distinction announces the most important difference between the linearized and the non-linear drag terms. Due to the non-linearity, the effect of the excitation will interact with itself, and the total energy will be leaked to another frequency. As indicated in equation (4.9), the frequency of the term $\frac{1}{4}\alpha_1 p_3 V_0^3 \cos(3\omega t)$ is different from the excitation $V_0 \cos(\omega t)$. This effect is fundamentally unpredictable for the linearized system, in which the excitations and responses are kept in same frequency.

The frequency leak property of the system results in two effects. First, the energy at the original frequency ω will be also leaked into the new frequencies and hence reduced. Second, the force component at the new frequency 3ω has different dynamic effect with the component at original frequency ω.

A typical phenomenon caused by the frequency leak is the higher order resonance. The force component at new frequency may trigger the resonance, while the force at original frequency will not. A demonstration is given as follows.

The coefficients are assumed for this SDOF system: m=100kg, c=20N.m/sec, k=100N/m, $\alpha_1 = 1$. The amplitude and frequency of the excitation are $V_0 = 5m/s$ and $\omega = 0.333rad/s$, expressed as follows,

$$100\ddot{r} + 20\dot{r} + 100r = |5cos(0.333t)|5\,cos(0.333t) \tag{4.10}$$

The natural frequency of the system equals 3 times the excitation's frequency

$$\omega_0 = \sqrt{\frac{k}{m}} = \sqrt{\frac{100}{100}} = \frac{1rad}{s} = 3\omega \tag{4.11}$$

This equals three times the excitation's frequency.

Based on the theory mentioned above, the higher order resonant will be triggered in this case. In order to calibrate the coefficients for the linearization, the mass m is first tuned to 0.001kg and 1kg to minimize the dynamic effect.

When the mass equals 0.001kg, the linearization coefficient C_{linear} is calibrated to 4.8997, as shown in figure 4.2. The natural frequency for this system is 316.228 rad/s. As observed from the plot, the motion from TD, FD and HFD matches each other quite well.

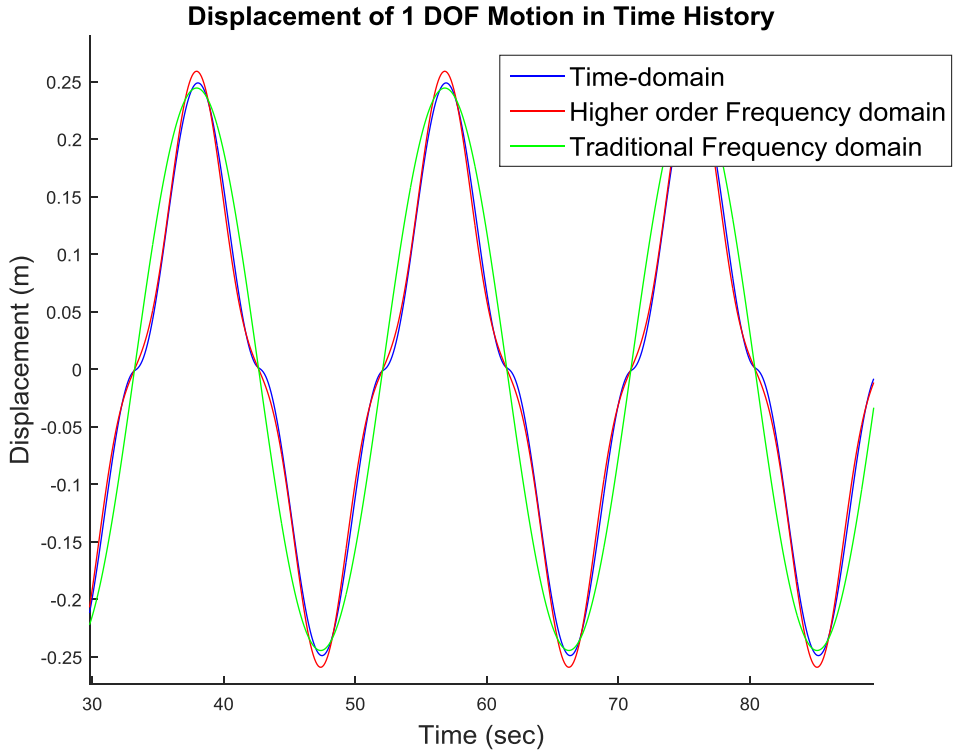

Figure 4.2. the plot of the displacement versus the time by the TD, FD and HFD methods (m=0.001kg)

To verify the validation of the linearization, the mass is tuned to 1kg, while this linearization coefficient is not changed ($C_{linear} = 4.8997$). The natural frequency is 10 rad/s for this system and the plot of the displacement versus time is shown in the figure 4.3.

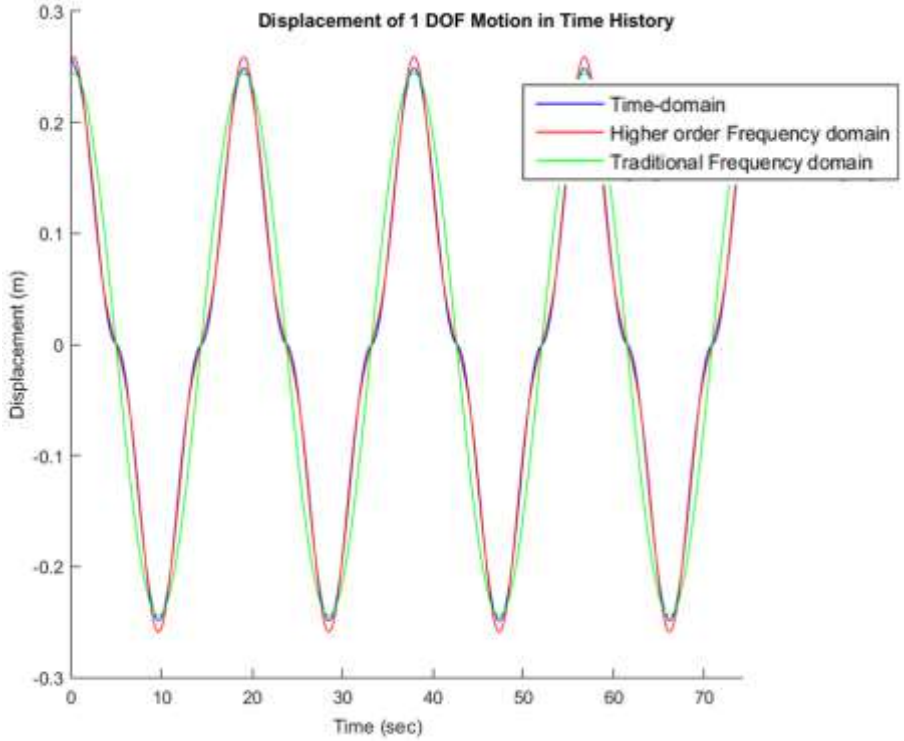

Figure 4.3. the plot of the displacement versus the time by the TD, FD and HFD methods (m=1kg)

As demonstrated in figure 4.2 and figure 4.3, the responses from the time-domain, the frequency domain and the higher order frequency domain is quite close to each other, independent from the structure. Therefore, it can be conclusion that, this linearization system is calibrated.

With the linearization being optimized, the mass is then tuned to 100kg to trigger the resonant. Figure 4.4 shows the plot of the displacement versus time, when m=100kg. As observed from figure 4.4, there is a clear difference occurs between the methods with linearized and non-linear drag term. Compared with figure 4.1 and figure 4.2, it can be concluded that this difference is induced by the dynamic effect. For further identification, the linear coefficient p_1 is set to be zero, and a new plot of the displacement versus time is made, as shown in figure 4.5. It is clear that the motion's shapes are dominated by the cubic part of the force. Therefore, the existence of the higher order resonance is verified and predicted.

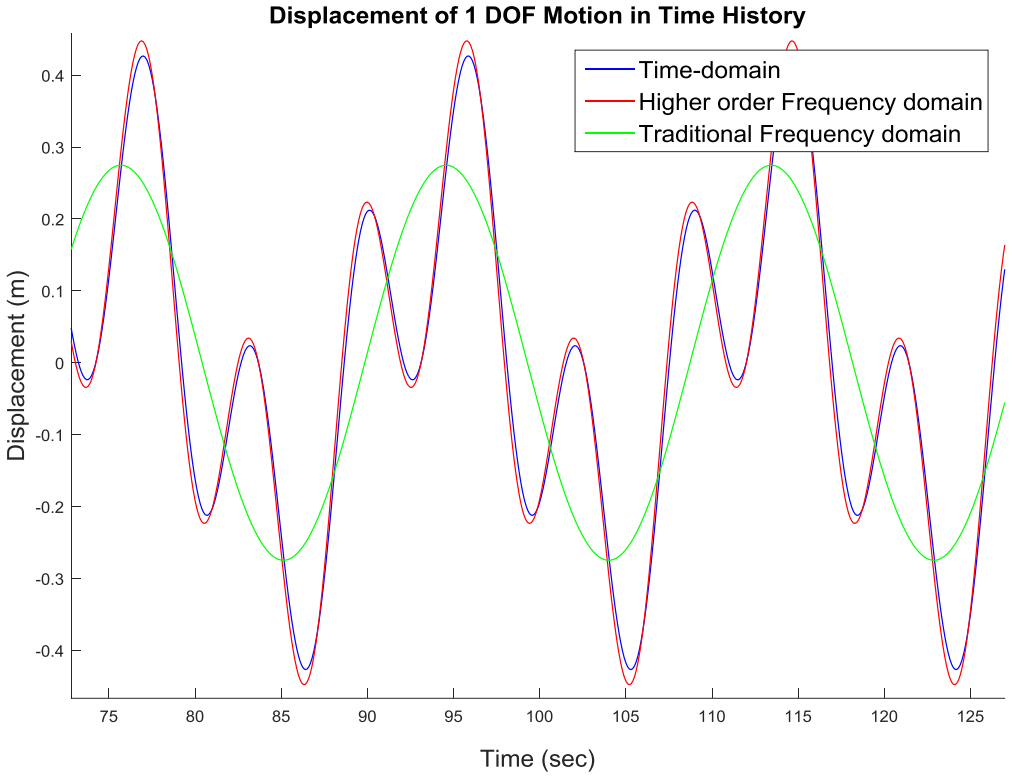

Figure 4.4. the plot of the displacement versus the time by the TD, FD and HFD methods (m=100kg)

In addition of this higher order resonant phenomenon, the linearization of the drag term may also overestimate the response, when the original frequency is coincident to the natural frequency of the system. As predicated previously, the energy at the original frequency ω will be also leaked to the new frequencies. Thus the energy at the original frequency ω will be reduced. However, for the optimized linearization of drag term the energy ω at higher order frequencies are compensated by the energy at the original frequency ω, expressed as,

$$\begin{aligned} E_{total} &= E_{\omega} + E_{3\omega} + \cdots, \quad for\ higher\ order\ approximation \\ E_{total} &= E_{\omega}, \quad for\ linearization \end{aligned} \tag{4.12}$$

Where, $E_{total}, E_{\omega}\ and\ E_{3\omega}$ are the total energy and energy at frequency $\omega\ and\ 3\omega$ respectively.

Therefore, when the excitation frequency ω equals the structural natural frequency ω_0, the total energy will contribute the resonant, while the only part of the total energy will be trigged in reality. This phenomenon results in the overestimation of the result from the traditional frequency-domain method.

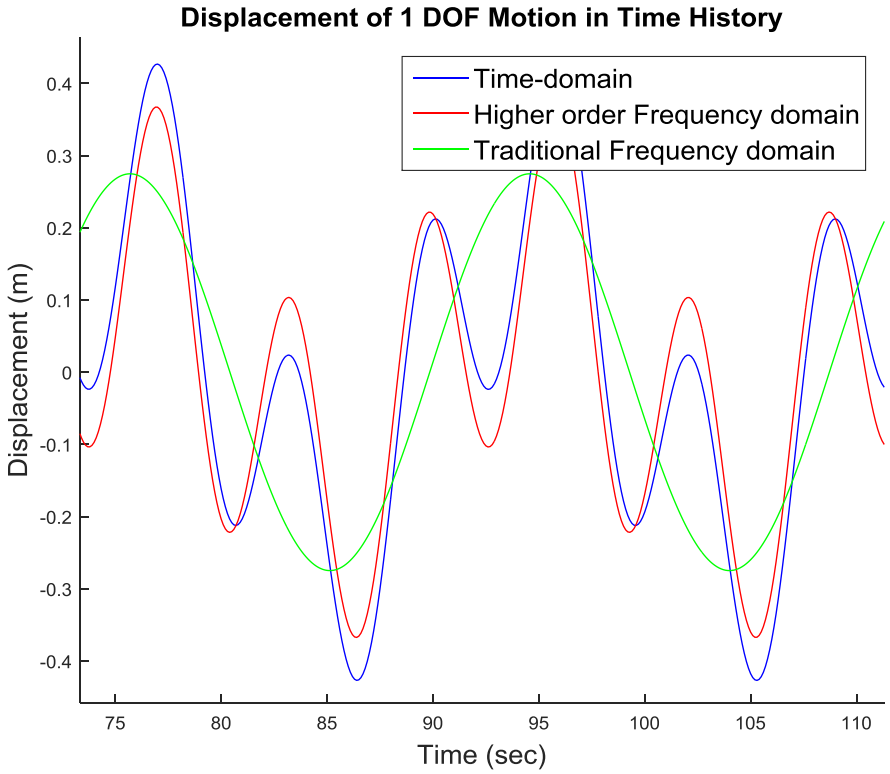

Figure 4.5. the plot of the displacement versus the time with only cubic part of the HFD methods (m=100kg)

To verify this prediction, the mass of the system is tuned into 900.18kg and then the natural frequency equals $\omega_0 = \sqrt{\frac{100}{900.18}} = 0.3333 rad/sec$, which is the same as the excitation. The figure 4.6 shows the plot of displacement versus time. It can be observed from the figure 4.6 that the amplitude of the motion calculated by FD method is larger than those from the time-domain and the higher frequency-domain methods. To avoid the special case effect, figure 4.7 shows another case, which natural frequency equals to the excitation. In summary, it is reasonable to conclude this assumption is valid.

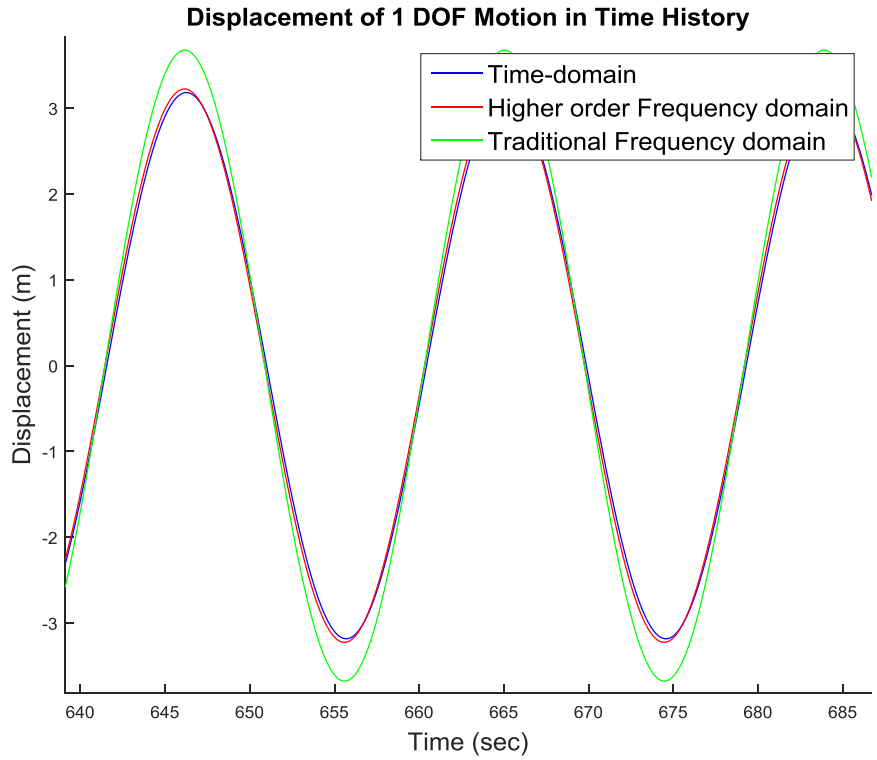

Figure 4.6. the plot of the displacement versus the time with the TD, FD and HFD methods(m=900.18kg)

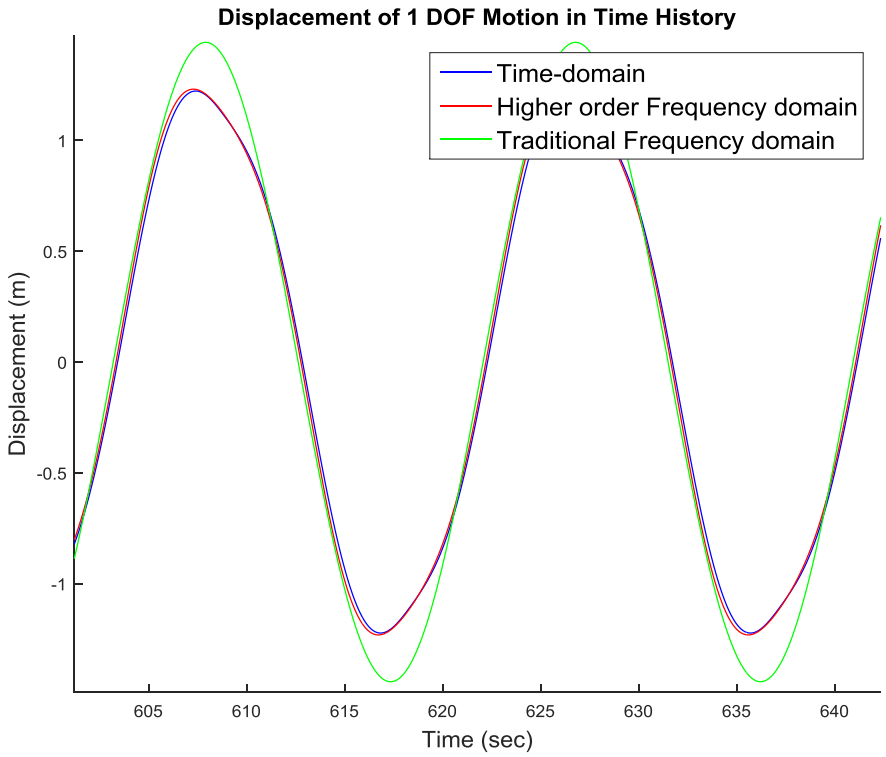

Figure 4.7. the plot of the displacement versus the time (m=20kg , c=50N*s/m , k=5.5544N/m)

In conclusion, from the basic study of the single sinusoidal excitation on the issue of the linearized versus non-linear drag term, two characteristics are listed as follows.

(1) The response component at the original frequency ω is not linearly proportional to the amplitude of the excitation. The application of one global set of the transfer functions may fail to be representative.
(2) The energy at the original frequency ω will be leaked to a new frequency, which may case higher order resonance. Besides, the optimized FD method may overestimate the response when the system is a status of the resonance at ω.

The next situation to be studied is the wave-current interaction. In this case, the fluid's velocity is assumed to be a single sinusoidal function plus a constant current, expressed as,

$$V = V_0 cos(\omega t) + V_{cur} \tag{4.13}$$

Where V_{cur} is the fluid of the current, which is assumed to be constant during the motion.

Thus the models for the TD, FD and HFD method then become,

The model for the time domain method (Newmark-beta method)

$$m\ddot{r} + c\dot{r} + kr = \alpha_1 |V_0 \cos(\omega t) + V_{cur}| (V_0 \cos(\omega t) + V_{cur}) \tag{4.14}$$

The model for the traditional frequency domain method

$$m\ddot{r} + c\dot{r} + kr = \alpha_1 C_{linear} V_0 \, cos(\omega t) + \alpha_1 C_{linear} V_{cur} \tag{4.15}$$

The model for the higher order frequency domain method

$$m\ddot{r} + c\dot{r} + kr = \alpha_1 (p_1 (V_0 \, cos(\omega t) + V_{cur}) + p_3 (V_0 \, cos(\omega t) + V_{cur})^3) \tag{4.16}$$

Expand (4.16), we have,

$$\begin{aligned} m\ddot{r} + c\dot{r} + kr = {} & (\alpha_1 p_1 V_0 \cos(\omega t) + \alpha_1 p_1 V_{cur}) \\ & + (\alpha_1 p_3 V_0^3 \cos(\omega t)^3 + 3\alpha_1 p_3 V_0^2 \cos(\omega t)^2 V_{cur} + 3\alpha_1 p_3 V_0 \cos(\omega t) V_{cur}^2 \\ & + \alpha_1 p_3 V_{cur}^3) \end{aligned}$$

$$\begin{aligned} m\ddot{r} + c\dot{r} + kr = {} & \alpha_1 \left(p_1 V_0 + \frac{3 p_3 V_0^3}{4} + 3 V_0 p_3 V_{cur}^2 \right) \cos(\omega t) + \frac{3\alpha_1 p_3 V_0^2 V_{cur}}{2} \cos(2\omega t) \\ & + \frac{\alpha_1 p_3 V_0^3}{4} \cos(3\omega t) + \alpha_1 (p_1 V_{cur} + \frac{3 p_3 V_0^2 V_{cur}}{2} + p_3 V_{cur}^3) \end{aligned} \tag{4.17}$$

Compare the (4.15) with (4.17), two distinctions are observed, which cannot be predicted by the traditional frequency-domain method fundamentally.

(1) The constant force component is not only depended on the current's velocity V_{cur}, but also depended on the amplitude of the varying motions V_0

(2) Besides the increase of the constant force component, the current and varying motion also interact with each other, with the change of the energy at the original frequency ω and the energy at the new frequency 2ω

To identify the existence of these two distinctions, another two numerical experiments have been made. The first numerical experiment is aimed to identify the change of the constant force with the increase of the amplitude of the sinusoidal excitation V_0. The second numerical experiment is aimed to identify the existence of the responses at the frequency 2ω, which is caused by the wave-current interaction.

Those numerical experiments are based on the following assumption of the SDOF system,

$$100\ddot{r} + 20\dot{r} + 100r = |V_0 cos(0.1t) + 3|(V_0 cos(0.1t) + 3) \tag{4.18}$$

Where the m=100, c=20 k=100, the $\omega = 0.1 rad/s$ and $V_{cur} = 3m/s$, compared with (4.14).

The first numerical experiment is carried out on the measurement of the average displacement for a period of the $24 * \frac{2\pi}{\omega} = 215.424\, sec$, with the increase of the V_0. Figure 4.8 shows the plot of the average displacement versus V_0. As shown in this figure, the average displacement of the TD increased quadratically, same as the prediction by the HFD method. It can be concluded that the first distinction is identified. (Still, the deviation can be observed between the TD and HFD's prediction. This is because; the 3rd order approximation can only hold the overall accuracy with in a velocity range. More details have been discussed in Chapter 3)

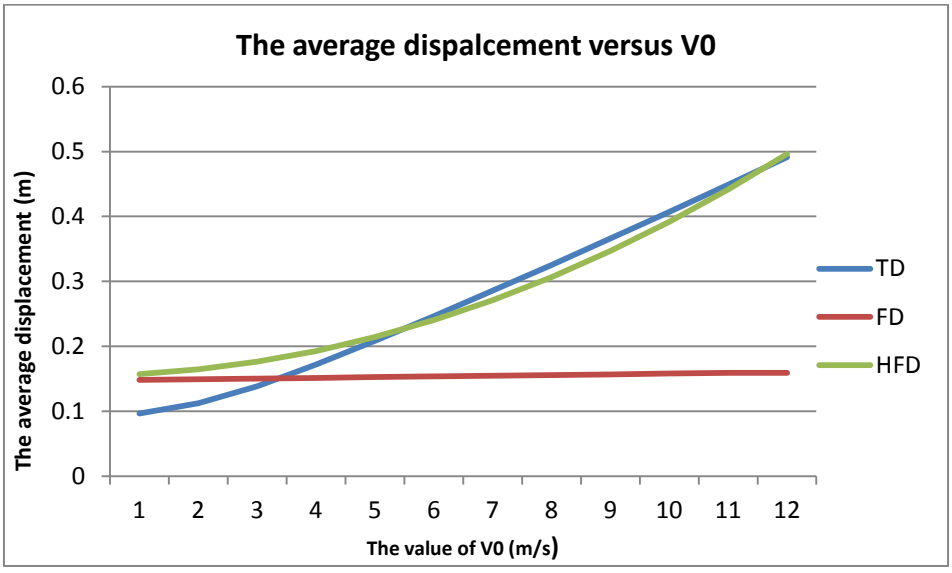

Figure 4.8 the plot of the average displacement versus V_0

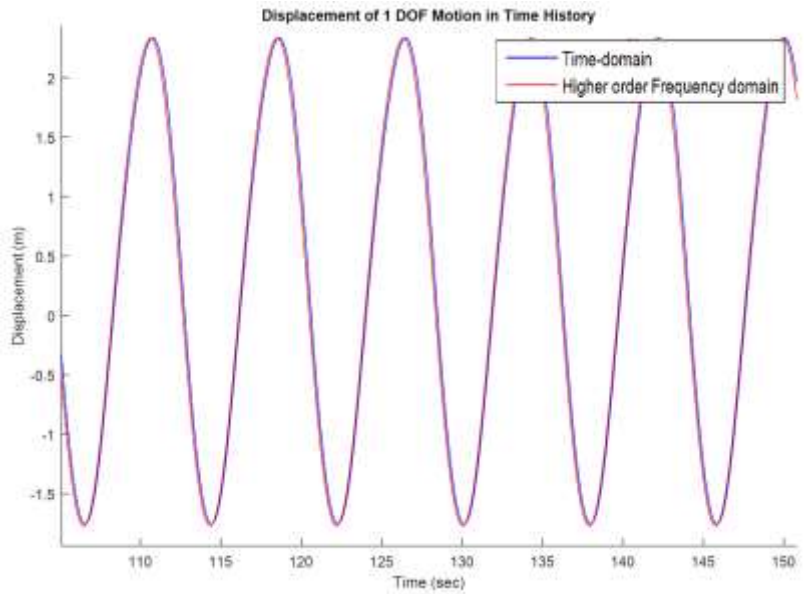

Figure 4.9 the plot of the displacement versus time for eqn.(4.18)

The second numerical experiment is to identify the responses at the second order frequency 2ω . The following system is assumed in this numerical experiment,

$$100\ddot{r} + 20\dot{r} + 100r = |9cos(0.8t) + 3|(9cos(0.8t) + 3) \tag{4.19}$$

The motions of this system are generated by using the time-domain and the higher order frequency-domain respectively. The figure 4.10 shows the plot of the displacement versus time. As observed, the motion from the time domain can be accurately reflected by the motions from the higher order frequency domain. To identify the motion's component at different frequencies, Fast Fourier transform (FFT) is used in this analysis to separate those motion's components. Figure 4.10 shows the amplitude- frequency plot of the motions. It can be clearly observed from the figure that there is motion's component at the frequency $2\omega = 2 * 0.8 = 1.6Rad/s$. And this motion can be accurately predicted by the higher frequency-domain method.

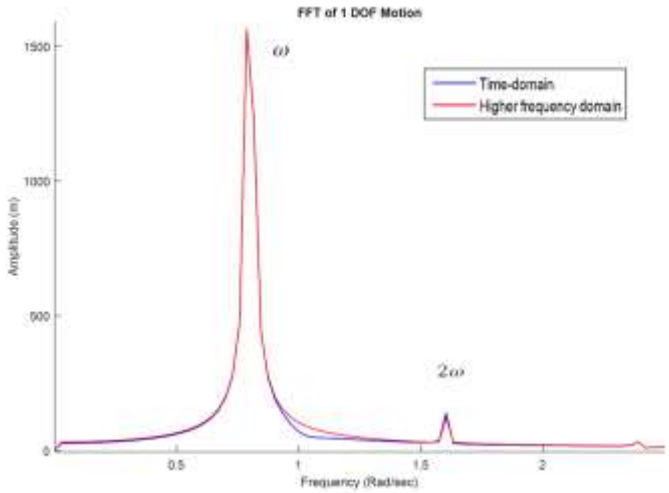

Figure 4.10 the FFT analysis of the motion

In conclusion, from the study of the single wave-current interaction on the non-linear drag term, two characteristics are listed as follows.

(1) The static response will increase quadratically with respect to the increase of the amplitude of the single-frequency excitation.

(2) The motion at a new frequency 2ω is generated by the wave-current interaction.

The study on the multi-wave interaction is similar to the study on the single-wave and the wave-current interaction. In this study, the excitation with two sinusoidal motions is assumed, expressed as,

$$V = V_1 \cos(\omega_1 t) + V_2 \cos(\omega_2 t) \tag{4.20}$$

Then the model for the TD, FD and HFD methods can be rewritten as,

The model for the time domain method (Newmark-beta method)

$$m\ddot{r} + c\dot{r} + kr = \alpha_1 |V_1 \cos(\omega_1 t) + V_2 \cos(\omega_2 t)|(V_1 \cos(\omega_1 t) + V_2 \cos(\omega_2 t)) \tag{4.21}$$

The model for the traditional frequency domain method

$$m\ddot{r} + c\dot{r} + kr = \alpha_1 C_{linear} V_1 \cos(\omega_1 t) + \alpha_1 C_{linear} V_2 \cos(\omega_2 t) \tag{4.22}$$

The model for the higher order frequency domain method

$$\begin{aligned} m\ddot{r} + c\dot{r} + kr &= \alpha_1 (p_1 (V_1 \cos(\omega_1 t) + V_2 \cos(\omega_2 t)) + p_3 (V_1 \cos(\omega_1 t) + V_2 \cos(\omega_2 t))^3) \\ &= \alpha_1 \left[\frac{1}{4} A_2^3 \, cos(3\omega_2 t) + \frac{1}{4} A_1^3 \, cos(3\omega_1 t) + \frac{3}{2} cos(\omega_2 t) \, A_1^2 A_2 \right. \\ &+ \frac{3}{4} cos(\omega_2 t) \, A_2^3 + \frac{3}{4} A_1^2 A_2 \, cos\big(t(2\omega_1 + \omega_2)\big) + \frac{3}{4} A_1^3 \, cos(\omega_1 t) \\ &+ \frac{3}{2} A_1 A_2^2 \, cos(\omega_1 t) + \frac{3}{4} A_1^2 A_2 cos\big(t(2\omega_1 - \omega_2)\big) + \frac{3}{4} A_1 A_2^2 \, cos\big(t(\omega_1 + 2\omega_2)\big) \\ &\left. + \frac{3}{4} A_1 A_2^2 \, cos\big(t(\omega_1 - 2\omega_2)\big) \right] \end{aligned} \tag{4.23}$$

As predicted by the HFD method, the motions are generated at following frequencies,

(1) Self-induced part: ω_1, ω_2, $3\omega_1$, $3\omega_2$

(2) Interaction-induced part: $\omega_1 + (\omega_2 - \omega_2)$, $\omega_2 + (\omega_1 + \omega_1), \omega_1 + 2\omega_2$, $2\omega_1 + \omega_2$, $|\omega_1 - 2\omega_2|$, $|\omega_2 - 2\omega_1|$

These interaction-induced parts can be divided into two groups: The high frequency group, which contains $\omega_1 + 2\omega_2, 2\omega_1 + \omega_2$, and the low frequency group, which contains $|\omega_1 - 2\omega_2|, |\omega_2 - 2\omega_1|$.

A FFT analysis for the system with excitations for $\omega_1 = 0.9\frac{rad}{s} and\ \omega_2 = 1.4\frac{rad}{s}; V_1 = V_2 = \frac{5m}{s}$ is plotted in figure 4.11. As identified in the plot, the motions at the frequencies of both self-induced part and interaction-induced part exist and are predicted. However, the cubic drag's approximation underestimates some higher order response component.

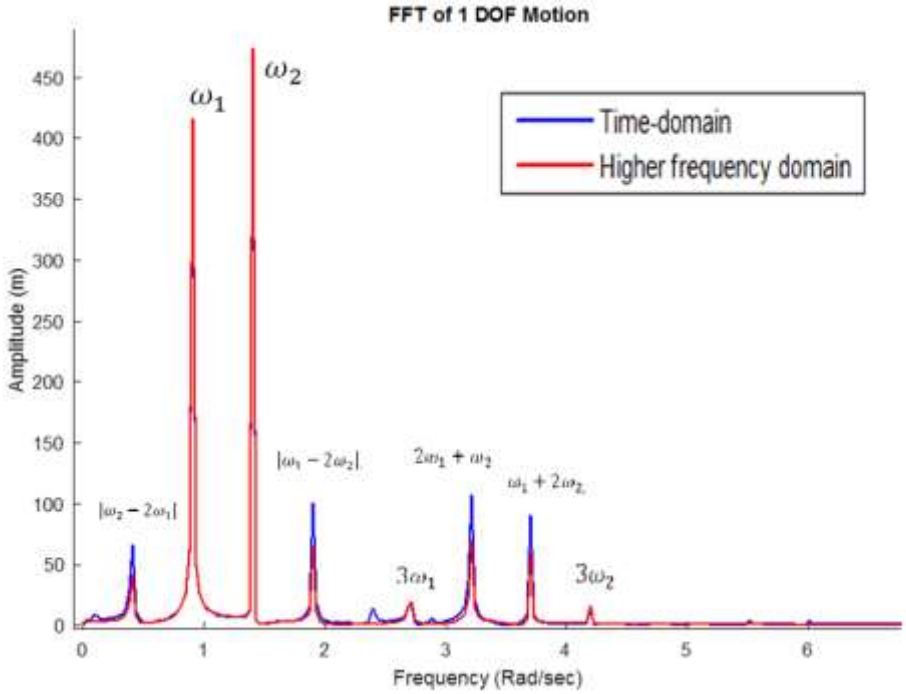

Figure 4.11 the plot of the FFT analysis for the system (4.16)

The waves are always given in the form of the spectrum and the non-linearity of the drag-force will lead to a shift of spectrum, and hence the resonance may be triggered, though the main band of the excitation's spectrum is beyond the region of the resonance. This phenomenon is similar to the second order slow drift force for floating structure. A demonstration is given in the figure 4.12, presents the 2nd order spectrum shift for a FPSO [20].

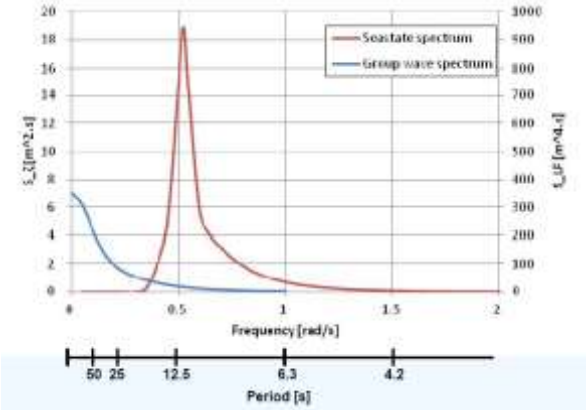

Figure 4.12 a demonstration of the spectrum shift for 2nd low-frequency interaction ref. [20]

4.2.2 The validation of the linearization method

From the previous section, it is concluded that the method of drag's linearization is conditionally valid. However, the traditional frequency-domain method is still generally used in the industry, because of its convenient and its conditionally accurate prediction. Therefore, the studies have been carried out to maximize the accuracy of the traditional frequency-domain method by proposing different linearization methods.

As mentioned in Chapter 2, two methods are recommended for the linearization [8]. Method I linearizes the drag term with respect to the reference wave height H_{ref} [10]. Method II linearizes the drag term with respect to its motion's deviations, and thus an optimization iteration is performed.

The first methods has been widely studied [19]. The previous studies have shown that the first method usually underestimates the motion of the drag forces.

The second linearization method, however, need to be carefully checked. Several studies [8][19] have been carried out on the accuracy of the second linearization method and they claimed that a reasonable result may be given for the initial design of the stinger [19]. However, those studies haven't provided a theoretically investigation on the validation of this linearization method.

The original study by Leon.E.Borgman [21] proposed a method for the spectrum assembly for the Morison type hydrodynamic force with the Gaussian distribution of the fluid's velocity. The hydrodynamic force model used in this study is,

$$\Phi(\mathrm{x},\mathrm{y},\mathrm{z},\mathrm{t}) = cV|V| + k\frac{\partial V}{\partial t} \tag{4.24}$$

Where c and k is the drag and inertia coefficients respectively. If the velocity and acceleration is Gaussian distributed with zero-mean value, then the auto-spectrum of $\Phi(\mathrm{x},\mathrm{y},\mathrm{z},\mathrm{t})$ will be,

$$S_{\phi\phi}(f) = \frac{c^2\sigma^4}{\pi}\left\{\frac{8S_{vv}(f)}{\sigma^2} + \frac{4[S_{vv}(f)]^{*3}}{3\sigma^6} + \cdots\right\} + k^2 S_{AA}(f) \tag{4.25}$$

Leon. E. Bergman has shown that the corresponding correlation coefficient ρ has only maximum 15% deviation for the linear approximation, while only maximum 1.1% deviation for the cubic approximation.

Therefore, an approach for the drag term's linearization based on Borgman's study is widely proposed by the offshore industry, expressed as,

$$|v_{n_i}|\boldsymbol{v}_{n_i} \approx \sigma_u \sqrt{\frac{8}{\pi}}\boldsymbol{v}_{n_i} \tag{4.26}$$

However, three challenges have been pointed out for this linearization.

(1) The original study by Borgman assumed that no-current is involved in fluid's velocity. Hence, it is invalid to apply this linearization when the current is presented.

(2) The original study by Borgman only showed the relation between the spectrum of the fluid's velocity and the spectrum of $\Phi(\mathrm{x},\mathrm{y},\mathrm{z},\mathrm{t})$. This mean the factor $\sigma_u\sqrt{\frac{8}{\pi}}$ only refers to the amplitude's ratio, without the any consideration of the phase shift between the fluid's velocity and $\Phi(\mathrm{x},\mathrm{y},\mathrm{z},\mathrm{t})$. Therefore, this linearization method may overestimate the motion in 1st order.

(3) The original study by Borgman only pointed out there is a highly correlation between the fluid's velocity and $\Phi(\mathrm{x},\mathrm{y},\mathrm{z},\mathrm{t})$. There's no improvement in mathematics on how the deviation could be for this 1st order and 3rd approximation in real-simulation. This linearization method induces uncertainties.

A new method of the drag's linearization is proposed in this study to include the effect of current. This new method is based on an approximation of the Morison's equation, expressed as,

$$\Phi = c|V + C_{cur}|(V + C_{cur}) + k\frac{\partial V}{\partial t} \approx c(V|V| + 2C_{cur}|V| + C_{cur}^2) + k\frac{\partial V}{\partial t} \tag{4.27}$$

Based on this approximation, the method can be proposed as

$$|v_n + v_{cur}|(v_n + v_{cur}) \approx |v_{cur}|v_{cur} + \sqrt{\frac{8}{\pi}}\sigma_u v_{cur} + \sigma_u\sqrt{\frac{8}{\pi}}v_n \tag{4.28}$$

Where v_n is the fluid's velocity with zero-mean value, the v_n is the constant velocity of current.

This linearization may include the effect of the current with certain simplification. As observed from the (4.22), the average force increased with the increase of the standard deviation of the fluid's velocity. The derivation procedure is attached in Appendix IV. And, due to the limitation of the study, the verification and sensitivity study may be carried out in the future.

The derivation of the explicit form of the optimized linearization coefficient is still a challenge. However, if we assumed such explicit form exists, the deviation of the linearization itself still introduces unignorable deviation, with the increase of the wave amplitude. The figure 4.11 shows the root mean squared error of 1st and 3rd fitting for the drag term approximation. As shown in this figure, the error of the linear approximation increases rapidly, compared with the 3rd order fitting. This figure indicates, the linearization itself, has the fundamentally defect, which cannot be compensated by any linearization method.

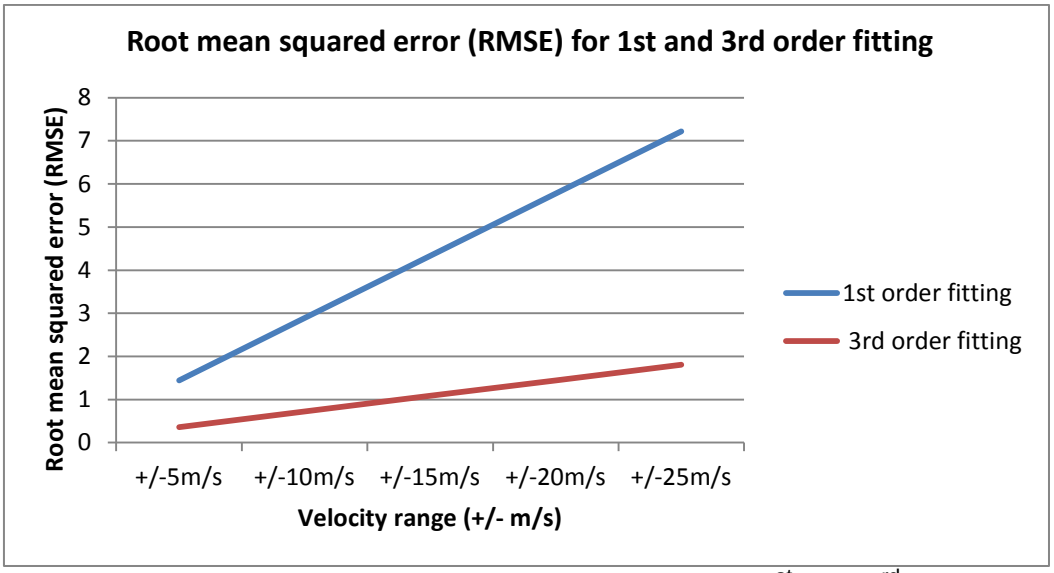

Figure 4.13 the root mean squared error for optimized 1st and 3rd order fitting

4.3 Varying free water surface effect

The analysis of the free surface effect is difficult. As mentioned in Chapter.3, the region that suffers wave loads is varying and the magnitude of wave load is difficult to be quantified. Therefore, the analysis of the free surface effect cannot be carried out on a SDOF system, similar to the analysis of the drag term's effect. Thus an alternative approach for the analysis needs to be proposed.

Therefore a MDOF system is assumed in this analysis. As shown in the figure 4.14, a vertical pipe is fixed at the seabed. The pipe is long enough to carry all the wave loads. The diameter of the pipe is set to 3.5m and the water depth is 94.03m, same as the legs of the Yme MOPUstor. The inertia coefficient is assumed to be 2 and the drag coefficient is assumed to be 0, to avoid the non-linear effect of the drag term. The coordinate of this system is set at the mean water level (MSL).

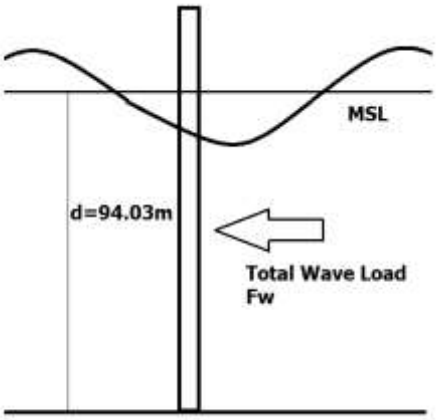

Figure 4.14 the graphical representation of the system

The total wave load of this system can be expressed as,

$$F = \int_{-d}^{\eta} f(z)dz \tag{4.29}$$

As observed in equation (4.23), two non-linearity factors can be identified from this calculation. First, the fluid's velocity in the calculation of the term "$f(z)$" will introduce non-linearity, because the fluid's velocity above the mean water level cannot be described in linear wave theory. Second, the upper bound of this integral is varying with the wave's motion, and thus this integral cannot be solved symbolically. Hence, those two factors need to be linearized before a linear analysis.

Therefore, the study of the linearization in the free surface treatment will focus on two aspects.

(1) The validation of the linear wave's approximation of the fluids above MSL

(2) The validation of the constant wave surface elevation assumption

There are two free surface treatment methods proposed for the linear wave's approximation of the fluids above MSL, which are the extrapolated wave treatment and the wheeler stretched wave treatment. The extrapolated treatment [7] assumes wave kinematic above mean sea level (z=0) constant and equal to the value at z=0 in wave crests, while extrapolated treatment uses airy wave kinematic up to surface elevation in wave toughs. The wheeler stretched treatment [7] calculates wave kinematics at the mean water level at the true surface and its corresponding distribution down to the seabed is stretched accordingly.

Figure 4.15 shows a graphical representation of both the extrapolated wave treatment and the wheeler stretched wave treatment.

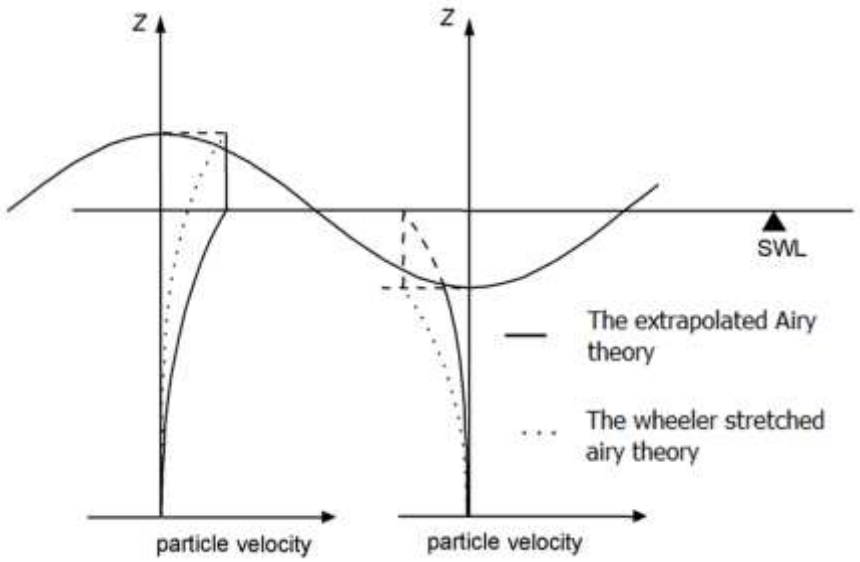

Figure 4.15 the graphical representation of the extrapolated Airy theory and the wheeler stretched airy theory, modified from ref [7].

In addition of the linear waves' approximation, the varying free surface itself also needs to be linearized, for the purpose of the analysis in the traditional frequency-domain method. As mentioned in Chapter 2, for the traditional frequency-domain analysis, a reference wave height is pre-assumed to determine a constant water elevation. The members below this level are assumed to be always submerged, hence the wave loads are only calculated on the structural member below this level.

As predicted by the HFD method in Chapter 3, the non-linear effect of the varying free surface can approximated to be quadratic. Therefore, a constant water surface elevation may neglect this quadratic order effect, and thus results in the deviation, with respect to both its extreme value and dynamic effect.

To analysis the effects of those two kinds of linearization, four cases are selected in this study with reasons. These are,

(1) The total wave load calculated by Stokes-V wave theory
(2) The total wave load calculated by using the extrapolated wave treatment
(3) The total wave load calculated by using the wheeler stretched airy wave treatment
(4) The total wave load calculated by using zero-elevation

Among those four cases, the total wave load calculated by Stokes-V wave theory is the most accurate theoretically and hence set as the reference. The total wave load calculated by using the extrapolated wave treatment and the wheeler stretched wave treatment are used to analysis the validation of the linear wave's approximation of the fluids above MSL. Also, this analysis can be used to assess the accuracy of those two methods. Besides, the total wave load calculated by using zero-wave elevation is used to analysis the validation of the constant wave surface elevation approximation.

The calculation of the wave load is carried out by the self-coded hydrodynamic analysis program, "hydro". The "hydro" is coded in Matlab^{TM} and capable to calculate hydrodynamic loads in time-domain. There are two advantages of the "hydro". First, the "hydro" is coded based on the hydrodynamic knowledge and seriously verified. Thus, the result from "hydro" is believed to be accurate. Second, the hydro is a self-coded program, while the most commercial hydrodynamic calculation programs are packaged and protected by the laws. This property makes the possible to modify the algorithm of the "hydro", especially for cases with the zero elevation assumption. More details of the "hydro" are attached in Appendix I.

The FFT analysis technique is applied in this study to separate the motion in different frequencies. This analysis technique can provide us a fundamental understanding of the non-linearity' influence, especially on the issue of the amplitude and frequency's shift.

To avoid the multi-wave interaction, the single regular waves are applied as the excitation. In order to link the study to the analysis of the Yme MOPUstor, the periods of the waves in this study are selected to be 7sec and 14.5sec, which represent the resonant and extreme wave conditions of the Yme MOPUstor, as shown in Chapter 5.

The first step of this non-linear analysis is to identify the frequencies component of the wave load. Figure 4.16 -Figure 4.19 shows the plots of the FFT analysis for four different sea states. Four characterizes can be observed from these plots. First, the component at the original frequency of the wave ω unquestionably dominates the wave load. Second, the besides the force component at ω, the force component at quadratic frequency 2ω is generated. This force component increases significantly, with the increase of the wave height. Third, with the increase of the wave height, the force's components at the higher order frequencies are observable in the wave load calculated by the Stokes V theory. But those components cannot be predicted by other methods. Fourth, the wave load calculated by both the extrapolation wave treatment and the wheeler stretched wave treatment can predict this quadratic effect of the non-linearity, while the zero wave elevation cannot. Therefore, it can be conclude that the quadratic interaction, as predicted by the HFD methods, exists in this numerical experiment. The non-linearity is mainly contributed by the quadratic interaction.

With the frequencies' component identified, the next step is to investigate the quantitative relation between the wave height and the force components at different frequencies. In this investigation, the two quadratic approximation methods proposed in Chapter 3 are carried out here. Figure 4.20-4.23 shows the plot of the wave height versus the component's amplitude for the linear and quadratic components. As observed from these figures, for the force's component at its original frequency ω, its amplitude increases linearly with respect to the increase of the wave height. This relation can be accurately predicted by all the methods. For the force component at quadratic frequency 2ω, the amplitude increases non-linearly with respect the increase of the wave height. This relation can be predicted by both the extrapolation wave treatment and the wheeler stretched wave treatment, among which the extrapolation treatment shows a better result. This conclusion contradicts to the traditional conclusion that wheeler extrapolation gives a better approximation [9].

In additions, as observed in figure 4.21 and figure 4.23, the two varying surface methods proposed in the HFD methods show a good predication for these two load cases. Therefore, the force component at frequency 2ω can be concluded that, its amplitude increases qudratically with respect to the increase of the wave height.

A dilemma is being faced for the selection of the reference wave height in the traditional frequency-domain methods (constant elevation). On one hand, the extreme value of the wave load predicted by the FD method is smaller than these in reality. This can be compensated by the increase of the reference wave height. On the hand, if the reference wave height is tuned to an optimized value to hold the real extreme value, the force component at the original frequency ω will be overestimated and hence the dynamic effect is distorted.

A recommendation is given for the application of the traditional frequency-domain method. If the analysis is not sensitive to the dynamic effect, the reference wave height should be increased compensate these quadratic forces. If the system is sensitive to the dynamic effect, then the reference wave height need to be tuned to be small enough to avoid the overestimation of the motion.

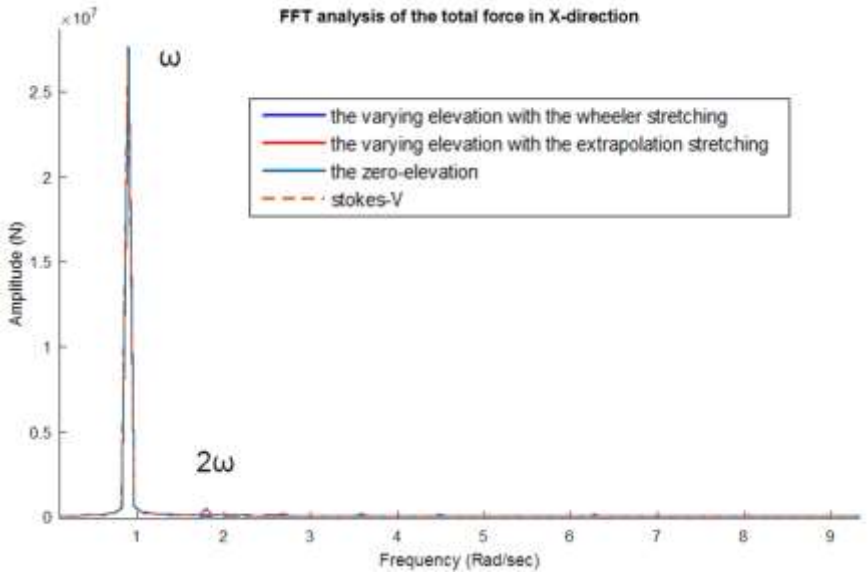

Figure 4.16. the plot of the FFT analysis for H=1m, T=7sec (Sample Frequency 100Hz)

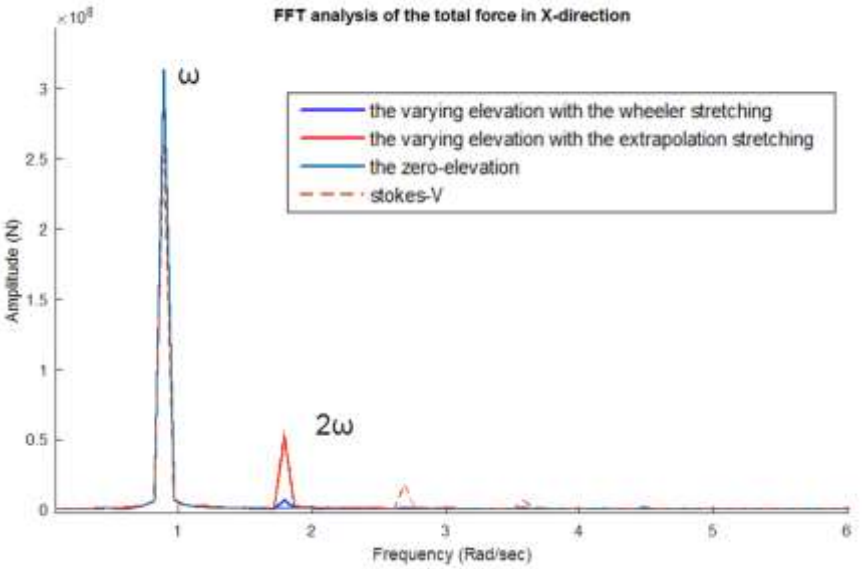

Figure 4.17 the plot of the FFT analysis for H=10m, T=7sec (Sample Frequency 100Hz)

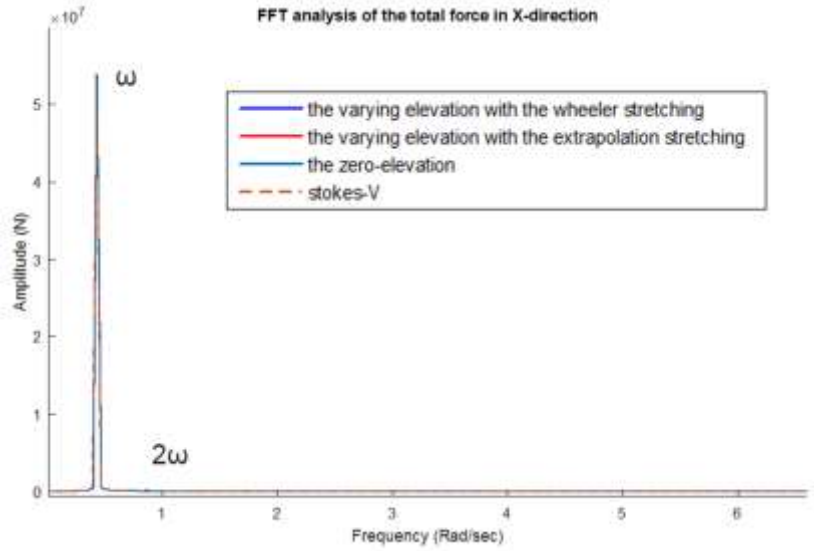

Figure 4.18 the plot of the FFT analysis for H=1m T=14.5sec (Sample Frequency 100Hz)

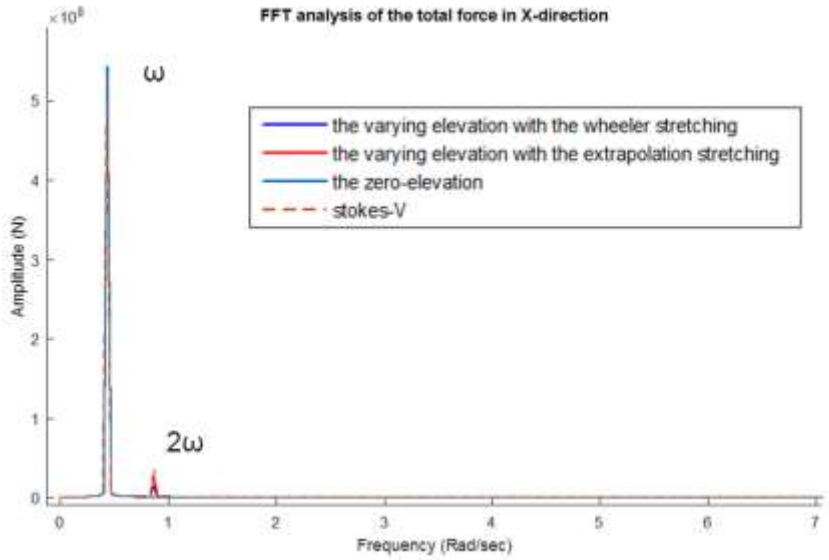

Figure 4.19 the plot of the FFT analysis for H=10m T=14.5sec (Sample Frequency 100Hz)

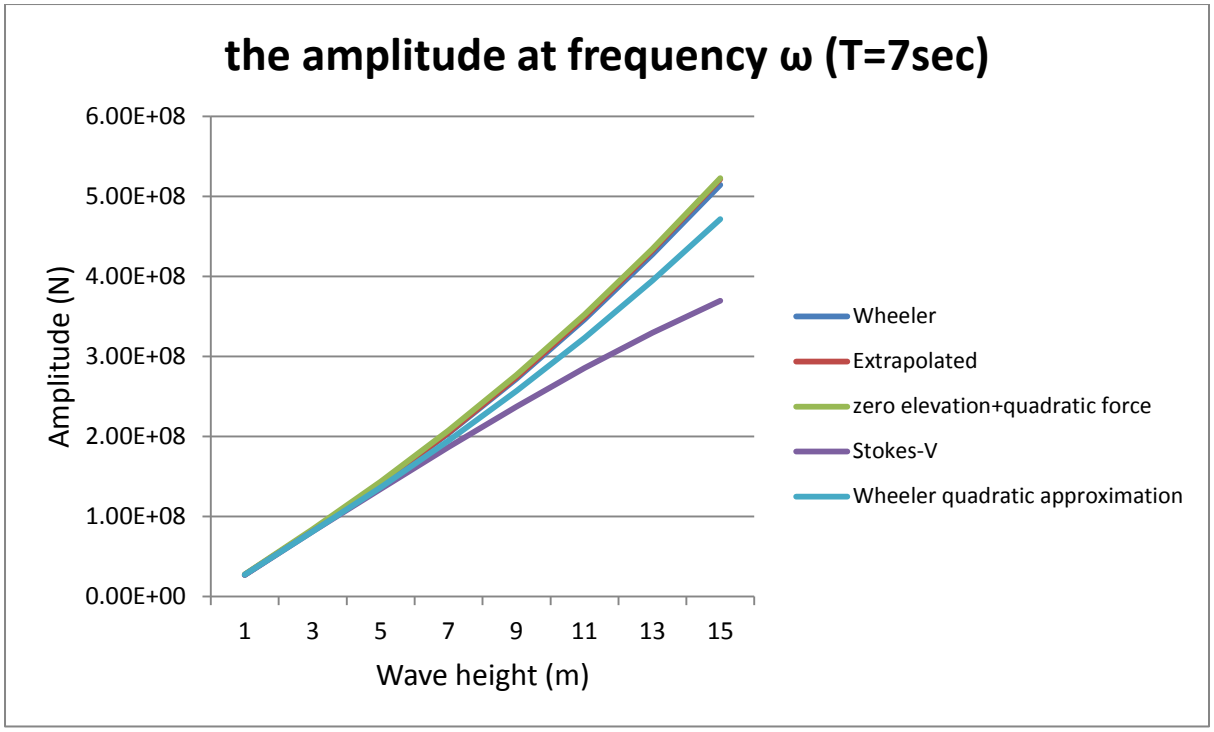

Figure 4.20 the plot of the amplitude at ω versus wave height for T=7sec

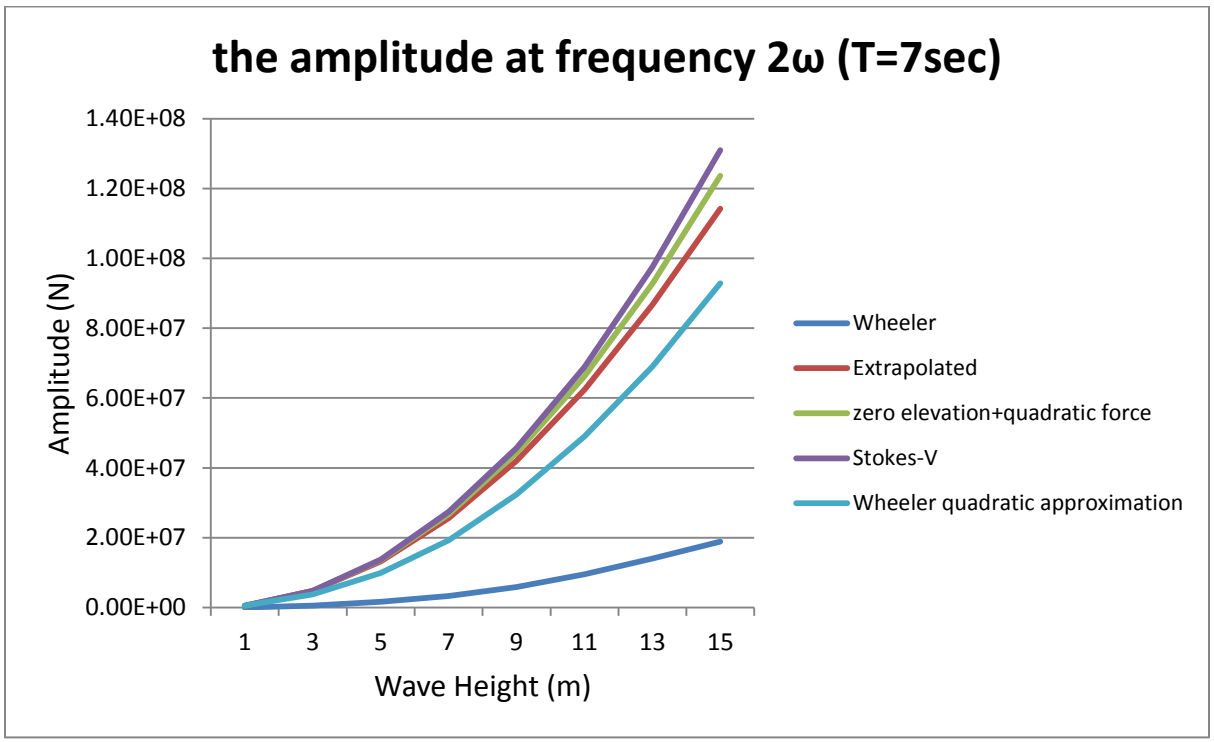

Figure 4.21 the plot of the amplitude at ω versus wave height for T=7sec

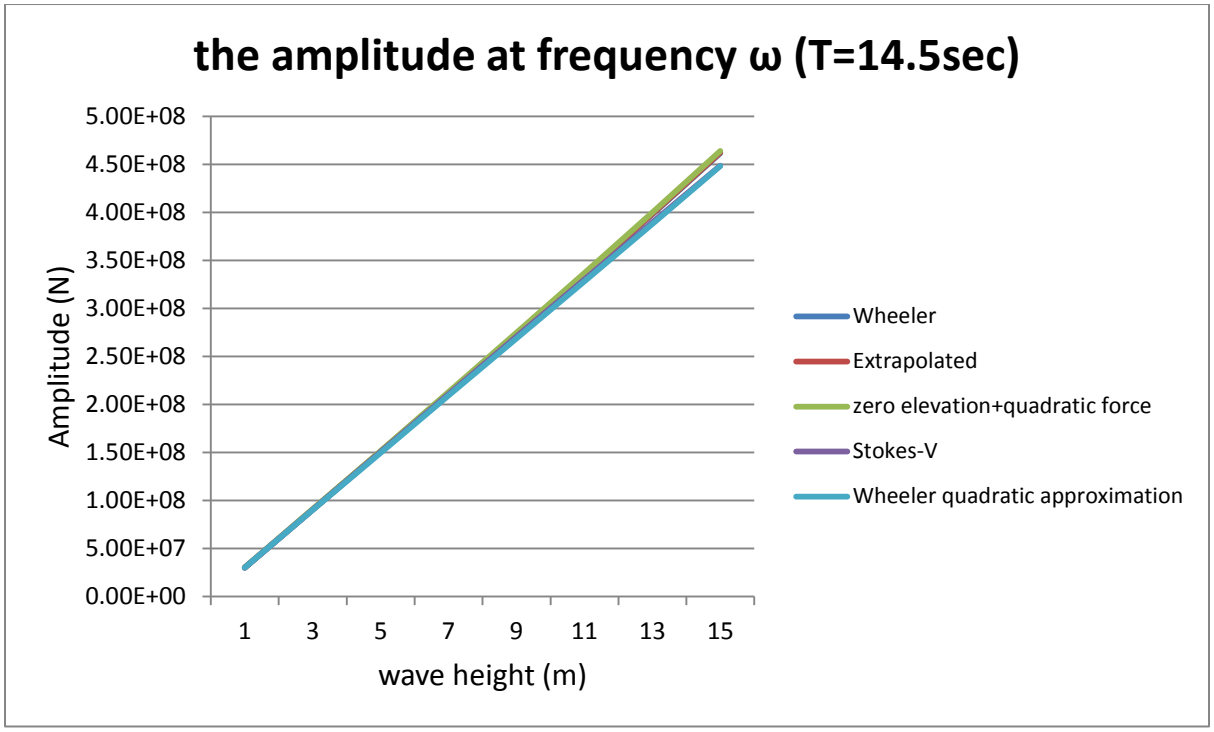

Figure 4.22 the plot for the amplitude at ω versus the wave height for T=14.5sec

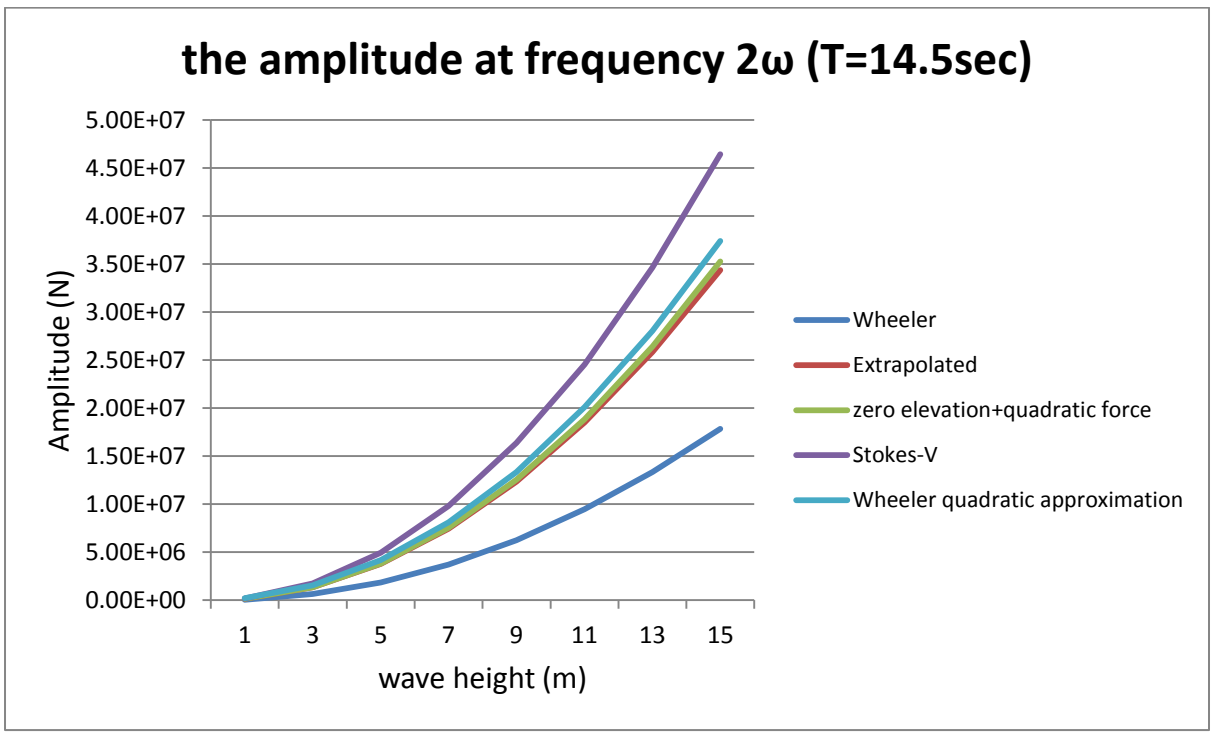

Figure 4.23 the plot for the amplitude at 2ω versus the wave height for T=14.5sec

4.4 Dynamic versus quasi-static analysis

This section presents the study on the issue of the dynamic versus quasi-static analysis. As mentioned previously, for the ultimate limit state analysis, the true dynamic status is sometime represented by an equivalent static status. Thus the study in this section mainly focuses on the validation of this representation.

To analysis the representation of the quasi-static method, two situations have been carried out, from the simple to the complex. These are,

(1) A SDOF system with the single-frequency excitation
(2) A SDOF system with the multi-frequency excitation

In this section, the studies on these two situations are carried out respectively. To analysis the differences between the real dynamic analysis and the quasi-static analysis, the calculations in both methods are presented and compared. The reasons of the deviations are identified and analyzed both qualitatively and quantitatively.

The study on a SDOF system with a single-frequency excitation is carried out first. A SDOF system is assumed and presented as follow.

$$m\ddot{r} + c\dot{r} + kr = f \tag{4.30}$$

Where, m represents the mass of the system, c represents the damping coefficient of the system and k represents the stiffness of the system. In this study, a hypothetical excitation, f, is used for this system.

The accurate "real" dynamic motion can be calculated via the transfer function. The transfer function of this system H_1 can be expressed as,

$$H_1 = \frac{1}{(k - m\omega^2) + \boldsymbol{j}\omega c} \tag{4.31}$$

If the f is a single sinusoidal harmonic excitation, expressed as

$$f = Fcos(\omega t) \tag{4.32}$$

Where F and ω are the amplitude and frequency of the excitation f respectively.

Then the response r can be given in an explicit form, expressed as

$$r = Re\left[\frac{Fe^{\boldsymbol{j}\omega t}}{(k - m\omega^2) + \boldsymbol{j}\omega c}\right] \tag{4.33}$$

For comparison, the equation (4.25) can be rewritten into the static form with only stiffness term and external force involved, expressed as,

$$Kr = f - (m\ddot{r} + c\dot{r}) = Re\left[\frac{KFe^{\boldsymbol{j}\omega t}}{(k - m\omega^2) + \boldsymbol{j}\omega c}\right] \tag{4.34}$$

Therefore, the "extreme value" of the response r can be expressed as,

$$R = Re\left[\frac{F}{(k - m\omega^2) + \boldsymbol{j}\omega c}\right] = \frac{F}{\sqrt{(k - m\omega^2)^2 + (\omega c)^2}}\cos\left(\text{atan}\left(\frac{\omega c}{k - m\omega^2}\right)\right) \tag{4.35}$$

In contrast, the quasi-static analysis defined an equivalent static status which represents the real dynamic situation, via the dynamic amplitude factor (DAF), expressed as,

$$KR_e = DAF * F = F_I + F \tag{4.36}$$

Where F is the equivalent static external force and F_I is the equivalent inertia force, where $F_I = (DAF - 1)F$. DAF is the dynamic amplification factor, which is defined as,

$$DAF = \frac{K}{\sqrt{(k - m\omega^2)^2 + (\omega c)^2}} \tag{4.37}$$

Therefore, the equivalent "static" extreme response of the system can be obtained as,

$$R_e = \frac{F}{\sqrt{(k - m\omega^2)^2 + (\omega c)^2}} \tag{4.38}$$

Compare the (4.35) with (4.38), it can be identified that there is a phase shift term "$\cos\left(\text{atan}\left(\frac{\omega c}{k - m\omega^2}\right)\right)$" exists in the real dynamic analysis, while the quasi-static analysis not. This existence of this phase shift has shown that the maximum external load and the maximum inertia load may not occur at the same time, while this phenomenon is not considered in the quasi-static analysis. Therefore, the quasi-static analysis may result in the overestimation of the extreme condition, expressed as

$$R \leq R_e \tag{4.39}$$

With the deviation factor identified, the next question is how this factor effects the representation of the quasi-static method. Rewrite the phase shift term, we have,

$$\cos\left(\text{atan}\left(\frac{\omega c}{k-m\omega^2}\right)\right) = cos\left(atan\left(\frac{1}{k}\frac{\omega c}{1-(\frac{\omega}{\omega_0})^2}\right)\right) \tag{4.40}$$

As observed from the equation (4.40), the value of this phase shift is dominated by two terms "$\frac{1}{1-(\frac{\omega}{\omega_0})^2}$" and "$\frac{\omega c}{k}$". The term "$\frac{\omega c}{k}$", is usually small for offshore platform. Taking the Yme MOPUstor as an example, with the topside's mass of 12900te and the natural period of 7sec, and damping ratio of 3%, the value of the term "$\frac{c}{k}$" is approximately 0.1130. Then the value of the term "$\frac{\omega c}{k}$" is around 0.0473-0.1420 for the wave period of 5sec – 15sec, which has almost no effect on the total deviation.

The value of the term "$\frac{1}{1-(\frac{\omega}{\omega_0})^2}$" is quite sensitive to the wave's period. The Figure 4.24 shows a plot of the frequency shift versus ω for the mass of 12900te and the natural period of 7sec. As shown in the figure, when the excitation's frequency is beyond the region of the natural frequency of the structure, the value of the "$\frac{1}{1-(\frac{\omega}{\omega_0})^2}$" is quite small and hence the quasi-static analysis is believed to be representative. However, when the wave's frequency is close to the natural frequency of the structure, the value of "$\frac{1}{1-(\frac{\omega}{\omega_0})^2}$" may be infinity large, then there will be an almost 90 degree shift between the maximum external force and the maximum inertia force. The analysis by the quasi-static method will be highly overestimated and then fails to be representative.

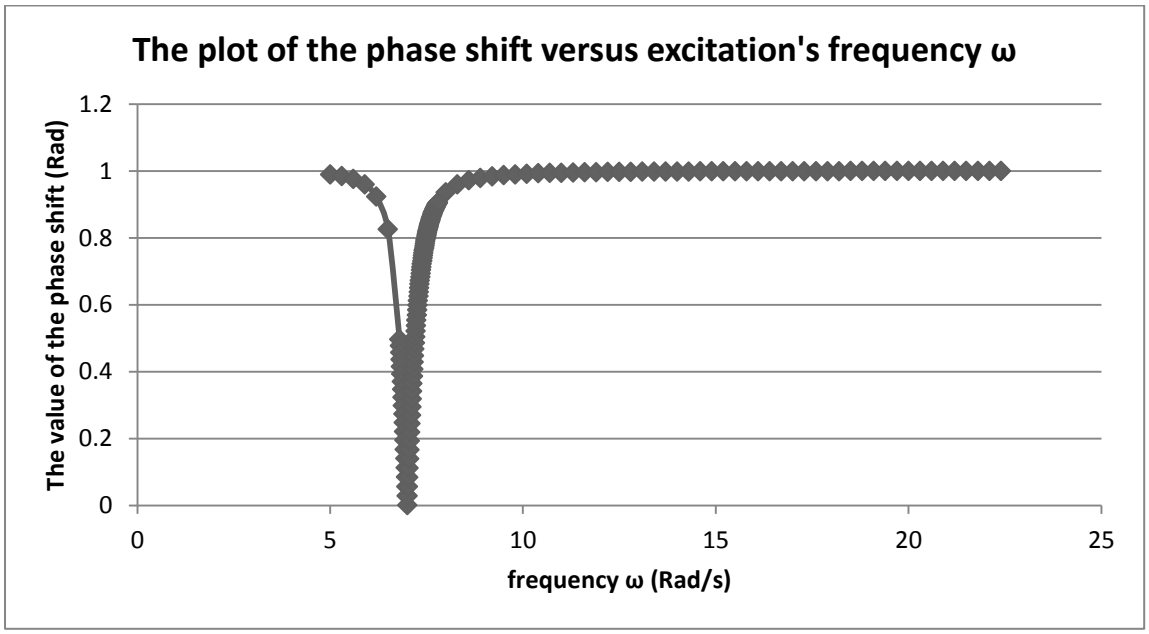

Figure 4.24 the plot of the phase shift versus excitation's frequency ω for the mass of 12900te and the natural period of 7sec

In addition of the study with the single-frequency excitation, the study of the SDOF system with the multi-frequency excitation is also important. As well discussed in the previous chapter, the real excitation of the offshore condition is stochastic in nature, which means the excitation component at different frequencies will contribute different dynamic effects. In the quasi-static analysis, however, only one DAF coefficient is applied to the estimate the inertia load. Thus it is critical to select a proper DAF estimation approach, in order to maximize the accuracy in a quasi-static analysis. The representation of DAF value for multi-frequency excitation is unavoidable to be checked.

As recommended [8], two methods are general proposed for the jack-up analysis, the simplified DAF method and the stochastic DAF method. The simplified DAF is calculated based on the peak frequency of the spectrum and the stochastic DAF is calculated as a balance of the response components at all the frequencies. Both methods are used in analysis of the Yme MOPUstor without further investigation. Therefore, in this study, both methods need to be analyzed fundamentally.

With all these considerations, a numerical experiment is carried out on a linear SDOF system. For the purpose of comparison and validation, this experiment is to calculation the extreme displacement with return period of 3hrs by three methods with different wave's characteristics:

(1) Simplified DAF
(2) Stochastic DAF
(3) Frequency-domain (True Dynamic)

The coefficients of this SDOF represent a simplified status of the Yme MOPUstor. Thus the mass, damping and stiffness coefficients for the SDOF system is assumed to be 12900te, 1.14E+06 Ns/m and 1.01E+07 N/m (calculated from (2.20) (2.21), based on 7sec natural period, 3% damping ratio). However, it should be clear this experiment is only intended for a more realistic study of the dynamic versus quasi-static method. The results have no representation of the real dynamic analysis of the Yme MOPUstor.

The external load is defined to be the linearized total external wave load in y direction with the wave direction of 90deg. The spectrum external total load f is calculated in the traditional frequency domain method, expressed as

$$S_{ff}(\omega) = S_{\eta\eta}\big(H_s, T_p, \gamma, \omega\big) RAO_f{}^2(\omega) \tag{4.41}$$

Where $S_{ff}(\omega)$ is the spectrum of the force. $RAO_f{}^2(\omega)$ refers to the transfer functions from the wave to the total wave load of the Yme MOPUstor in Y-direction. These transfer function is calculated from Sesam^{TM}-Wajac, for the purpose of the demonstration. The FEM model for calculation is given in Chapter 5. $S_{\eta\eta}(\omega)$ refers to the Jonswap spectrum of the waves. In this calculation, the significant wave height H_s is assumed to be 5m and the enhance peak factor γ is assumed to be 3, for convenience.

To begin with, for the quasi-static calculation by the simplified and stochastic DAF method, the extreme value of the f within 3hrs is determined statically, based on the Rayleigh distribution, which are,

$$f_{max,3hrs} = \sqrt{2M_{f0} \ln\left(\frac{3x3600sec}{T_{f,x}}\right)} \tag{4.42}$$

Where, the terms $T_{f,x}, M_{f0}\ and\ M_{f2}$ are the mean zero-crossing period, zeroth moment and second moment of the force spectrum, as introduced in Appendix II.

The simplified DAF and stochastic DAF are calculated based on the structural and hydrodynamic property of this SDOF system. The peak frequency of the wave spectrum is adopted as the reference frequency of simplified DAF calculation, based on the equation (2.18). The calculation of the stochastic DAF value is based on the force spectrum, expressed as,

$$SDAF = \sqrt{\frac{\int H_{dyn}(\omega)^2 S_{ff}(\omega) d\omega}{\int H_{static}(\omega)^2 S_{ff}(\omega) d\omega}} \tag{4.43}$$

Where $H_{dyn}(\omega)$ is the dynamic transfer function of the SDOF system, same as $H_1(\omega)$ in the equation (3.35), $H_{static}(\omega)$ is the static transfer function, which equals 1/K.

Hence, the extreme displacement in 3hrs predicted by the simplified and stochastic DAF method can be expressed as,

$$r_{DAF} = \frac{DAF \cdot f_{max,3hrs}}{K} \tag{4.44}$$

$$r_{SDAF} = \frac{SDAF \cdot f_{max,3hrs}}{K} \tag{4.45}$$

Where, r_{DAF} and r_{SDAF} are the extreme responses predicted by the simplified and stochastic DAF method respectively.

With these quasi-static methods defined, the extreme value from true dynamic calculation is performed by the traditional frequency-domain method. The expression of the responses spectrum is expressed as

$$S_{rr}(\omega) = H_{dyn}^2(\omega) * S_{ff}(\omega) \tag{4.46}$$

$$r_{max,3hrs} = \sqrt{2M_{r0} \ln\left(\frac{3x3600sec}{T_{r,x}}\right)} \tag{4.47}$$

Where, the terms $T_{r,x}, M_{r0}\ and\ M_{r2}$ are the mean zero-crossing period, zeroth moment and second moment of the response spectrum $S_{rr}(\omega)$.

Figure 4.25 shows the plot of the wave peak frequency T_p versus the extreme displacements predicted by these three methods. Three characteristics can be clearly observed from this plot. First, the stochastic DAF method accurately predicts the extreme displacement of the real dynamic analysis, while the simplified method cannot. Second, the simplified method overestimates the displacement in resonant zone, underestimates the displacement in non-resonant zone. Third the extreme displacements calculated by both the simplified DAF and the stochastic DAF are overestimated, as predicted previously.

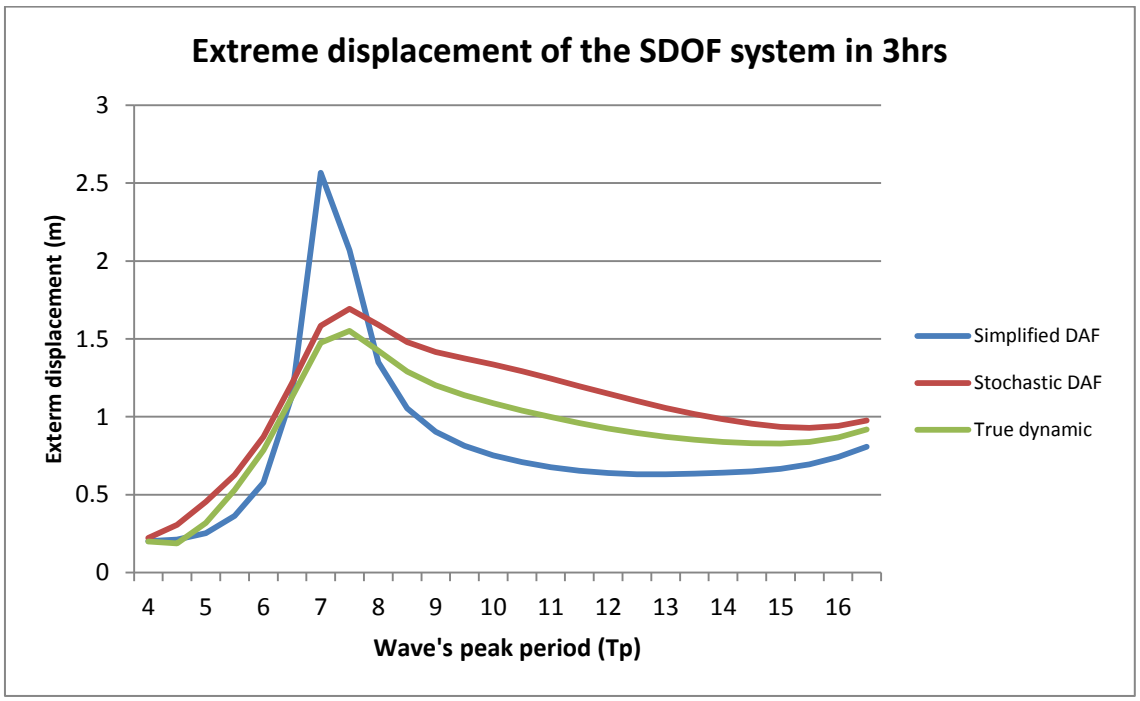

Figure 4.25 the extreme displacement of the SDOF system in 3hrs

The reason causes the unrepresentative of the simplified DAF method is that, in reality, the energy is distributed along frequencies for the stochastic wave. For the simplified DAF calculation, however, the total energy is concentrated in the peak frequency of the spectrum. Some energy will be split into the resonant region for the stochastic wave in non-resonant condition so that the actual dynamic effect is increased. In opposite, some energy will be split beyond the resonant zone for random wave in resonant condition so that the actual dynamic effect is decreased. These phenomenon cannot be predicted by only peak frequency of the spectrum, and thus results in the unrepresentative of the simplified DAF method.

In addition of those differences, the representation of the SDOF model for a MDOF system is also debatable. First, the MDOF system usually has several dominate natural periods, which cannot be reflected by a SDOF model. Taking the example of the Yme MOPUstor, as mentioned, there are three dominated natural periods for this platform, which are sway, surge and yaw. These three natural periods may have a combination effect on the global dynamic behavior. However, the DAF calculation based on SDOF assumption can only introduce the dynamic effect for one single natural period, and hence fails to be representative. Second, the actual inertia load distribution cannot be reflected by the DAF estimation. This part will be further discussed in Chapter 6.

To sum up, in the study of the dynamic versus the quasi-static analysis, the conclusion can be summarized as follows.

(1) In real dynamic situation, there may be a phase shift between the maximum external load and the maximum response. This frequency shift cannot be considered in the quasi-static analysis. Therefor the quasi-static analysis may overestimate the motion.

(2) The quasi-static analysis based on stochastic DAF is believed to be more accurate than the quasi-static analysis based on the simplified DAF. The analysis based on the simplified DAF may underestimate the motion for non-resonant condition. It also may overestimate the motion for the resonant condition.

(3) The representation of the SDOF model for a MDOF system is debatable. This simplification may cannot reflect the real dynamic effect and load distribution.

5.0 METHODOLOGY FOR THE COMPARATIVE STUDY

5.1 General

This chapter presents the methodology for the comparative study on the Yme MOPUstor platform. As mentioned previously, this comparative study focuses on the ultimate limit state check. There, the analyses are carried out to determine the extreme responses in 3hrs simulation for two given sea states, as shown in Table 5.1. These two sea states are selected based on the study of Atkins [4]. The load case 1 represents the resonant condition of the platform, which gives the maximum dynamic effect. The load case 2 represents the extreme wave condition of the platform, which gives the maximum wave loads.

Table 5.1. the selected environmental conditions for this comparative study

Environmental Condition	$H_s(m)$	T_p (sec)	$H_{max}(m)$	$T_{ass}(sec)$	Wave direction
Load Case 1	6.03	7.03	11.43	7.1	90 deg
Load Case 2	14.2	15.9	24.58	14.58	90 deg

The dynamic analysis methods applied in this comparative study are,

- The quasi-static analysis method
- The traditional frequency domain analysis method
- The time-domain analysis method

The dynamic analyses of all these three methods are performed by the DNV software, Sesam^{TM}-Genie^{TM}. The Sesam^{TM}-Genie^{TM} is a package of software for the design and analysis of the offshore structures, integrating the concept modelling, FEM mesh, static and dynamic analysis and the result evaluation, as shown in figure 5.1.

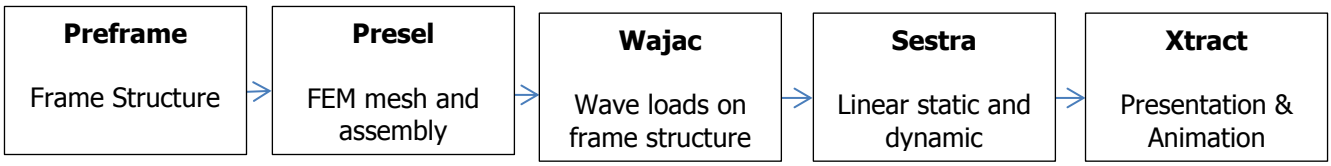

Figure 5.1 the calculation procedure of the Sesam^{TM}-Genie^{TM}

As observed in figure 5.1, each function of the Sesam^{TM}-Genie^{TM} is performed by an independent sub-program. However, the integral interface of the Sesam^{TM}-Genie^{TM} is only limited to the quasi-static analysis and no package for the post-processing is contained in the Sesam^{TM}-Genie^{TM}. Therefore, the dynamic analysis in this comparative study is executed with each package independently and a self-made post-processing program.

To sum up, the configuration of the dynamic analysis methods in this study is summarized in table 5.2.

Table 5.2. the configuration of the dynamic analysis methods			
	Quasi-static	Frequency-domain	Time-domain
Sesam™ - Genie™ interface	The FEM model of the Yme MOPUstor		
Sesam™ - Wajac™	The maximum single wave load	Fully non-linear stochastic wave	Linearized drag force and constant elevation ($H_{ref} = 1m$)
Sesam™ - Sestra™ + Xtract™	SDAF (based on natural period of 7sec)	Explicit Newmark-beta method (time step $\Delta t = 0.25sec$)	Structural transfer function
Self-code in Matlab™	No-need	Generalized extreme value distribution	Rayleigh distribution

This comparative study will focus on four aspects, which are

(1) The effect of the linearized versus non-linear
(2) The effect of the dynamic versus quasi-static analysis
(3) The effect of the stochastic versus deterministic
(4) Efficiency

The study of the non-linearity is mainly based on the spectrum analysis of the external force and the responses between the frequency-domain method and the time-domain method. To control variables, the dynamic analysis with only the drag coefficient presented and only the inertia coefficient presented are also performed respectively in study. Since the structure is linearized, the dynamic analysis follows the principle of superposition, and hence these separated studies are believed to be representative. The non-linearities involved these separated dynamic analyses are identified in the table 5.3 respectively.

Table 5.3. the nonlinearity identification of the separated dynamic analysis		
Method	Inertia	Drag
Frequency domain	Constant elevation	Constant elevation + Linearized drag force
Time domain	Varying elevation with the wheeler treatment	Varying elevation with the wheeler treatment + non-linear drag force

The study of the dynamic versus the quasi-static analysis is carried out on the inertia loads comparison between the quasi-static analysis and the frequency domain analysis. To control variables, however, the DAF in this part of the study will be estimated by the linearized wave load to synchronize the frequency domain method. Both the magnitude and the distribution of these loads are analysed in this study.

The study of the stochastic versus deterministic consists of two parts. The first part focuses on the representation of the single wave load, with respect to the real stochastic wave load. The second part of this study focuses on the representation of the design wave load method, which is used to reconstruct a load distribution when the response is maximized.

5.2 FEM model for the comparative study

The structural model of Yme MOPUstor used in study is the global FEM model of Yme MOPUstor provided by Atkins Ltd, as shown in the figure 5.2.

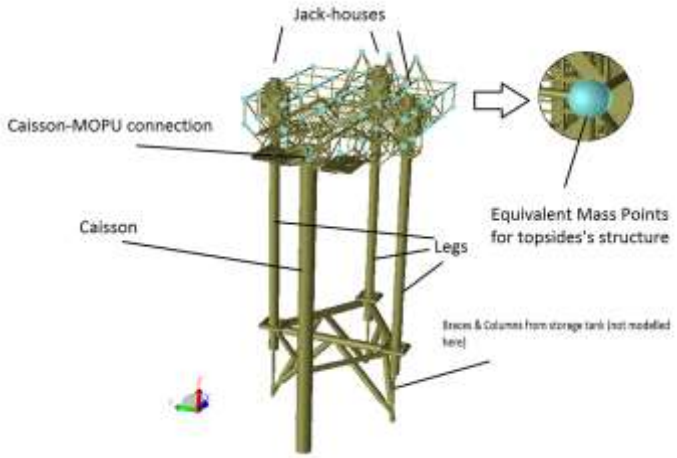

Figure 5.2. Overview of the Atkins's Model

The Atkins's model is a simplified linear elastic beam model of the Yme MOPUstor. The storage tank is not modelled directly. Instead, the local flexibility of the tank is accounted for in the supports of tower. All the relative geometries and connections have been modelled and verified by Atkins [4] based on the basic properties of the Yme MOPUstor.

The coordinate system is set at the seabed level of the model. The x-direction is set to be the caisson to forward legs direction, and then the starboard side and port board side's legs can be defined as figure 5.3.

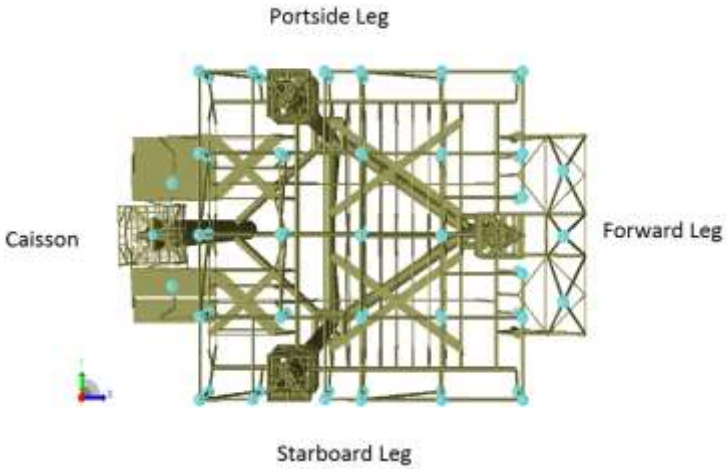

Figure 5.3 Nomenclature of the Yme MOPUstor

Three interest elevation levels (or EIs) for the legs' responses are highlighted. Those are the level at bottom of the legs: EI 39.9m, the level at the top of the legs: EI 119.4m and the level at the cut level: EI 100.125, as shown in Figure 5.4.

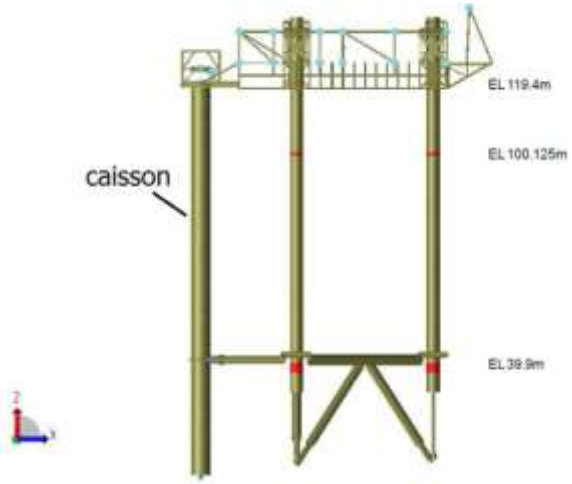

Figure 5.4 elevations of interest leg section's locations

The total mass of the MOPU is 1.29×10^7 kg, the model stiffness has been tuned so that the natural periods of the three main modes (Surge, Sway and Yaw, see Figure 2.5 below) closely match those measured, as listed in table 5.4

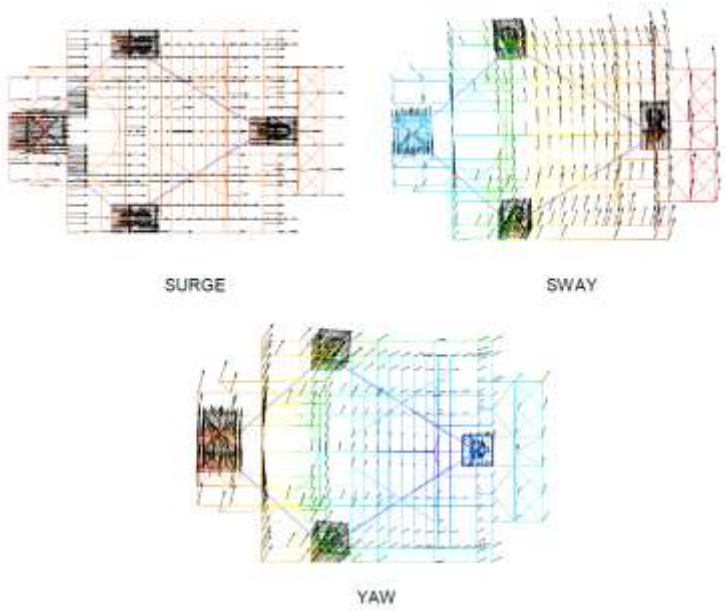

Figure 5.5 the graphical representation of the global modes.

The damping coefficients of the Yme MOPUstor are estimated based on the ratio of critical damping. A study on damping term has been carried out by Atkins two years ago [34]. The total damping consists of four major components: structural damping, viscous damping, radiation damping and wind damping. According to Atkins's studies, the total is estimated as 3% of critical damping for each mode.

Due the misalignment between axial force and deformed legs, second order effect exists. The second order effect, or $P-\Delta$ effect will provide an extra bending moment on the legs. In Atkins model the $P-\Delta$ effect is modelled as a negative spring at the location of jack-houses.

In conclusion, with all relative characteristics properly modelled, it is reasonable to assume the Atkins's model has capable of reflecting the dynamic response properties of the real Yme MOPUstor and thus is valid to be adopted as this model for the comparative study.

Table.5.4 Natural period of platform (measured) and model

Mode	Natural Period (Sesam^{TM} Model) (Sec)	Natural Period (Measured) (Sec)
Sway	6.97	7.1
Surge	6.53	6.7
Yaw	5.15	5.3

Several reference responses are selected for this comparison. First, the displacement at the top of the legs and the caisson are selected as the references, since they directly reflect the total deformation of the Yme MOPUstor platform and the relative movement between the caisson and the topside. Furthermore, in order to inspect the inner interaction of each leg, the total shear forces and bending moments at the base of each leg are also chosen. The table.5.5 and figure 5.6 show the corresponding result type of the nodes or element extracted from Sesam^{TM} model.

Table 5.5 Result used as reference response

Type	**Number**	**Output Component**	**Comment**
Shear Force and Bending Moment at base level (EL39.9m)	Element 200	Displacement: Translational Component in global coordinate: TX, TY, TZ (Unit: m)	Caisson
	Element 1405		Starboard leg
	Element 1580		Portside Leg
	Element 3224		Forward Leg
Displacement at top level (EL119.4m)	Node 102	Element average sectional force (G-Force) Axial Force: NXX (Unit: N) Shear Force in local y and z direction: NXY, NXZ (Unit: N) Torsional Moment: MXX(Unit: Nm) Bending moment in local y and z direction: MXY, MXZ (unit: Nm)	Caisson
	Node 864		Starboard leg
	Node 870		Portside Leg
	Node 1612		Node (32.7,9,117.5) close to gravity center of the topside
	Node 2070		Forward Leg

The table.5.5 and figure 5.6 show the corresponding result type of the nodes or element extracted from Sesam^{TM} model.

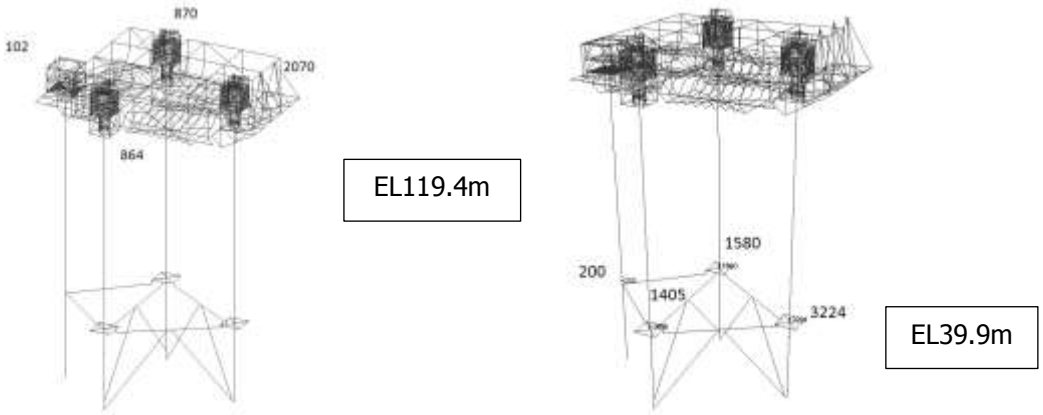

Figure 5.6. Example of a set of reference response in Sesam^{TM} Xtract GUI

6.0 RESULT AND ANALYSIS

This chapter presents the results and analyses of the comparative study with respect to the dynamic analysis of the Yme MOPUstor platform. As mentioned in Chapter 5, the comparative study is carried out between the quasi-static method, frequency-domain method and time-domain method, in four aspects.

These aspects are the effect of the non-linearity (drag term and free surface elevation), the issue of the dynamic versus the quasi-static, the issue of the deterministic versus the stochastic and the efficiency. The results and analyses on these four aspects are carried out respectively. A table of conclusion and practice advice is also provided in this chapter.

6.1 The effect of the non-linearity

To begin with, the result and analysis of the non-linearity is carried out. This study focuses on the difference between the frequency domain and the time domain method. This analysis in this section consists of two parts.

(1) Free surface treatment
(2) Linearized versus non-linear drag term

For a better understanding, a qualitative analysis of these two non-linearity factors are carried out first. Then, the spectrums of the total external force in Y direction (sample frequency 2Hz) are used to identify and analysis these effects quantitatively.

The non-linearity effect of the drag-force term is evaluated first. The influence of the drag force can be estimated by the Keulegan–Carpenter number. A higher KC-number indicates a higher influence of the drag force term. According to ref. [9], section 6.6.1.5, the KC-number in the stochastic wave can be defined as

$$K_c = \frac{TV_{max}}{D} \cong \frac{T_z V_{max}}{D} \tag{6.1}$$

Where $T_z = 2\pi\sqrt{\frac{M_0}{M_2}}$, $V_{max} = \sqrt{2M_2 \ln(\frac{3hr}{T_z})}$, M_o, M_2 are the zeroth and second moment of the wave spectrum, D is the diameter of the legs.

Table 6.1. corresponding KC-number of all the load cases

Load Case	H_s (m)	T_p (sec)	Diameter (m)	KC-Number
1	6.03	7.03	3.5	1.41
2	14.2	15.9	3.5	8.99

Table.6.1 shows the corresponding KC-number for each load case. According to ref [6], section 6.7.2, KC=3 can be treated as a threshold of the drag force's influence.

Hence the load case 1 satisfies the KC criteria for the linearized calculation, while the drag force's influences in the load case 2 are significant.

Second, the non-linearity effect of the free surface elevation is evaluated. As indicated in ref [6], section 3.2.1, the steepness can be used to determine how strong the free surface elevation effects are, in a specific conditions. A higher steepness indicates a higher non-linearity of varying wave elevation. According to ref [6], section 3.5.3, the significant steepness of a sea state can be defined as,

$$S_{m02} = \frac{2\pi}{g}\frac{H_s}{T_z^2} = \frac{2}{\pi g}\frac{M_2}{\sqrt{M_0}} \tag{6.2}$$

Where the term "S_{m02}" is defined to be the average steepness.

Table.6.2 shows the significant steepness of each load case. From table.6.2, it is obvious that the steepness in the extreme wave conditions is four orders higher than these in the "resonant" conditions. Hence, it can be predicted that the non-linear effect of the varying free surface should be much stronger in the load case 2 than the load case 1.

Table 6.2. the corresponding steepness for all the load cases

Load Case	H_s(m)	T_p(sec)	D (m)	Significant Steepness
1	6.03	7.03	3.5	9.8E-08
2	14.2	15.9	3.5	2.2E-04

In summary, the pre-assessment of the drag and steepness' influence has shown that the non-linear effect in the load case 2 is much stronger than these in the load case 1. Therefore, it should be observed larger deviation for the analysis of the load case 2 than the load case 1 by the traditional frequency domain method.

With all the non-linearity factors pre-assessed, the next step is to analysis the spectrum of the total external force in Y direction. As discussed in Chapter 4, the nonlinear effect of the varying free surface elevation can be approximated to be quadratic and the nonlinear effect of the drag term can be approximated to be cubic. Therefore, the frequency shifts should be observed in the spectrum plot. These shifts should consist of two parts: the frequency shift due to the varying free surface elevation and the frequency shift due to the non-linear drag force. To identify the influence of these two parts, the analyses with only the drag term presented and only the inertia term presented are also performed respectively. Table 6.3 shows the identification of the non-linearity contained in each analysis.

Table 6.3. the identification of the non-linearity contained in each analysis

Method	Inertia	Drag
Frequency domain	Constant elevation	Constant elevation + Linearized drag force
Time domain	Varying elevation with the wheeler treatment	Varying elevation with the wheeler treatment + non-linear drag force

The analysis of the varying free surface elevation is carried out first. Figure 6.1- Figure 6.2 show the spectrum of the external force in Y-direction with only the inertia term presented for the load case 1 and the load case 2 respectively. As marked in these figures (marked by the blue circles), two trends of the frequency shifts occurred in these figures. One trend occurs at the region lower than the main frequency band. These frequency shifts represents the substraction part of the original frequency. The other trend occurs at the region higher than the main frequency band. These frequency shifts represent the summation part of the original frequency. Besides with the increase of the wave height (from LC1 to LC2), these trends become more observable.

In addition, the extreme values predicted by the time-domain method and the frequency-domain methods also provide some information. Table 6.4 shows the 3hrs extreme value predicted by the time-domain method and the frequency-domain method respectively. As observed from the table 6.4, however, there is no decrease of the accuracy of the load case 1 compared with the accuracy of the load case 2 with respect to the extreme value.

Table 6.4. the 3hrs extreme value predicted by the time-domain and the frequency domain method with only the inertia term presented

Method	LC 1		LC 2	
	3hrs extreme value	Error	3hrs extreme value	Error
Time – domain	$3.89MN$	--	$19.3MN$	--
Frequency - domain	$3.25MN$	16.5%	$16.8MN$	12.95%

Therefore, it can be concluded that the frequency shift caused by the varying wave elevation can be identified in the spectrum. However, the varying wave elevation effect with respect to the extreme value is not clear for the dynamic analysis of the Yme MOPUstor.

With the effect of the varying free surface elevation analysed, the next step is to analysis the effect of the non-linear drag force. Figure 6.3 - 6.4 show the spectrum of the total external force in Y direction with only the drag term presented for the load case 1 and the load case 2 respectively. As marked in these plots (the drag force marked by the dark circles and the varying free surface effect marked by the blue circles), the non-linearity effect are significant. Three characters can be clearly observed in those figures. First, it is quite clear that the frequency-domain severely underestimated the drag force. Second, due to the present of the non-linearity drag force, two significant frequency shifts occur at the low frequency region and the high frequency region, which cannot be observed in the figure 6.1 and the figure 6.2. Third, the effect of the varying wave surface can still be observed in the figure 6.3 and figure 6.4, as marked by the blue circles.

Table 6.5. The 3hrs extreme value predicted by the time-domain and the frequency domain method with only the drag term presented.

Method	LC 1		LC 2	
	3hrs extreme value	Error	3hrs extreme value	Error
Time – domain	$2.387MN$	--	$19.3MN$	--
Frequency - domain	$0.884MN$	62%	$0.910MN$	94%

Table 6.5 shows the 3hrs extreme value predicted by the time-domain and the frequency domain method with only the drag term presented. The drag force of current is added to the extreme value separately. It can be clearly observed from the table that the linearized drag term significantly underestimates the result and with the increase of the drag effect (or KC-number), this underestimation has become even worse (62% to 94%).

Therefore, it can be concluded that the frequency shift caused by the drag force can be identified in the spectrum. And the linearization of the drag force in this calculation thus may be invalid.

Finally, the spectrum of the total force with both the drag and the inertia force are presented. Figure 6.5- figure 6.6 show the spectrum of the total external force in Y direction for the load case 1 and the load case 2 respectively. As observed from these two plots, due to the superposition of the drag forces and the inertia forces, the spectrum at peak frequency have been enhanced and the non-linearity effect has been reduced. However, the superposition of the drag forces and inertia force is not the simple summation. As indicated in the Morison equation, there is a 90 degrees phase shift between the inertia force and the drag force. Therefore, this phase shift will result in a moderate extreme value, instead of the simple summation. Table 6.6 shows the 3hrs extreme value with both drag and inertia term presented. As shown in the table, the deviations of the frequency domain method are moderate, with in a certain range. Also, the deviation of the frequency domain method increases, with the increase of the wave height. The extreme topside's displacement in 3hrs simulation has verified this prediction, as shown in table 6.7.

Table 6.6. the 3hrs extreme value predicted by the time-domain and the frequency domain method with both the drag term and the inertia term presented.

Method	LC 1		LC 2	
	3hrs extreme value	Error	3hrs extreme value	Error
Time – domain	$4.09MN$	--	$24.5MN$	--
Frequency - domain	$3.22MN$	6%	$17.4MN$	29%

Table 6.7. the 3hrs extreme topsides' displacement predicted by the time-domain and the frequency domain method with both the drag term and the inertia term presented.

Method	LC 1		LC 2	
	3hrs extreme value	Error	3hrs extreme value	Error
Time – domain	0.7436	--	0.9469	--
Frequency - domain	0.8051	-8.27%	0.5577	41.10%

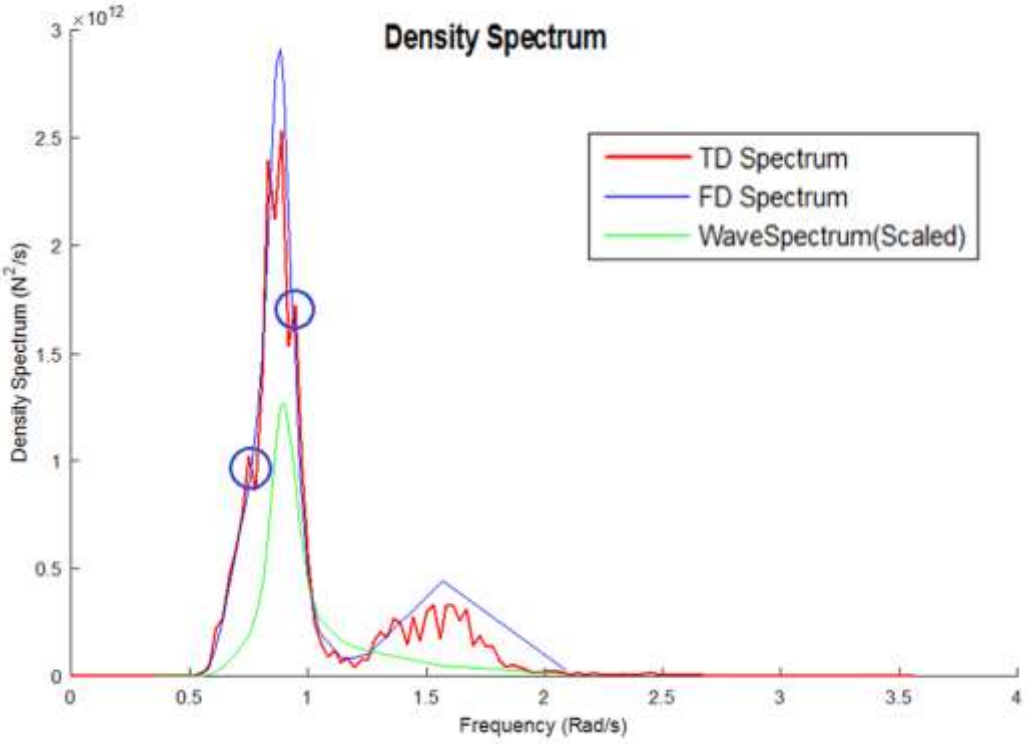

Figure 6.1. the density spectrum of the total external force in Y direction (inertia only) for the LC 1 (Sample Frequency 3Hz)

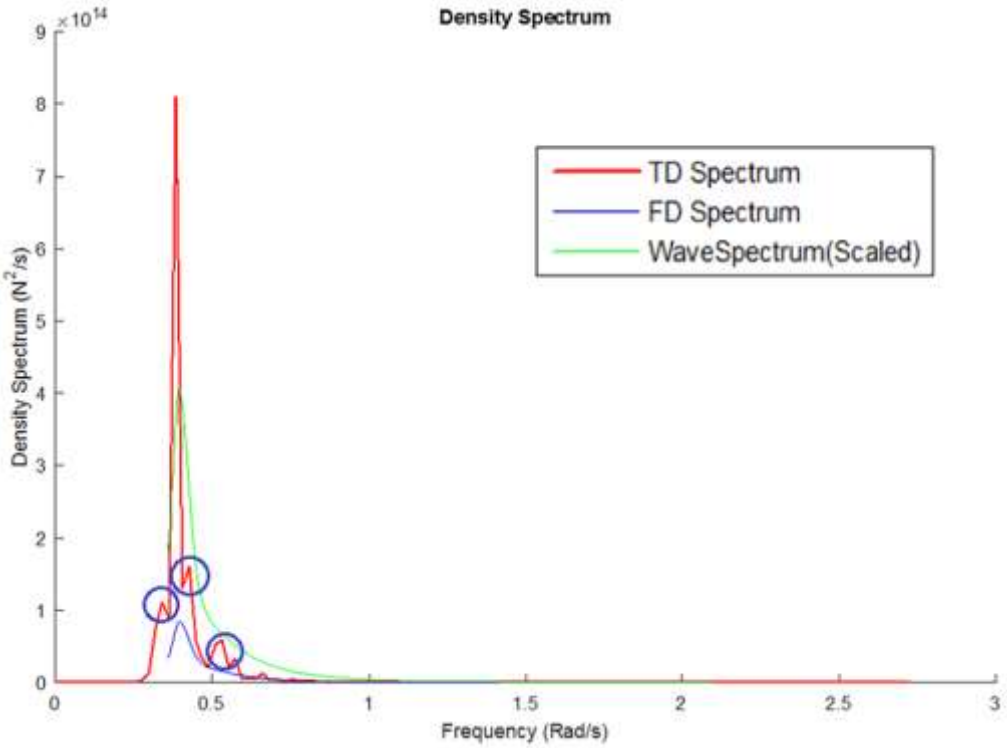

Figure 6.2. the density spectrum of the total external force in Y direction (inertia only) for the LC 2 (Sample Frequency 3Hz)

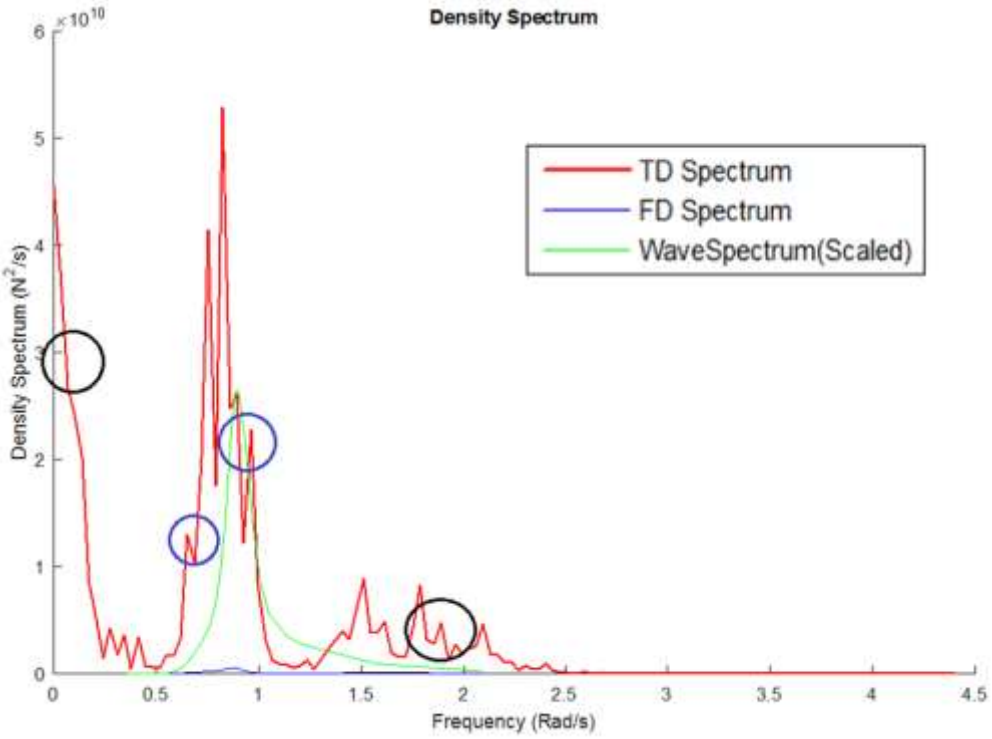

Figure 6.3. The density spectrum of the total external force in Y direction (drag only) for the LC 1 (Sample Frequency 3Hz)

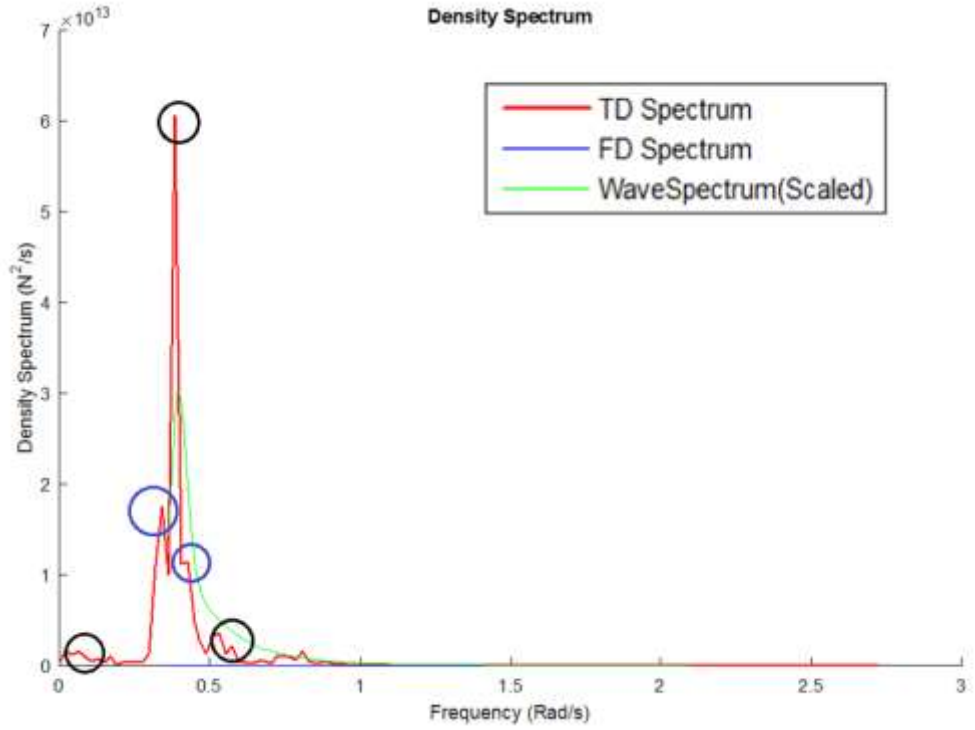

Figure 6.4. The density spectrum of the total external force in Y direction (drag only) for the LC 2 (Sample Frequency 3Hz)

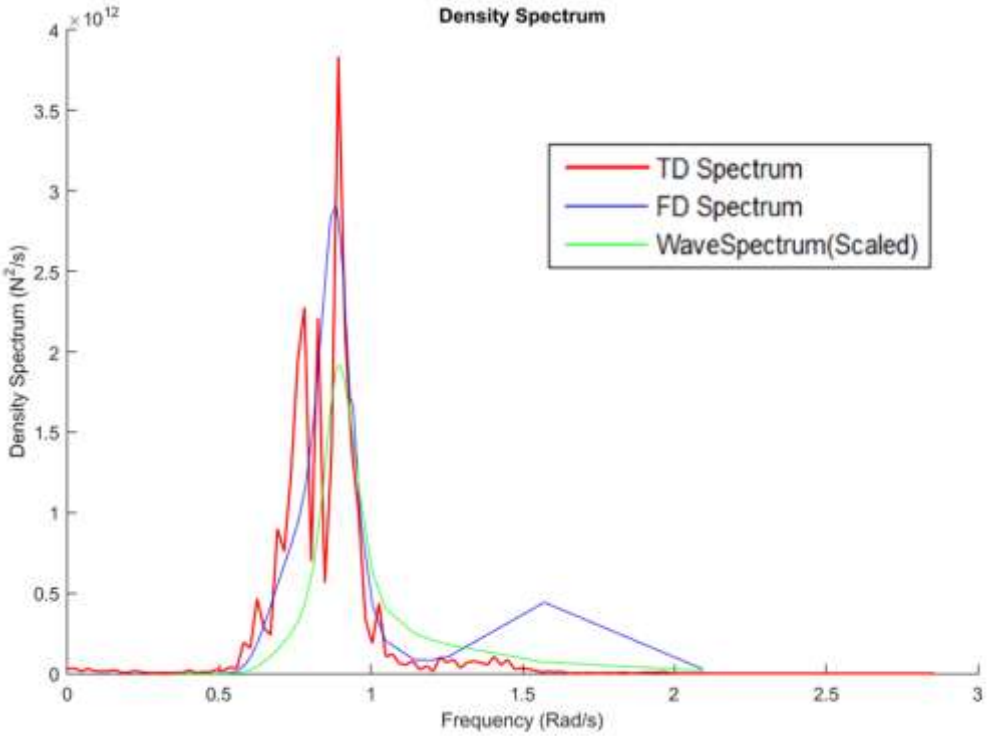

Figure 6.5. The density spectrum of the total external force in Y direction (drag and inertia) for the LC1 (Sample Frequency 3Hz)

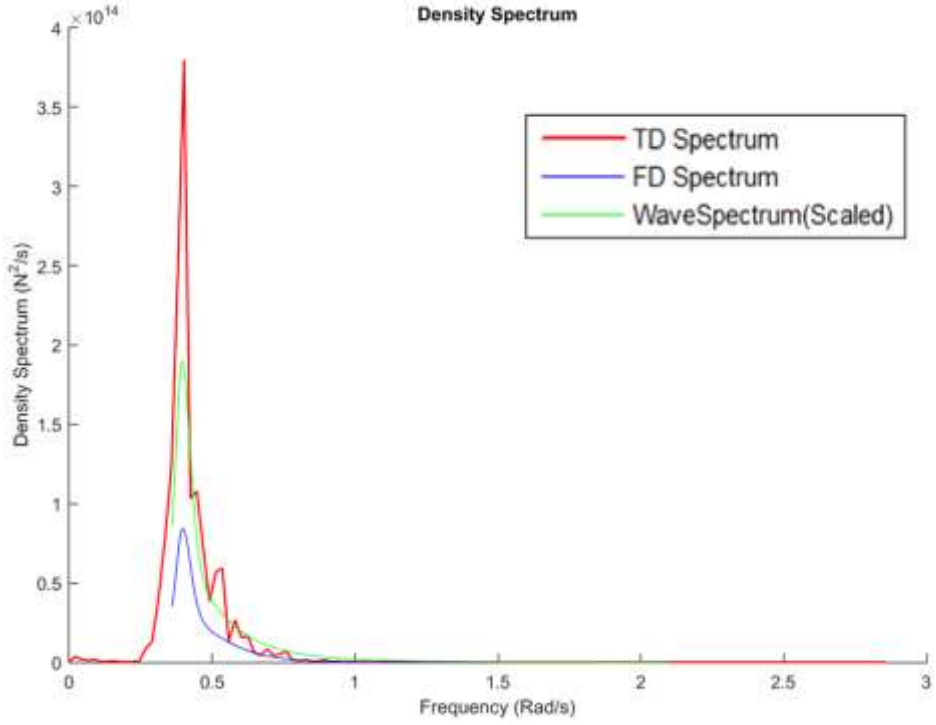

Figure 6.6. The density spectrum of the total external force in Y direction (drag and inertia) for LC 2 (Sample Frequency 3Hz)

6.2 The dynamic versus the quasi-static

As discussed in Chapter 4, the study of the dynamic versus the quasi-static will focus on two aspects:

(1) The validation of DAF on SDOF system
(2) The representation of SDOF system for MDOF system

Based on these two principles, the analysis is carried out by comparing the inertia load when the displacement of the CoG is the maximum in 3hrs, estimated by different methods. To control variables, the wave load used in DAF estimation is linearized, and thus only the issue of dynamic versus the quasi-static is involved in this analysis. Therefore, the analysis result in this section does not represent the real quasi-static analysis of the platform.

For the study on the validation of DAF estimation on SDOF system, the SDOF used in this analysis is the simplified model of the Yme MOPUstor based on the natural period of 7sec and the topsides' mass of 129000te, expressed as

$$1.29 \times 10^7 \ddot{r} + 1.14 \times 10^6 \dot{r} + 1.01 \times 10^7 r = F \tag{6.3}$$

Where r is the hypothesis displacement, F is the total wave load in Y direction.

The calculation procedure for the simplified DAF(DAF), stochastic DAF (SDAF) and the frequency-domain method are introduced in the Chapter 4. The calculation of the inertia loads for the multi degree of system (MDOF) is based on the linear time-domain method, introduced in Appendix III.

Table 6.8 the inertia loads estimated by the simplified DAF(DAF), the stochastic DAF (SDAF) and the frequency-domain method (SDOF and MDOF) (Unit: MN)

Load Case	SDOF			MDOF
	DAF	SDAF	FD	FD
LC 1	29.30MN	17.85MN	16.5MN	8.60MN
LC 2	3.972MN	9.378MN	8.6MN	7.52MN

As observed from table 6.8, as predicted in Chapter 4, the DAF method overestimates the inertia load, due to the lack of the frequency shift. The stochastic DAF method, however, provides a reasonable result compared with the FD's result for the SDOF system. Therefore, the stochastic DAF method is believed to be valid for the SDOF system.

For the issue of SDOF's representation, however, the results are not very satisfactory. By comparing the FD calculated in SDOF and MDOF system, it can be clearly observed that the inertia load has been overestimated, while the total extreme external load are the same. Therefore, the representation of a SDOF system in the Yme MOPUstor's dynamic analysis is debatable.

In additions, the load distribution of the Yme MOPUstor also cannot be fully reconstructed by the DAF method. As shown in figure 5.5, the three dominated modes of the Yme MOPUstor can only approximately be treated as the Surge, Sway and Yaw shapes. Taking the Sway shape as an example, the real "Sway" mode of the platform is an combination of the true Sway and the true Yaw's motion. This shape is so complex that it cannot be represented by a single inertia load at centre. Therefore, the deviation occurs between the quasi-static analysis and the real motion, with respect to the SDOF representation.

6.3 The deterministic versus the stochastic

The study of the stochastic versus deterministic is carried out in two aspects:

(1) The representation of a single wave load with respect to the external force

(2) The representation of a single wave load with respect to the maximum response

The study on the representation of a single wave load with respect to the external force is carried out first. As mentioned in Chapter 5, the table 6.9 shows the maximum wave heights with their associated wave periods for each load case. (The conversion approach is attached in Appendix I) In this study, the wave loads of both the stochastic waves and the single wave are calculated and compared, with respect to its extreme value.

Table 6.9 the selected environmental conditions for this comparative study

Environmental Condition	$H_s(m)$	$T_p\ (\mathrm{sec})$	γ	$H_{max}(m)$	$T_{ass}(sec)$	Wave direction
LC 1	6.03	7.03	5	11.43	7.1	90 deg
LC 2	14.2	15.9	3.3	24.58	14.58	90 deg

Table 6.10 shows the 3hrs- extreme external force predicted by the stochastic waves and the single wave for each load case. As observed from the table, the result from the single wave is quite close to the result from the stochastic. However the accuracy of single wave load in the load case 1 is higher than those in the load case 2. This may be caused by the wide band spectrum for the load case 2. Therefore, it can be concluded that, with respect to the total extreme value, the single wave load is representative for these two load cases.

Table 6.10 the extreme total wave load in 3hrs simulation

Method	LC 1		LC 2	
	3hrs extreme load	Error	3hrs extreme load	Error
Stochastic wave	$4.09MN$	--	$24.5MN$	--
Single wave	$4.50MN$	10.0%	$24.2MN$	-1.22%

However, with respect to the extreme overturning moment, the single wave load method results in a large deviation. Table 6.11 shows the extreme overturning moment predicted by the single wave and the stochastic wave method. As observed

from table 6.11, the deviations of the single wave load are significant. This phenomenon indicates the load distribution of the single wave load may fail to be representative.

Table 6.11 the extreme overturning moment in 3hrs simulation				
Method	LC 1		LC 2	
	3hrs extreme load	Error	3hrs extreme load	Error
Stochastic wave	$244.96MNm$	--	$294.25MNm$	--
Single wave	$411.17MN$	68%	$1411.4MNm$	380%

Due to the limitation of this study, this representation of this analysis is limited. The validation of single wave load for these load cases doesn't mean it is general applicable for the sea state. A sensitivity study of this effect should be presented in future.

With the representation of a single wave load with respect to the external force analysed, the next step is to analysis the representation of a single wave load with respect to the maximum response. To control variables, this analysis is carried out only in the frequency domain methods.

The study is based on the static load reconstruction when the topside's displacement is maxima for a 3hrs simulation. Two methods are adopted in this load reconstruction: the design wave method and the linear time-domain method. The design wave method is to reconstruct the load distribution via the equivalent single wave at the peak frequency of the response's spectrum. The linear time domain method, on the other hand is to reconstruct the load distribution via a pseudo sea state. More details of these two methods are attached in Appendix III.

The load case 1 is used and the maximum horizontal displacement of the top level of the forward leg (EL119.14m) is adopted to perform the comparative study, because the linearized method is only valid in the load case 1. The goodness of converted loads will be judged based on two criteria: total static wave load in Y direction and total inertia loads on three translational direction (Global X,Y,Z direction).The static load in Y-direction is calculated by applying the RAO of total shear force and overturning moment calculated in Wajac^{TM}.

For regular wave load conversion method, the result based on short-term based approach is listed in table 6.12.

Table 6.12 the conversed regular wave						
Short-term Sea state			Statistical extreme response			
Hs	Tp	Wave direction	Y-displacement	Peak frequency in response spectrum	Corresponding RAO	Wave Height H
6.03m	7.03sec	90deg	1.1109m	0.902Rad/s	0.599	1.852m

Thus the equivalent single wave has a wave height of 2.008m and frequency of 0.902Rad/s. Its corresponding static wave load and inertia load are shown in the table 6.13

Table 6.13 the load of the conversed regular wave						
Conversed Wave		Maximum Wave load		Inertia Load		
Wave Height H	Wave Frequency w	Total Shear force (Y)	Overturning Moment (Y)	FX	FY	FZ
1.852m	0.902Rad/s	1.087MN	1.300MNm	1.83MN	8.41MN	0.15MN

For linear time-domain method, four load cases have been generated. Their maximum horizontal displacements are listed in the table 6.14

Table 6.14 the load cases based on linear time domain method					
Load Case	Maximum Total horizontal Response			Maximum Component Reponses(m)	
	Total horizontal response (m)	Corresponding Time Point T_{max}	Error **	X-direction(error)**	Y-direction(error)**
1	1.121	3151.4sec	1.1%	$4.70x10^{-3}$(-8%)	1.13 (1%)
2	1.060	7577.6sec	-4.5%	$4.62x10^{-3}$(-9.7%)	1.06 (-4.5%)
3	1.084	3296.8sec	-2.3%	$4.34x10^{-3}$(-15.2%)	1.09(-2.3%)
4	1.081	3794.8sec	-2.5%	$4.77x10^{-3}$(-6.9%)	1.08 (-2.5%)
Statistical value	1.109	N/A	N/A	$5.12\ x10^{-3}$	1.11

*: Different from component of the maximum total horizontal displacement
**: Error compared with statistical value.

As known in the table 6.14, the maximum response in 3hrs simulation is stable and their values are quite close to extreme value based on statistical analysis. Another three cases are generated for further inspection, listed in table 6.15

Table 6.15 the load cases based on linear time domain method (extra)				
Load Case	Maximum Total horizontal Displacement		Maximum Component Reponses	
	Total horizontal response	Corresponding Time Point T_{max}	X-direction	Y-direction
5	1.0807	1066sec	$4.304\ x10^{-3}$ m	1.0806m
6	1.0492	2776sec	$4.314\ x10^{-3}$ m	1.0492m
7	0.9038	6918.6sec	$4.290\ x10^{-3}$ m	0.9038m

It is interesting to observe that the relative deviation between each load case is rather small, while small but constant deviation between simulated response and statistical value occurs. A possible reason is that the Rayleigh distribution is just approximation curve fit to the real response distribution, and the Rayleigh distribution may overestimate the actual response within tolerable range. Another reason such as frequency discretion may also contribute the deviation. It can be conclude the error of simulation is acceptable and the simulation is valid for load conversion.

The static and inertia load for load case 1 - 4 is list in table 6.16.

Table 6.16 the static and inertia load for the load case 1 - 4

Load Case	Wave load		Inertia Load		
	Total Shear force (Y)	Overturning Moment (Y)	FX	FY	FZ
1	0.3MN	1.28MNm	0.040MN	9.25MN	-2.14×10^{-4}MN
2	0.5MN	1.35MNm	0.039MN	8.43MN	-5.69×10^{-4}MN
3	1.23MN	1.01MNm	0.022MN	8.02MN	-4.91×10^{-5}MN
4	-0.25MN	0.0221MNm	0.037MN	8.2MN	-2.07×10^{-4}MN

In order to make a comparison between two methods, load from linear time-domain method is linear scaled to the statistical value, as shown in table 6.17

Table 6.17 the comparison between the single wave method and the linear time domain method

Load Case	Wave load		Inertia Load	
	Total Shear force (Y)	Overturning Moment (Y)	FX	FY
1	0.3MN	1.27MNm	0.040MN	9.15MN
2	0.5MN	1.41MNm	0.040MN	8.83MN
3	1.26MN	1.03MNm	0.023MN	8.21MN
4	-0.25MN	0.023MNm	0.038MN	8.4MN
Single Wave	-0.1MN	1.41MNm	0.031MN	9.10MN

The inertia load shows its stable properties for different load cases. The inertia load in Y-direction contributes most and is within the range of 8.2-9.2MN. However, the single wave method may overestimate inertia load in X-direction compared with the linear time domain simulation. In contrast, the static wave load varies a lot for different load cases. This is indicated the stochastic intrinsic quality of the structural response: that the different distribution of the static wave load and the inertia load will lead to same response for the horizontal displacement at the top of the forward leg.

Nevertheless, a high caution should be paid to the single wave conversion method, though it shows a really good case in this calculation. The Yme MOPUstor is dominated by three dynamic modes: surge, yaw and sway, which mean the RAO of the response, will have three peaks, instead of one. Combining with the wave spectrum (especially for wide band spectrum), the response spectrum may be wide band, or even has multi-peaks. In this case, the assumption for the peak frequency equivalent in the single wave conversion method will be invalid, and its corresponding result will fail to be representative. Besides, the regular wave conversion method is invalid for the non-linear load combination. Therefore, the regular wave conversion and the linear-time domain method are recommended to be performed at same time for one load conversion.

In conclusion, the single wave representation shows its validation in this numerical experiment. The validation of this method is limited to the band width of the spectrum. Therefore, a pre-assessment needs to be carried out before its engineering practise.

6.4 The efficiency

The efficiency is a balance between the time-consuming and the accuracy. As mentioned before, all the dynamic analysis methods are imperfect in nature. On one hand, some methods give quite accurate results, but its time-consuming is unacceptable for a commercial project. On other hand, the time-consuming of the analysis by some methods is acceptable for engineering practise, but its analysis results can only be considered to be representative, under a certain condition, within certain accuracy. There, in this section, the study on efficiency consists of two topics: the time-consuming and the accuracy.

The time-consuming for each analysis are listed in the table 6.18, and the results of the 3hrs extreme responses are shown in table 6.19 – table 6.21. The responses at the local coordinates have been converted into the global coordinate. Due to the involvement of the negative spring, the fake shear forces are generated at the bottom of the legs. However, these fake shear forces are generated for the results by all the methods, and hence are not considered here.

Table 6.18 the time-consuming for each analysis

		Sesam™ Wajac™	Sesam™ Sestra™	Comments
Load case 1	Quasi-static	≈37sec	≈8sec	For one load case
	Frequency-domain	22sec	1251sec	Applicable for all load cases
	Time domain	29102sec	116460sec	For one load case
Load case 2	Quasi-static	≈37sec	≈8sec	For one load case
	Frequency-domain	22sec	1251sec	Applicable for all load cases
	Time domain	1818sec	50514sec	For one load case

As observed in table 6.18, the time-domain method is the most time-consuming method among the all the dynamic analysis methods. Hence, because of its large time consuming, it is impossible to run all the dynamic analysis cases by using the time-domain method. The time-consuming of the frequency domain method and the quasi-static method are relatively small. With respect to one load case analysis, the quasi-static analysis is faster than the frequency-domain analysis. However, with respect to the complete sea states analysis, the frequency domain method is believed to be faster. To sum up, the quasi-static method or frequency-domain method are recommended to be performed initially before the time-domain analysis.

In addition, the issue of the accuracy also needs to be contained into the consideration. Ae mentioned previously, the time-domain method is believed to be the most accurate in principle and thus set to be the reference. As observed from table 6.19 - 6.21, for the load case 1 analysis, the frequency domain's results are more accurate. This is consistent with the prediction that the frequency domain is more accurate in the resonant zone [6]. For the load case 2 analysis, the quasi-static's analysis results are more accurate. This is consistent with the prediction that the quasi-static is more accurate in the extreme wave condition [6].

However, this conclusion is not generally applicable to all the dynamic analysis cases. For the dynamic analysis of the Yme MOPUstor, the dynamic effect is not significant at the extreme wave condition, vice versa, as discussed in section 6.1. For the cases which the natural period is coincident with period of the extreme wave condition, both the frequency-domain method and the quasi-static method fail to be representative. Only the time-domain method is available in these cases. Therefore, as recommended in section 6.1, the non-linearity needs to be pre-assessed for the selection for a proper dynamic analysis method.

Table 6.19 The maximum displacement in Y-direction (3hrs, Unit: meter)				
The topside's CoG (node: 1612)				
	Time-domain	Frequency-domain	Quasi-static (DAF)	Quasi-static (SDAF)
Load case 1	0.7367	0.8051	2.4896	1.5599
Load case 2	0.9469	0.5325	0.7658	1.3092
The top of the forward leg (node: 2070)				
	Time-domain	Frequency-domain	Quasi-static (DAF)	Quasi-static (SDAF)
Load case 1	1.009	1.1109	2.8844	1.7950
Load case 2	1.3298	0.6346	0.7972	1.4344
The top of the caisson (node: 102)				
	Time-domain	Frequency-domain	Quasi-static (DAF)	Quasi-static (SDAF)
Load case 1	0.5637	0.5062	2.0850	1.3273
Load case 2	0.8892	0.5055	0.7875	1.2302
The top of the starboard leg (node: 864)				
	Time-domain	Frequency-domain	Quasi-static (DAF)	Quasi-static (SDAF)
Load case 1	0.6806	0.6886	2.3885	1.4981
Load case 2	0.8423	0.5094	0.7808	1.2929
The top of the portside leg (node: 870)				
	Time-domain	Frequency-domain	Quasi-static (DAF)	Quasi-static (SDAF)
Load case 1	0.6775	0.6880	2.3669	1.4744
Load case 2	0.8412	0.5093	0.7576	1.2698

Table 6.20 The maximum shear force in Y direction (3hrs, Unit: MN)				
The base of the caisson (Element:200)				
	Time-domain	Frequency-domain	Quasi-static (DAF)	Quasi-static (SDAF)
Load case 1	2.601	2.655	7.342	4.473
Load case 2	6.588	4.953	1.231	2.908
The base of the starboard leg (Element:1405)				
	Time-domain	Frequency-domain	Quasi-static (DAF)	Quasi-static (SDAF)
Load case 1	2.500	2.852	9.181	5.535
Load case 2	4.170	2.982	1.413	3.549
The base of the portside leg (Element: 1580)				
	Time-domain	Frequency-domain	Quasi-static (DAF)	Quasi-static (SDAF)
Load case 1	2.780	2.803	9.471	5.842
Load case 2	4.610	2.980	1.724	3.854
The base of the forward leg (Element: 3224)				
	Time-domain	Frequency-domain	Quasi-static (DAF)	Quasi-static (SDAF)
Load case 1	4.108	3.138	11.002	6.704
Load case 2	5.188	3.063	1.845	4.359

Table 6.21 The overturning moment about X direction (3hrs, Unit: MNm)				
The base of the caisson (Element:200)				
	Time-domain	Frequency-domain	Quasi-static (DAF)	Quasi-static (SDAF)
Load case 1	126.31	150.55	430.77	262.40
Load case 2	218.41	160.19	72.07	170.54
The base of the starboard leg (Element:1405)				
	Time-domain	Frequency-domain	Quasi-static (DAF)	Quasi-static (SDAF)
Load case 1	92.20	107.69	333.06	260.26
Load case 2	131.1	87.23	52.94	129.15
The base of the portside leg (Element: 1580)				
	Time-domain	Frequency-domain	Quasi-static (DAF)	Quasi-static (SDAF)
Load case 1	97.15	111.92	336.68	206.36
Load case 2	136.6	88.76	59.05	135.26
The base of the forward leg (Element: 3224)				
	Time-domain	Frequency-domain	Quasi-static (DAF)	Quasi-static (SDAF)
Load case 1	148.2	169.22	406.70	247.83
Load case 2	187.6	111.34	68.23	161.14

6.5 Conclusion and practise advise

Table 6.22. The conclusion and the practise advise

Load Cases		Load Case 1 (Resonant Condition)	Load Case 2 (Extreme Wave Condition)
Linear versus nonlinear	Drag force effect	Inertia Dominated; Drag's linearization strongly underestimates the drag force but has no fatal effect on the accuracy.	Non-inertia Dominated; Drag's linearization strongly underestimates the drag force and has fatal effect on the accuracy
	Free surface effect	The free surface effect is not significant; For the linearized calculation, the constant elevation should be tuned close to the mean water level to avoid overestimation on the dynamic effect.	The free surface effect is significant; For the linearized calculation, the linearized calculation will underestimate the result.
Quasi-static versus dynamic		Sensitive to the dynamic effect; A large phase shift occurs between the external load and the inertia load. Thus the quasi-static analysis will highly overestimate the result.	Not very sensitive to the dynamic effect; The quasi-static analysis provides a reasonable result. However, due to the band of the wave spectrum, parts of the energy are presented in resonant zone. Hence the stochastic DAF estimation, instead of the simplified DAF estimation, provides a better result.
Deterministic versus stochastic		The stochastic load case can be reasonably represented by a deterministic load case.	The stochastic extreme wave load can be represented by a deterministic single wave load
Efficiency		Quasi-static and FD methods are much faster than the TD method.	
Practise advice		The load case at the resonant condition can be solved by the time domain method or the frequency-domain method. The reference wave height needs to set to be 1m to reflect the true dynamic effect. The design wave conversion method is valid for this load case.	The load case at the extreme wave condition can be solved by the quasi-static method or the time-domain method. The stochastic DAF method provides a better result.

7.0 FURTHER STUDY

As pointed out previously, the biggest challenge with respect to the improvement of the frequency-domain method's efficiency is the non-linearity. The issues of the stochastic excitation and the dynamic can be perfectly handled by the frequency-domain method. And the time-consuming of the time-domain methods is acceptable. However, the traditional frequency-domain method fails to serve when the non-linearities are significant. Therefore, several attempts have been made to include the non-linearity into this efficient method.

As pointed out in ref [39], the non-linearities involved in the Jack-up design can be cataloged as,

Structural:
1) Leg to hull interface
2) Overall leg hull structure
   - P-Δ effect
   - Euler effect
3) Leg to soil interface

Environmental:
4) Coupled Morison drag force calculation
5) Wave elevation and crest kinematics
6) Combination current-wave interaction

In this thesis, the higher order frequency domain method is developed to involve some of environmental non-linearities, which are hydro-structure decoupled drag force, wave elevation and crest kinematics. However, it is still not enough. Taking an example of the Yme MOPUstor, for the decommissioning operation of the the Yme MOPUstor, one plan proposed is to install a stabilization tool in the cut leg as a temporary support, in case of the Pieter Schelte cannot lift the platform immediately. Figure 7.1 shows a graphical representation of the stabilization tool. This stabilization tool is functioned based on the fiction force, and thus the global force-deformation properties of it show significant non-linearity. This structural non-linearity cannot be considered by the HFD method. Therefore, some further studies need to be carried out.

Several ideas have been inspired by the research work from the Aerospace industry and may be applicable for the hydro-structure models. These possible methods are,

(1) Describing function method with the non-linear modal techniques[26]

(2) Direct spectrum conversion method [14]

(3) Volterra series [27]

(4) Linearized structure with non-linear component [41]

Due to the limitation of this study, no further research work is carried out on those aspects.

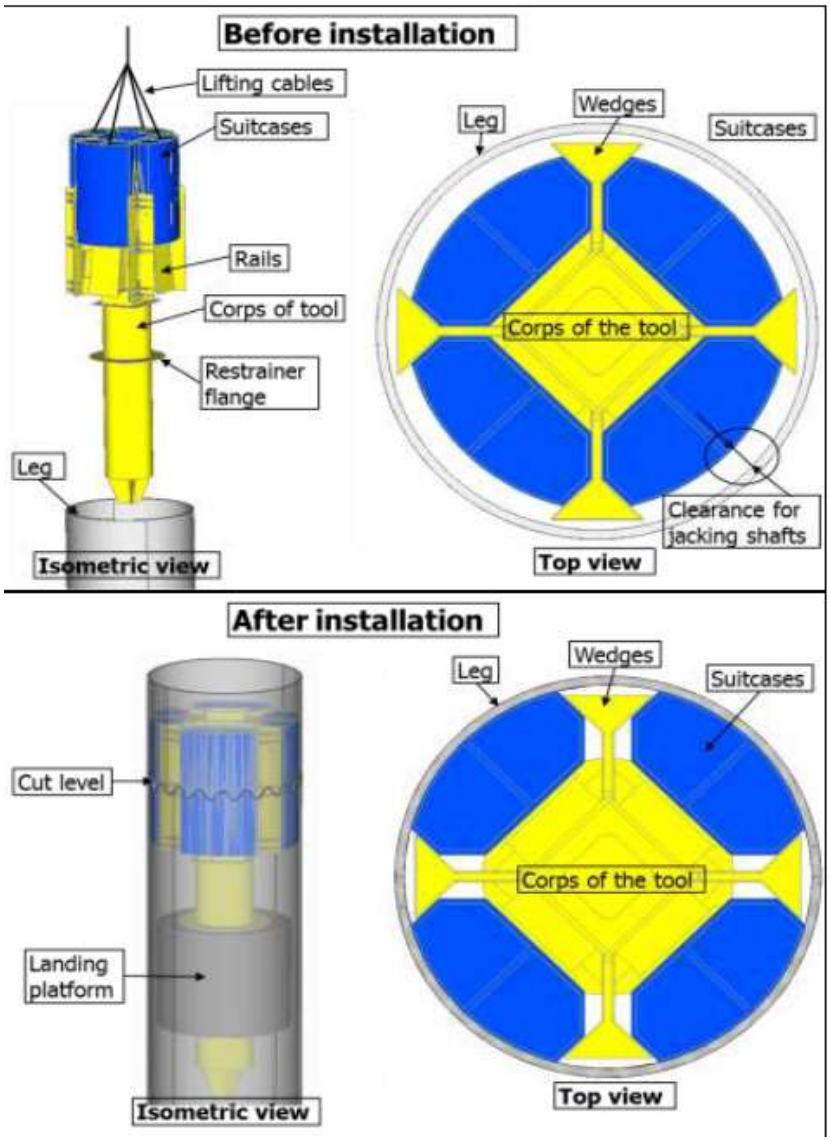

Figure 7.1. The graphical representation of the stabilization tool, from ref [40]

8.0 REFERENCE

[1] "Yme Oil Field, Egersund Basin, Norway". Offshore-Technology. Net Resources International. Retrieved 2010-08-29.

[2] Overall Basic Design for MOPU and caisson for Yme Location, MSC ref P 11028-5550 rev D, October 30th, 2009

[3] Yme - Sensitivity Analyses for Dynamic wave response on Yme platform Report No./DNV Reg No.: 2011-1258/ 13P7H1D-1 Rev Draft, 2011-11-07

[4] Yme Structural Assessment Report, Atkins, 20/04/2012

[5] SESAM Theory Manual Riflex, DNV, 23-06/2014.

[6] YME 100 Years Motions Clarification, Atkins ref. TN-5113072-YME-168-048, 22-Aug-2013

[7] Usfos hydrodynamic manual, DNV, 10/02/1010

[8] Self-elevating units, DNV-RP-C104, DNV, Nov.2012

[9] Environmental conditions and environmental loads, DNV-RP-C205, Oct.2010

[10] Sesam User Manual Wajac, DNV, Dec.15th, 2013

[11] Borgman, L. E. (1965). A Statistical Theory for Hydrodynamic Forces on Objects: Wave Res. Rep. HEL 9-6, Hydraulic Eng. Lab., Univ. of Calif., Berkeley, Calif.

[12] Sesam User Manual Sestra, DNV, Feb 27th, 2013

[13] Abaqus 6.11 theory manual, Dassault Systèmes, 2011

[14] Y.Lu, Y.Chen, P.Tan, Y.Bai, Prediction of most probable extreme values for jack-up dynamic analysis, Marine Structure 15 (2002) 15-34, 2002

[15] X.Y.Zheng, C.Y.Liaw, Inundation Effect and Quartic Approximation of Morison-Type Wave Loading, Proceedings of the Eleventh (2001) International Offshore and Polar Engineering Conference Stavanger, Norway, June 17-22, 2001

[16] J.M.J. Journée and W.W. Massie, offshore hydrodynamics, first edition, TU Delft, January 2001.

[17] Gaussian quadrature. (2015, May 18). In Wikipedia, The Free Encyclopedia. Retrieved 09:32, May 31, 2015, from http://en.wikipedia.org/w/index.php?title=Gaussian_quadrature&oldid=662972730

[18] Taylor series. (2015, May 30). In Wikipedia, The Free Encyclopedia. Retrieved 09:44, May 31, 2015, from http://en.wikipedia.org/w/index.php?title=Taylor_series&oldid=664671155

[19] Riaan van't Veer, Application of linearized Morison load in pipe lay stinger design, GustoMSC, June 15, 2008

[20] Ir. Jorrit-Jan Serraris & Ir. Willemijn Pauw, Analysis of Mooring Systems, TU Delft, Feb. 25 2013

[21] Leon E. Borgman, Random Hydrodynamic Forces on Objects, The Annals of Mathematical Statistics, Volume 38, Number 1 (1967), 37-51

[22] John D. Fenton, A fifth-order stokes theory for steady waves, the Journal of Waterway, Port, Coastal and Ocean Engineering, Vol.111, No.2 March, 1985

[23] SESAM USER MANUAL Postresp, DNV, 10/10/2013

[24] Lammeren, van Jasper, Yme MOPUstor Platform – proposal for structural assessment method, Allseas technical notes, 26/09/2014

[25] P.Liu, Dynamic of elevated Jack-up structures, PhD thesis, 1991

[26] H. Siller, Non-linear modal analysis methods for engineering structures, PhD thesis, Imperial College London, August, 2004

[27] D.Storer, Dynamic analysis of non-linear structures using higher order frequency response function, PhD thesis, Univ. Manchester, Oct 1991

[28] L.Holthuijsen, Waves in oceanic and coastal waters, Cambridge university press, 2007.

[29] Z.K.Peng, Comparisons between harmonic balance and non-linear output frequency response function in non-linear system analysis, Journal of Sound and Vibration 311(2008) 56-73

[30] M.Chrolenko, Dynamic analysis and design of mooring lines, Msc Thesis, NTNU

[31] G. Rodenbusch, Random directional wave forces on template offshore platforms, OTC 5098

[32] K.G. Grenda, Wave dynamic of Jackup Rigs, OTC 5304

[33] R.Rand, Lecture Notes on non-linear Vibrations, Cornell University, 2005

[34] Addendum to Yme Structural Assessment Report, Atkins, TN/5081357/YME/162/016, 4.10.2013

[35] Yme MOPUstor Platform – Global Stiffness, Mass & Motion Study, Atkins, YME02-23484-N-RA-0009, 15.03.2013

[36] WAFO – a Matlab Toolbox for Analysis of Random Waves and Loads, verison 2.5, Lund Univ., March 2011

[37] Generalized extreme value distribution. (2015, May 8). In Wikipedia, The Free Encyclopedia. Retrieved 20:04, June 14, 2015, from https://en.wikipedia.org/w/index.php?title=Generalized_extreme_value_distribution&oldid=661410599

[38] Xtract user manual, DNV, March, 2014

[39] C.J.Moommaas & W.W.Dedden, the development of a stochastic non-linear and dynamic Jack-up design and analysis method, Marine Structures 2 (1989) 335-363

[40] K. Rafik, Integrity check of the MOPU after cutting without stabilization tool Rev A, YME02-10837-N-RA-0017, 10/11/2014

[41] J.Ferreira, Dynamic Response Analysis of structures with Non-linear components, PhD thesis, Imperial college London, 1998

Appendix I: The hydrodynamic model and the program “Hydro”

I.1. Mathematical Model of waves

The knowledge of this section is mainly from ref [9].

Several wave models are applied to simulate a regular wave with a given height H and a given period T. The mathematical model of such regular wave is based on the potential theory with the non-viscous stationary assumption.

The motion of the water particle in waves is assumed to be fully represented by the potential function $\phi(x,z)$ in 2-D frame as shown in figure I.1. Thus, the velocity of the water particle at (x,z) can be expressed as

Velocity in x- direction

$$v_x = \frac{\partial \phi}{\partial x}(x,z) \qquad (I.1)$$

Velocity in z- direction

$$v_y = \frac{\partial \phi}{\partial y}(x,z) \qquad (I.2)$$

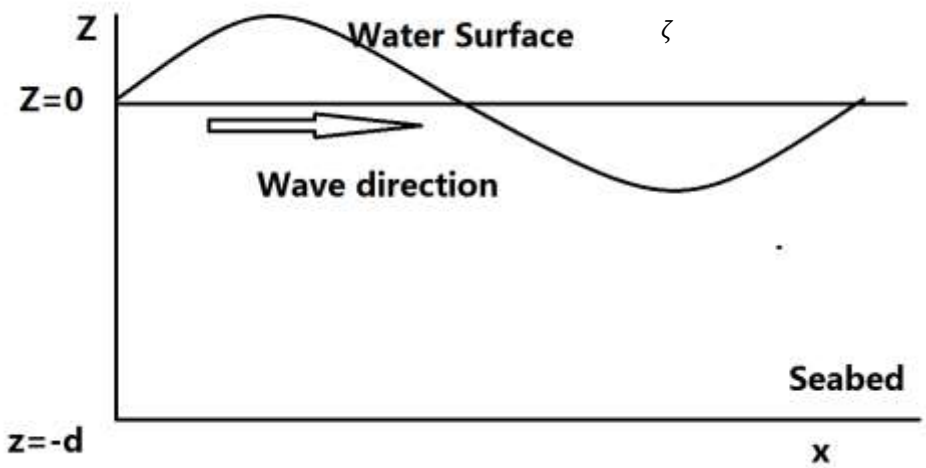

Figure I.1 the 2-D frame for wave definition

The kinematic condition (A.3) and the dynamic condition (A.4), derived from conservation law and the boundary condition, fully determine the potential function $\phi(x,z)$. The perturbation theory (A.5) is applied to expand the potential function by the order of wave steepness and thus can be solved within a limited accuracy.

$$\left(\frac{\partial \zeta}{\partial t} + \nabla\phi\nabla\zeta\right)_{z=\zeta} = \left(\frac{\partial \phi}{\partial z}\right)_{z=\zeta} \tag{I.3}$$

$$\zeta(x,y,t) = -\frac{1}{g}\left(\frac{\partial \phi}{\partial t} + \frac{1}{2}\nabla\phi\nabla\phi\right) \tag{I.4}$$

$$\begin{aligned} \zeta &= \zeta_1 + \zeta_2 + \cdots \\ \phi &= \phi_1 + \phi_2 + \cdots \end{aligned} \tag{I.5}$$

Where, ζ is the free-surface elevation of water and ϕ is the potential function. $\zeta_1, \zeta_2 \ldots, \phi_1, \phi_2, \ldots$ are first, second.. order of surface elevation and potential function with respect to the steepness of wave.

Many studies have been carried out for the solution of the wave governing equation. Among those, the airy wave, the Stokes wave and the conical wave are generally used in the engineering problems. The application range is indicated in the figure I.2 from ref [9].

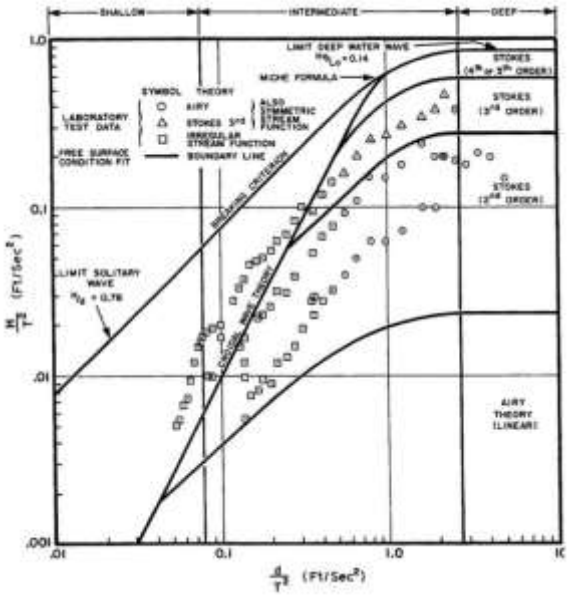

Figure I.2 Application range for different wave theory

As shown in the figure I.2, the airy wave is the simplest wave model and limited to infinitesimal wave height sea state. The Stokes' wave is more applicable for the high steepness wave, while the conical wave model is usually considered in the shallow water case.
In this section, the 5th order stokes wave and the airy wave model will be introduced.

I.1.1. Airy wave model

Airy wave is the simplest wave and the most commonly applied theory. Ignoring all higher order effect, the airy wave represents the regular wave's elevation in a perfect sinusoidal form,

$$\eta = A\sin(\omega t + \varphi) \tag{I.6}$$

Where η_a, ω, φ is the wave's amplitude (half of wave height H), the wave's frequency and the initial phase.

Applying the continuity equation and the kinematic boundary equation, the velocity potential ϕ is then obtained,

$$\phi = \frac{\omega}{k} A \frac{\cosh(kz)}{\sinh(kh)} \sin(kx - \omega t) \tag{I.7}$$

Where h is the water depth and z is the water level (z is between 0 and negative water depth –h). k is the wave number, which can be determined by the linear dispersion relation

$$\omega^2 = gktanh(kh) \tag{I.8}$$

The flow velocity component in a 2D frame U_x (along the wave direction) and U_z(along the water depth) is then calculated by

$$u_x = \frac{\partial \phi}{\partial x} \; and \; u_z = \frac{\partial \phi}{\partial z} \tag{I.9}$$

To interpolate the velocity above the still water level, two stretching methods are proposed [7].

Extrapolated wave treatment assumes wave kinematic above mean sea level (z=0) constant and equal to the value at z=0 in wave crests, while the extrapolated wave treatment uses airy wave kinematic up to surface elevation in wave toughs, as shown in Figure I.3. The same rule is applied for the particle speed and the accelerations, i.e. the values at the mean sea surface, z = 0, is used for all z > 0.

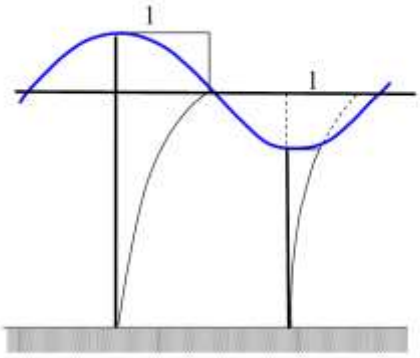

Figure I.3 Extrapolated airy wave theory

An alternative method for the wave interpolation is called the stretched wave treatment (or wheeler modification). This method calculates wave kinematics at the mean water level at the true surface and its corresponding distribution down to the seabed is stretched accordingly, as illustrated in Figure I.4.

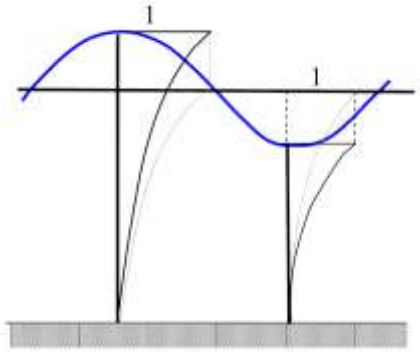

Figure I.4 Stretched airy wave theory

I.1.2. Stokes's wave

Stokes's Wave theory is a more generalized wave theory which includes the higher order effects. With the involvement of the higher order steepness, the accuracy of Stokes's wave increased. An airy wave thus can be treated as 1st order stokes wave. 5th stokes waves theory is recommended for ultimate limit state check, according to DNV-RP-C104 and thus introduced here [8].
Two method of expressing the Stokes 5th wave exist in previous studies. Skjelbreia and Hendrickson (1961) first introduce an expression for the Stokes 5th wave and is widely adopted as the engineering standards. However, Fenton (1985) gives another expression of 5th order Stokes' wave theory and demonstrates it is more accurate than Skjelbreia and Hendrickson's theory. While theory of Skjelbreia and Hendrickson (1961) is used in Sesam system, theory of Fenton is illustrated and

adopted as the reference theory in “Hydro”. Its procedure can be summarized as follow,

(1) Determine wavenumber k

$$\left(\frac{k}{g}\right)^{0.5} U_{cur} - \frac{2\pi}{\tau(gk)^{\frac{1}{2}}} + C_0(kd) + \left(\frac{kH}{2}\right) C_2(kd) + \left(\frac{kH}{2}\right)^4 C_4(kd) = 0 \qquad (I.10)$$

Where k is wavenumber
d is the water depth
H is the wave height
τ is the wave period
U_{cur} is the velocity of current.
Newton-Raphson method is used here to solve this implicit equation.

(2) Surface Elevation $\eta(x,t)$

The surface elevation is given by,

$$\eta(x,t) = d + (\sum_{i=1}^{5} \varepsilon^i \sum_{j=1}^{i} B_{ij} cosjk(x - ct))/k \ , \qquad where\ \varepsilon = \frac{kH}{2}, c = \frac{2\pi}{Tk} \qquad (I.11)$$

Where the system coordinate is set at the seabed fixed with earth.

(3) Velocity potential $\phi(x,y,t)$

The velocity potential is given by

$$\phi(x,y,t) = C_0 \left(\frac{g}{k^3}\right)^{0.5} \sum_{i=1}^{5} \epsilon^i \sum_{j=1}^{i} A_{ij} \cosh(jky) \sin(jk(x - ct)) \qquad (I.12)$$

$$v_x = \frac{\partial \phi}{\partial x}, \qquad v_z = \frac{\partial \phi}{\partial y}$$

For matrix A and B, their values are given in figure 1.5 , where $S = \sec kd$.

$$
\begin{aligned}
A_{11} &= 1/\sinh kd \\
A_{22} &= 3S^2/(2(1-S)^2) \\
A_{31} &= (-4-20S+10S^2-13S^3)/(8\sinh kd\,(1-S)^3) \\
A_{33} &= (-2S^2+11S^3)/(8\sinh kd\,(1-S)^3) \\
A_{42} &= (12S-14S^2-264S^3-45S^4-13S^5)/(24(1-S)^5) \\
A_{44} &= (10S^3-174S^4+291S^5+278S^6)/(48(3+2S)(1-S)^5) \\
A_{51} &= (-1184+32S+13232S^2+21712S^3+20940S^4+12554S^5-500S^6-3341S^7-670S^8) \\
&\quad /(64\sinh kd\,(3+2S)(4+S)(1-S)^6) \\
A_{53} &= (4S+105S^2+198S^3-1376S^4-1302S^5-117S^6+58S^7)/(32\sinh kd\,(3+2S)(1-S)^6) \\
A_{55} &= (-6S^3+272S^4-1552S^5+852S^6+2029S^7+430S^8)/(64\sinh kd\,(3+2S)(4+S)(1-S)^6) \\
B_{11} &= 1 \\
B_{22} &= \coth kd\,(1+2S)/(2(1-S)) \\
B_{31} &= -3(1+3S+3S^2+2S^3)/(8(1-S)^3) \\
B_{33} &= -B_{31} \\
B_{42} &= \coth kd\,(6-26S-182S^2-204S^3-25S^4+26S^5)/(6(3+2S)(1-S)^4) \\
B_{44} &= \coth kd\,(24+92S+122S^2+66S^3+67S^4+34S^5)/(24(3+2S)(1-S)^4) \\
B_{51} &= -(B_{53}+B_{55}) \\
B_{53} &= 9(132+17S-2216S^2-5897S^3-6292S^4-2687S^5+194S^6+467S^7+82S^8) \\
&\quad /(128(3+2S)(4+S)(1-S)^6) \\
B_{55} &= 5(300+1579S+3176S^2+2949S^3+1188S^4+675S^5+1326S^6+827S^7+130S^8) \\
&\quad /(384(3+2S)(4+S)(1-S)^6) \\
C_0 &= (\tanh kd)^{1/2} \\
C_2 &= (\tanh kd)^{1/2}\,(2+7S^2)/(4(1-S)^2) \\
C_4 &= (\tanh kd)^{1/2}\,(4+32S-116S^2-400S^3-71S^4+146S^5)/(32(1-S)^5) \\
D_2 &= -(\coth kd)^{1/2}/2 \\
D_4 &= (\coth kd)^{1/2}\,(2+4S+S^2+2S^3)/(8(1-S)^3) \\
E_2 &= \tanh kd\,(2+2S+5S^2)/(4(1-S)^2) \\
E_4 &= \tanh kd\,(8+12S-152S^2-308S^3-42S^4+77S^5)/(32(1-S)^5)
\end{aligned}
$$

Figure I.5 Matrix A and B

I.2. Stochastic wave theory

I.2.1. Wave Spectrum

The wave in the real ocean are stochastic in nature, the simplification of the equivalent single wave thus fails to reflect the real situation of forces acted on the offshore structure. Especially for the fatigue limit state design (FLS) and the ultimate limit state design (ULS), where dynamic effects, true surface level treatment, buoyancy and hydrodynamic damping, etc become significant, the simulation contains all those non-linearity provides the best prediction of “reality”.
For the stochastic sea states, the wave’s motions may be generated on the basis of a wave spectrum. So-called “spectrum” is a measurement of how energy density is distributed among frequencies, as defined in (I.13).

$$\mathrm{S}_{\eta\eta}(\omega)\mathrm{d}\omega = \mathrm{E}\left[\frac{1}{2}A(\omega)^2\right] \qquad (I.13)$$

The typical spectrums for the waves are like Jonswap spectrum and PM-spectrum. Jonswap spectrum is used to model the under-developed sea like the case in North Sea and Golf of Mexico, while the PM-spectrum is usually applied in the fully-developed sea like the case in the pacific Ocean.
The general spectrum for both Jonswap and PM spectrum can be expressed as

$$S_J(\omega) = A_\gamma S_{pm}(\omega)\gamma^{\exp(-0.5\left(\frac{\omega-\omega_p}{\sigma\omega_p}\right)^2)} \quad (I.14)$$

Where

$$S_{PM}(\omega) = \frac{5}{16}H_s^2\omega_p^4\omega^{-5}\exp(-\frac{5}{4}\left(\frac{\omega}{\omega_p}\right)^{-4}) \quad (I.15)$$

Where $\omega = \frac{2\pi}{T_p}$ is the angular spectral peak frequency. $S_{PM}(\omega)$ is the PM spectrum, γ is the non-dimensional peak shape parameter. $A_\gamma = 1 - 0.287\ln(\gamma)$ is a normalizing factor.
For $\gamma = 1$, the general Jonswap spectrum reduces to the PM-spectrum.

I.2.2. Stochastic wave generation

Conventional stochastic wave generation treats the stochastics wave as a combination of the Airy waves. According to DNV-RP-C104, the waves may be simulated by the velocity potential on the form:

$$\phi = \sum_{i=1}^{M} A_i \frac{\omega_i}{k_i}\frac{\cosh(k_i(z+h))}{\sinh(kh)}\cos(\omega_i t - k_i x - \phi_i) \quad (I.16)$$

Possibly extended to more wave direction, where

$\phi(x, y, z)$ =velocity potential at location x, z and time t
A_i= amplitude of partial wave number i
=$\sqrt{2S(\omega_i)\Delta\omega_i}$
h= water depth
ω_i=angular frequency of wave number i
k_i=wave number connected to ω_i through the dispersion relationship
ϕ_i= random phase, uniformly distributed between 0 and 2π
$\Delta\omega_i$=frequency band width associated with ω_i, i.e. $(\omega_{i+1} - \omega_i)$
$S(\omega)$= wave spectrum

I.3. Introduction to "Hydro"

To further investigate the sea's motion and engineering application, programme "hydro" has been coded and verified. The Highlights of "Hydro" are,

(1) Quasi-static load calculation
(2) Decoupled time-domain load calculation
(3) Wave model in Calculation: Airy wave, 5th order Stokes's wave, 1st order stochastic wave

The wave base shear calculation of Yme's SBM model has been performed in Hydro and Sesam^{TM}-Wajac. The direction of wave is assumed to be 60 deg, while same current profile as original SBM design report is set to be same direction as the waves.

Load Case	Hmax[m]	Tass[s]	Hydro[N]	Wajac[N]	Error
1	4.796	6.439	9.53E+05	9.14E+05	4.218%
2	5.710	7.025	1.43E+06	1.40E+06	2.378%
3	7.488	8.045	2.40E+06	2.39E+06	0.622%
4	9.236	8.935	3.30E+06	3.28E+06	0.721%
5	10.101	9.344	3.71E+06	3.69E+06	0.687%
6	10.948	9.728	4.10E+06	4.07E+06	0.698%
7	11.790	10.095	4.44E+06	4.43E+06	0.089%
8	12.639	10.452	4.83E+06	4.79E+06	0.913%
9	14.322	11.126	5.52E+06	5.49E+06	0.652%
10	15.990	11.756	6.24E+06	6.20E+06	0.632%
11	17.655	12.353	6.99E+06	6.96E+06	0.442%
12	19.307	12.918	7.84E+06	7.78E+06	0.735%
13	20.935	13.452	8.76E+06	8.67E+06	0.977%
14	22.540	13.958	9.69E+06	9.64E+06	0.531%
15	24.075	14.425	1.07E+07	1.07E+07	0.302%
16	24.303	14.494	1.09E+07	1.08E+07	0.833%
17	23.863	14.362	1.06E+07	1.05E+07	0.553%
18	22.081	13.815	9.44E+06	9.35E+06	0.931%
19	20.357	13.265	8.39E+06	8.35E+06	0.499%
Error Analysis for Load Case 1&2: There are two factors that cause the errors: (1) Different Wave Theory Selection (Fenton vs Skjelbreia & Hendrickson) (2)The wave height corresponding to associated wave is quite close to "breaking wave". This may cause the deviation at that point.					

Table 2.7 Base Shear comparison between Sesam^{TM}-Wajac and Hydro

More verifications for the hydro are attached in next section.

I.3. The verification of “Hydro”

All Verifications are carried out based on Hydrodynamics manual of Usfos [7]. The reference is based on the result from the Usfos calculation.

A.1. Current

The current speed is assumed to vary linearly with depth, with 0 m/s at sea floor and 1.5 m/s at sea surface.

	Period [s]	Height [m]	Theory
	15	0.0002	Stokes
	Depth [m]	Diameter [m]	Wave dir
	70	0.2	330
	C_d	C_m	
	1	0	
	Coord 1 [m]	Coord 2 [m]	V_curr
X	0	30	1.5
Y	0	30	Curr dir
Z	-70	20	270
	Reaction SP [N]	Reaction Usfos [N]	Deviation
X_max	-515.432	-513.979	0.0028
X_min	-515.778	-516.361	0.0011
Y_max	5156.271	5162.840	0.0013
Y_min	5155.834	5140.540	0.0030
Z_max	-1546.777	-1542.180	0.0030
Z_min	-1546.855	-1548.840	0.0013

	X[N]	Y[N]	Z[N]
Hydro	-516.155	5160.986	-1548.277
Usfos	-515.778	5162.840	-1548.84
Error(%)	0.07%	-0.04%	-0.04%

A.2. Airy wave kinematics-deep water

	Period [s]	Height [m]	Theory
	5	5	Deep
	Depth [m]	Diameter [m]	
	20	0.2	
	C_d	C_m	
	1	0	
	Coord 1 [m]	Coord 2 [m]	
X	0	0	
Y	0	0	
Z	-20	7	

	Depth	Hydro[m/s]	Usfos[m/s]	Error
Velocity	3	3.152	3.15	0.1%
	-5	1.414	1.3643	3.6%
	-10	0.6511	0.6571	-0.9%
	-15	0.3341	0.2741	21.9%
Acceleration	0	3.9561	3.8857	1.8%
	-5	1.777	1.7357	2.4%
	-10	0.8182	0.8143	0.5%
	-15	0.4213	0.3857	9.2%
Error Analysis: There will be two factors that cause the large error at z=-15m: (1) Usfos adopted deep water simplification equation for his calculation, while hydro adopted general equation. (2) The data for Usfos is measured from its original data plot by hand. That may lead to a large deviation for small value.				

A.3. Airy wave kinematics-finite water depth

	Period [s]	Height [m]	Theory
	8	5	Finite
	Depth [m]	Diameter [m]	
	20	0.2	
	C_d	C_m	
	1	0	
	Coord 1 [m]	Coord 2 [m]	
X	0	0	
Y	0	0	
Z	-20	7	

	Depth	Hydro[m/s]	Usfos[m/s]	Error
Velocity	0	1.7347	1.7098	**1.46%**
	-5	1.2662	1.2900	**-1.84%**
	-10	0.9972	1.0039	**-0.67%**
	-15	0.8401	0.8465	**-0.76%**
	-20	0.7985	0.7960	**0.31%**
Acceleration	0	2.2089	2.2096	**-0.03%**
	-5	1.6229	1.6400	**-1.04%**
	-10	1.2763	1.2782	**-0.15%**
	-15	1.0638	1.0770	**-1.23%**
	-20	0.9991	1.0135	**-1.42%**

A.4. Extrapolated Airy Wave Kinematics-finite water depth

Seafloor z=5.0m, Depth z=85m, Surface level z=90m. Wave Height H=18m, Wave period=14.0 seconds.

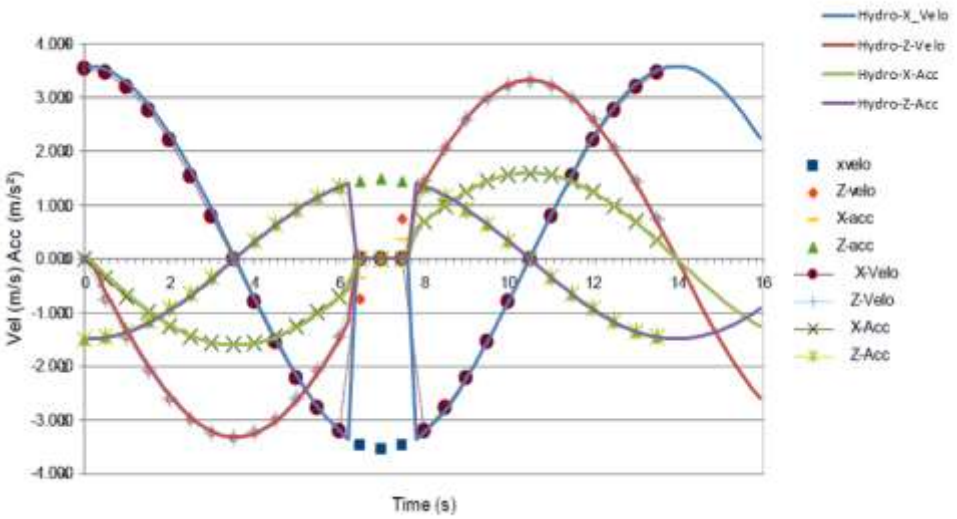

Wave particle velocity and acceleration for z=81.5m (close to trough)

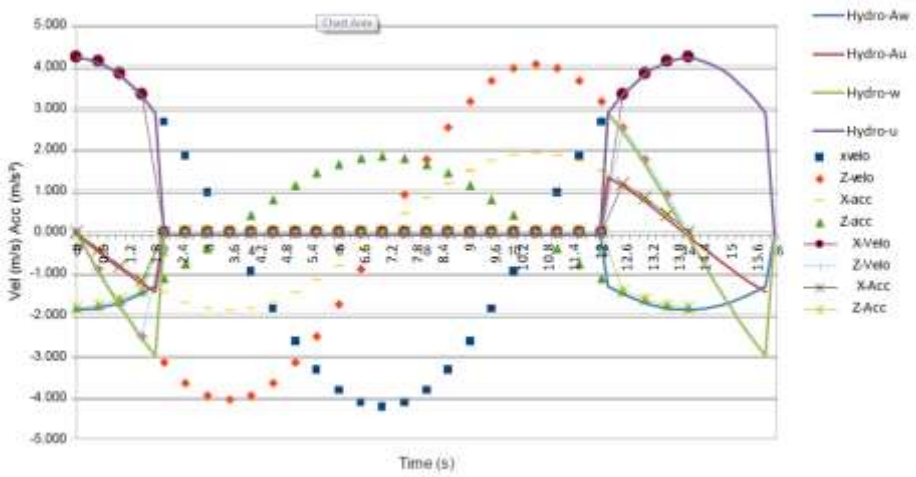

Wave particle velocity and acceleration for z=96m

A.5. Stretched Airy Wave Kinematics-finite water depth

Seafloor z=5.0m, Depth z=85m, Surface level z=90m. Wave Height H=18m, Wave period=14.0 seconds.

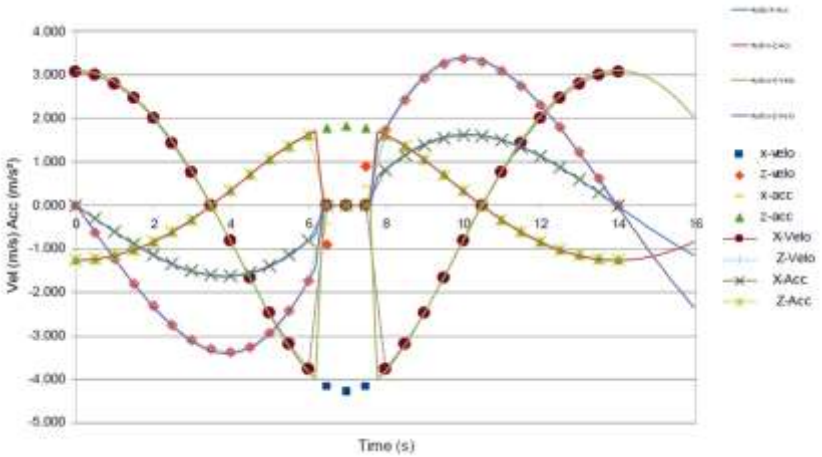

Wave particle velocity and acceleration for z=81.5m (close to trough)

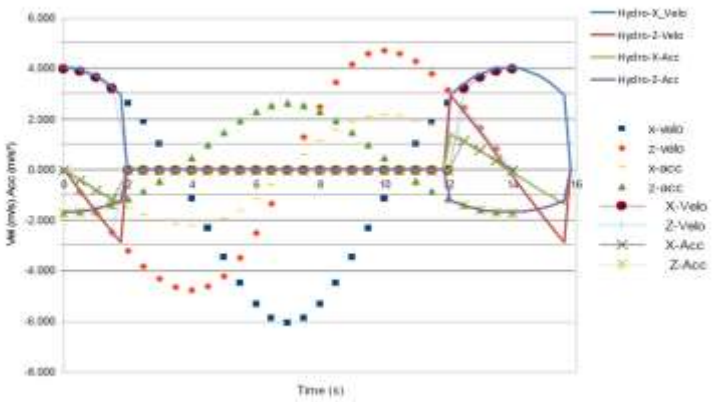

Wave particle velocity and acceleration for z=96m

A.6. Stokes wave kinematics –Wave height 30m

	Period [s]	Height [m]	Theory
	16	30	Stokes
	Depth [m]	**Diameter [m]**	
	70	0.2	
	C_d	**C_m**	
	1	0	
	Coord 1 [m]	**Coord 2 [m]**	
X	0	0	
Y	0	0	
Z	-70	20	

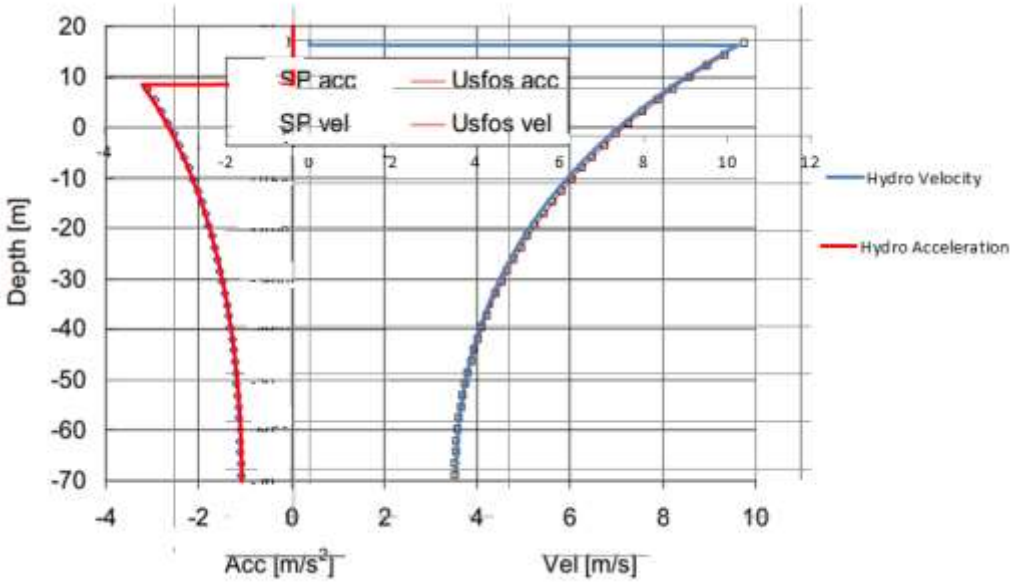

Velocity (t=0s) – and acceleration (t=2.0s) profile

A.7. Stokes wave kinematics –Wave height 33 m

	Period [s]	Height [m]	Theory
	16	33	Stokes
	Depth [m]	Diameter [m]	
	70	0.2	
	C_d	C_m	
	1	0	
	Coord 1 [m]	Coord 2 [m]	
X	0	0	
Y	0	0	
Z	-70	20	

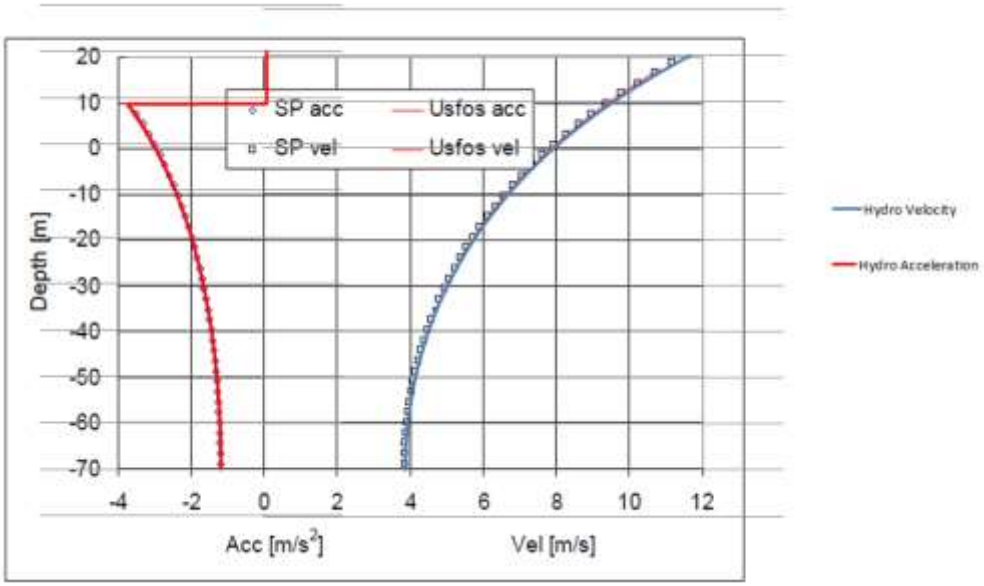

Velocity (t = 0 s) - and acceleration (t = 2.0 s) profile

A.8. Wave forces oblique pipe, 20m depth – Airy deep water theory

	Period [s]	Height [m]	Theory
	5	5	Deep
	Depth [m]	Diameter [m]	
	20	0.2	
	C_d	C_m	
	1	0	
	Coord 1 [m]	Coord 2 [m]	
X	0	10	
Y	0	10	
Z	-20	7	

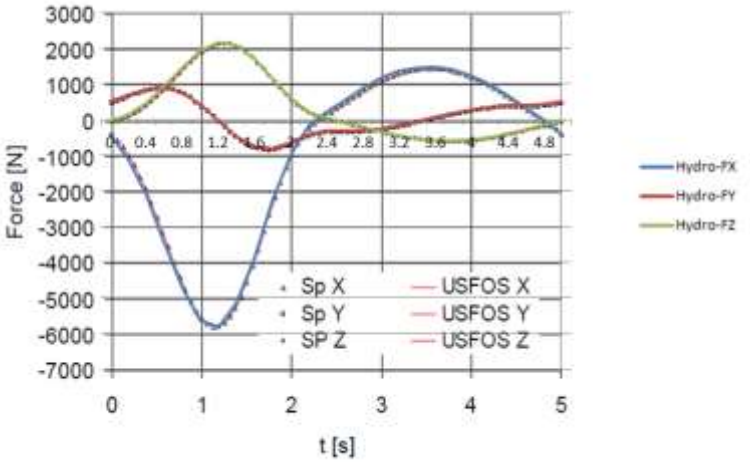

	Period [s]	Height [m]	Theory
	5	5	Deep
	Depth [m]	Diameter [m]	Wave dir
	20	0.2	0
	C_d	C_m	
	0	2	
	Coord 1 [m]	Coord 2 [m]	V_curr
X	0	10	0
Y	0	10	Curr dir
Z	-20	7	0

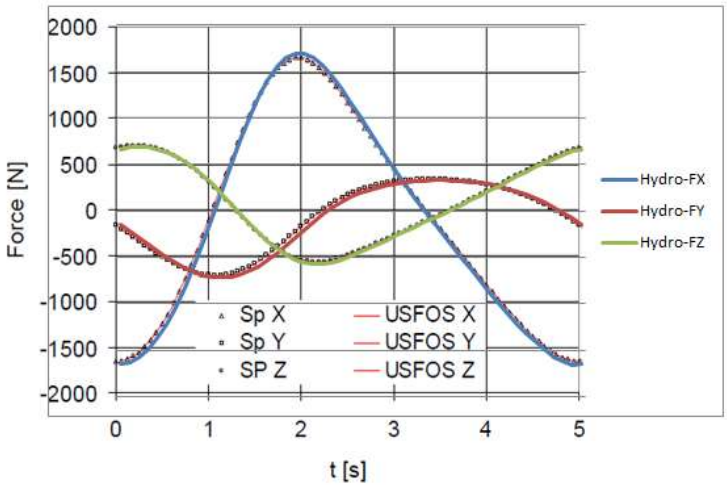

A.9. Wave forces oblique pipe, 20 m depth – Airy finite depth theory

	Period [s]	Height [m]	Theory
	8	5	Finite
	Depth [m]	Diameter [m]	Wave dir
	20	0.2	0
	C_d	C_m	
	1	0	
	Coord 1 [m]	Coord 2 [m]	V_curr
X	0	10	0
Y	0	10	Curr dir
Z	-20	7	0

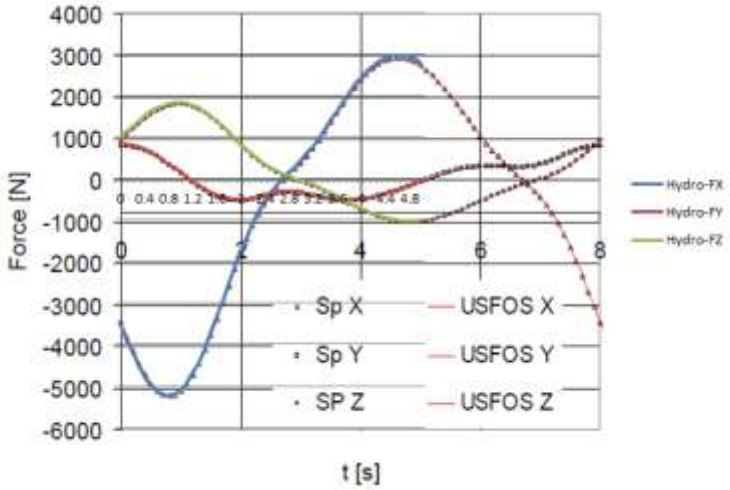

	Period [s]	Height [m]	Theory
	8	5	Finite
	Depth [m]	Diameter [m]	Wave dir
	20	0.2	0
	C_d	C_m	
	0	2	
	Coord 1 [m]	Coord 2 [m]	V_curr
X	0	10	0
Y	0	10	Curr dir
Z	-20	7	0

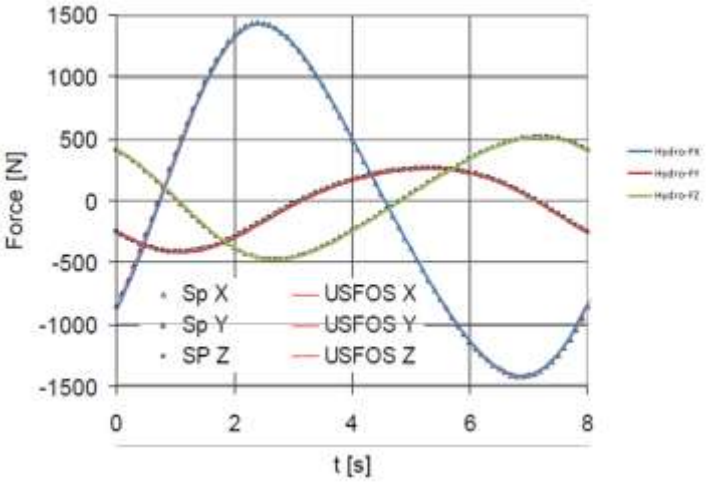

A.10. Wave and current forces oblique pipe, 20 m depth – Stokes theory

Period [s]	Height [m]	Theory
8	5	Stokes
Depth [m]	**Diameter [m]**	
20	0.2	
C_d	**C_m**	
1	0	

	Coord 1 [m]	Coord 2 [m]
X	0	10
Y	0	10
Z	-20	7

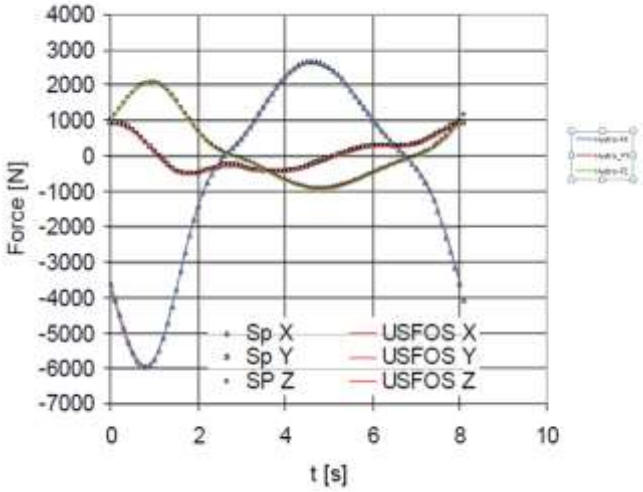

Period [s]	Height [m]	Theory
8	5	Stokes
Depth [m]	**Diameter [m]**	
20	0.2	
C_d	**C_m**	
0	1	

	Coord 1 [m]	Coord 2 [m]
X	0	10
Y	0	10
Z	-20	7

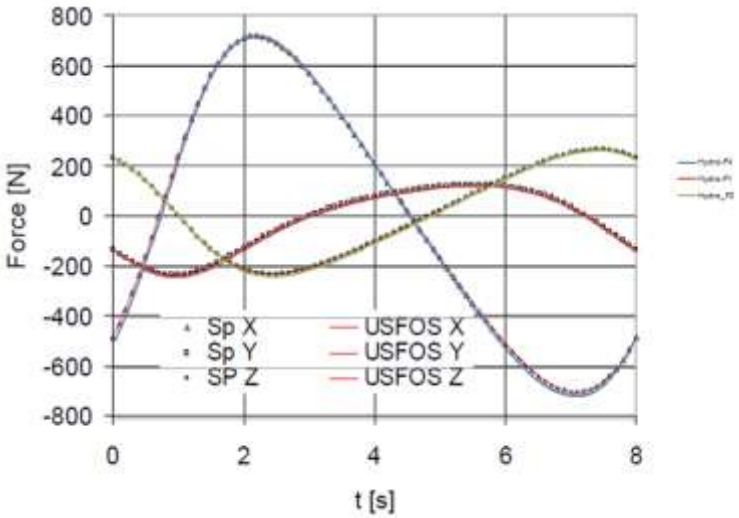

A.11. Wave forces vertical pipe, 70 m depth – Airy finite depth theory

	Period [s]	Height [m]	Theory
	15	30	Finite
	Depth [m]	Diameter [m]	Wave dir
	70	0.2	0
	C_d	C_m	
	1	0	
	Coord 1 [m]	Coord 2 [m]	V_curr
X	0	20	0
Y	0	0	Curr dir
Z	-70	17	0

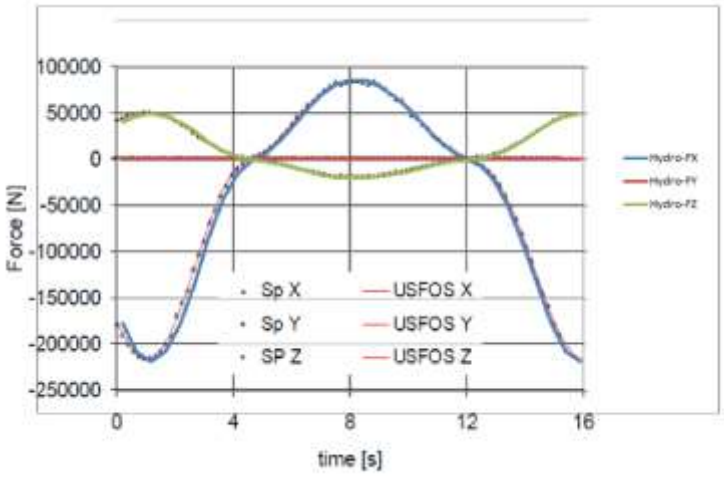

	Period [s]	Height [m]	Theory
	15	30	Finite
	Depth [m]	Diameter [m]	Wave dir
	70	0.2	0
	C_d	C_m	
	0	2	
	Coord 1 [m]	Coord 2 [m]	V_curr
X	0	20	0
Y	0	0	Curr dir
Z	-70	17	0

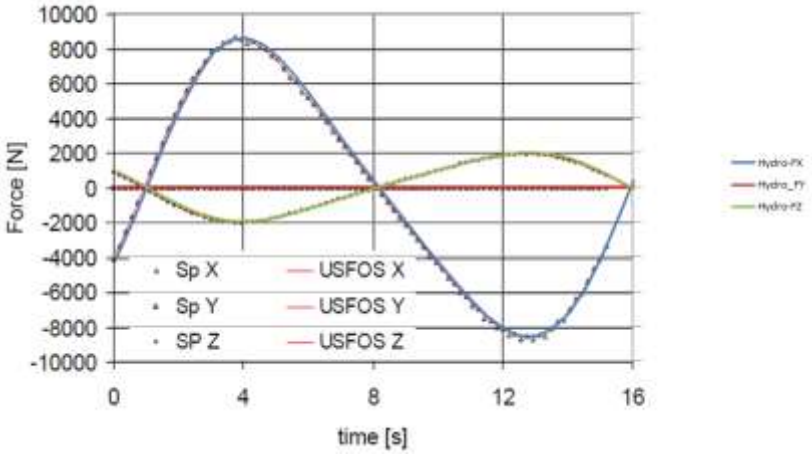

A.13. Wave forces vertical pipe, 70 m depth – Stokes theory

Period [s]	Height [m]	Theory
15	30	Stokes
Depth [m]	**Diameter [m]**	**Wave dir**
70	0.2	**0**
C_d	**C_m**	
1	0	
Coord 1 [m]	**Coord 2 [m]**	**V_curr**
X 0	20	0
Y 0	0	**Curr dir**
Z -70	17	0

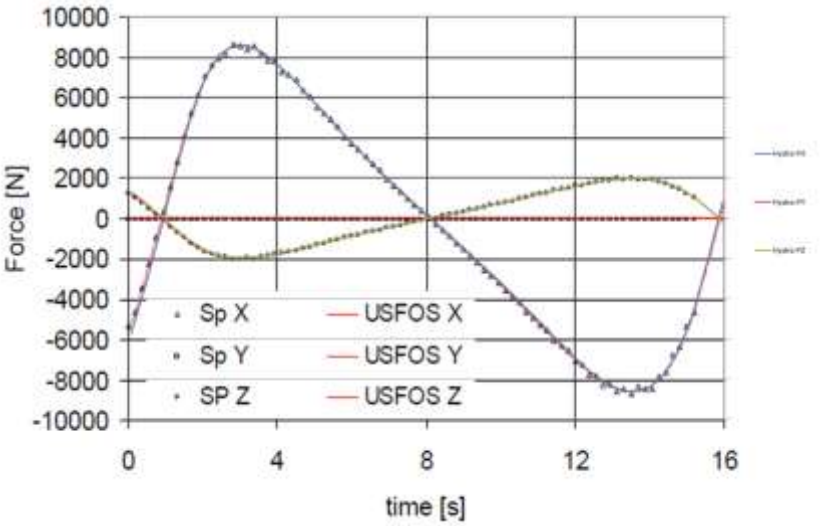

Period [s]	Height [m]	Theory
15	30	Stokes
Depth [m]	**Diameter [m]**	**Wave dir**
70	0.2	**0**
C_d	**C_m**	
0	2	
Coord 1 [m]	**Coord 2 [m]**	**V_curr**
X 0	20	0
Y 0	0	**Curr dir**
Z -70	17	0

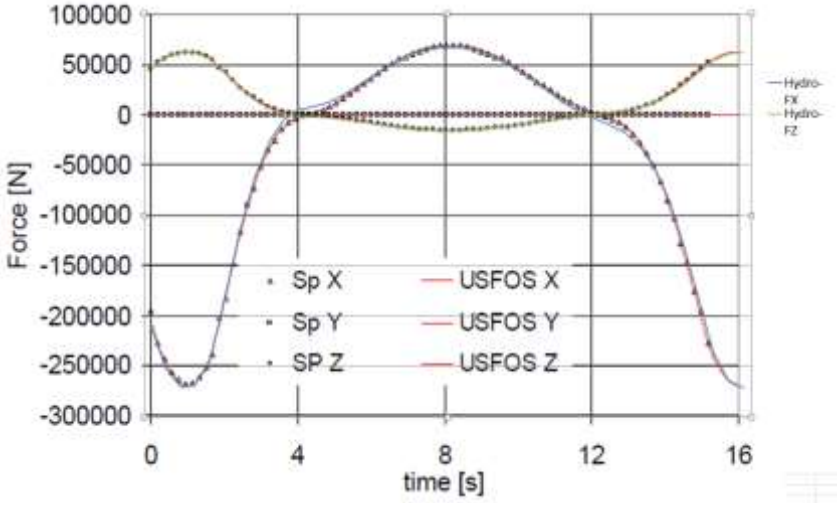

A.14. Wave forces oblique pipe, 70 m depth – Stokes theory

	Period [s]	Height [m]	Theory
	15	30	Stokes
	Depth [m]	Diameter [m]	Wave dir
	70	0.2	0
	C_d	C_m	
	1	0	
	Coord 1 [m]	Coord 2 [m]	V_curr
X	0	30	0
Y	0	30	Curr dir
Z	-70	20	0

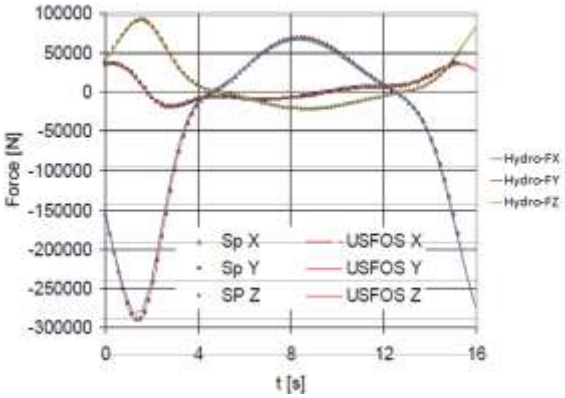

A.15. Wave forces oblique pipe, 70 m depth, diff. direction – Stokes theory

	Period [s]	Height [m]	Theory
	15	30	Stokes
	Depth [m]	Diameter [m]	Wave dir
	70	0.2	330
	C_d	C_m	
	1	0	
	Coord 1 [m]	Coord 2 [m]	V_curr
X	0	30	0
Y	0	30	Curr dir
Z	-70	20	0

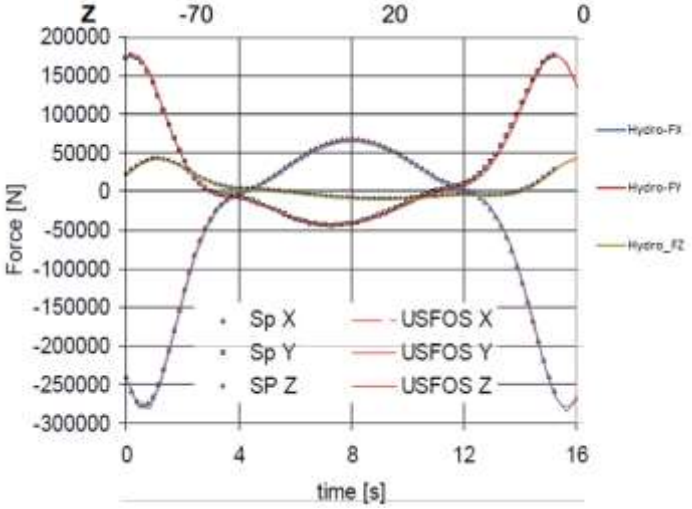

	Period [s]	Height [m]	Theory
	15	30	Stokes
	Depth [m]	Diameter [m]	Wave dir
	70	0.2	330
	C_d	C_m	
	0	2	
	Coord 1 [m]	Coord 2 [m]	V_curr
X	0	30	0
Y	0	30	Curr dir
Z	-70	20	0

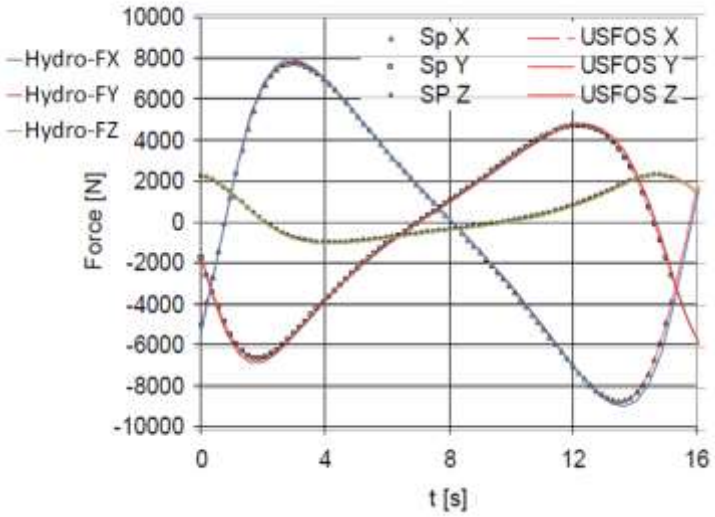

A.16. Wave forces horizontal pipe, 70 m depth – Airy theory

	Period [s]	Height [m]	Theory
	15.48	30	Finite
	Depth [m]	Diameter [m]	Wave dir
	70	1	330
	C_d	C_m	Doppler
	1	0	
	Coord 1 [m]	Coord 2 [m]	V_curr
X	0	20	1.5
Y	0	30	Curr dir
Z	-5	-5	270

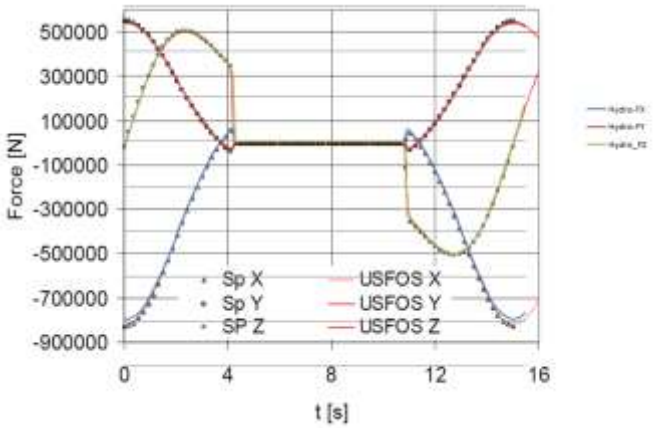

APPNEDIX II: Post-processing

This appendix presents the post-processing method for the frequency domain method and the time domain method.

II.1. The frequency domain method

As mentioned in Chapter 2, in hydromechanics, the amplitude of the transfer function $|H(\omega_i, \beta_i)|$ from the wave spectrum to the response is known as the Response Amplitude Operator (RAO). Here the equation is written as,

$$S_{\eta\eta}(\omega_i) * RAO(\omega_i, \beta_i)^2 = S_{rr}(\omega_i) \tag{II.1}$$

Where, $S_{\eta\eta}(\omega_i)$ is the wave spectrum and $S_{rr}(\omega_i)$ is the response spectrum.

Several statistical techniques may be applied to determine the characteristic values of response [23].
The N[th] spectral moment M_c is given by

$$M_N = \int \omega^N S_{\eta\eta}(\omega_i) * RAO(\omega_i, \beta_i)^2 d\omega \tag{II.2}$$

The significant response of R_s (double amplitude) is related to 0[th] spectral moment and given by

$$R_s = 4\sqrt{M_0} \tag{II.3}$$

The mean zero- crossing period T_x of the response is relate to zero order and second order of spectrum and given by

$$T_R = 2\pi \sqrt{\frac{M_0}{M_2}} \tag{II.4}$$

For N-years return period, the extreme response may be calculated based on short-term distribution. First, the extreme short-term sea state (H_s, T_p) is determined based on N years wave contour plot. Next, the largest response under determined sea state is calculated.

The accumulated distribution of narrow-band response's maxima in a short-term sea state may be described by Rayleigh distribution

$$F_s(r) = F_s(r_a \leq r) = 1 - e^{-\left(\frac{r^2}{2M_0}\right)} \tag{II.5}$$

Where $F_s(r)$ is accumulative distribution under a short-term sea state, r_a is the maxima of response

For a 3hr short-term sea state, the most probable maximum response $r_{max,s}$ may be defined as,

$$F_s(r_{max,s}) \approx 1 - \frac{1}{N} \tag{II.6}$$

Where N is the total number of response cycles during the 3hrs storm period, estimated by

$$N \approx \frac{3 \times 3600sec}{T_X} \tag{II.7}$$

Thus,

$$r_{max,s} = \sqrt{2M_0 \ln(N)} \tag{II.8}$$

Alternatively, long-term distribution of response maxima may also be treated as a weighted combination of all short-term distributions based on the probability of such sea state happens in specific site, e.g. scatter diagram. According to Ref [23] section B5, the long-term accumulated distribution is given as,

$$F_L(r) = F_s(r_a \leq r) = T_{rl} \iint \frac{f(H_s, T_p) F_s(r|H_s, T_p)}{T_x(H_s, T_p)} dH_s dT_p \tag{II.9}$$

Where H_s, T_p is the significant wave height and peak frequency of short-term sea state, $f(H_s, T_p)$ is joint probability of sea state $f(H_s, T_p)$, which is defined as account number n of such sea state divided by the total number of cycles N in scatter diagram. T_{rl} is defined as

$$T_{rl} = \left[\iint \frac{f(H_s, T_p)}{T_r(H_s, T_p)} dH_s dT_p \right]^{-1} \tag{II.10}$$

Within n years, the total number of response cycles N_n in wave direction β is given by

$$N_n = \frac{n \cdot 365 \cdot 24 \cdot 60 \cdot 60 \cdot F_\beta(\beta)}{\sum f(H_s, T_p) T_r(H_s, T_p) dH_s dT_p} \tag{II.11}$$

Where F_β is probability of wave occurs in direction β within n years.

Thus the long-term maximum response $r_{max,l}$ is given by

$$F_L(r_{max,l}) \approx 1 - \frac{1}{N_n} \tag{II.12}$$

$$r_{max,l} \approx F_L^{-1}\left(1 - \frac{1}{N_n}\right) \tag{II.13}$$

Normally Weibull distribution may be applied to fit F_L. However, Weibull distribution is just approximation to the real distribution and may fails to be representative in this case. Instead, Newton bisection method is used to approach $r_{max,l}$ numerically within tolerable error (1e-8 in this case).

All process mentioned above can be summarized in one Flow Chart, shown as follow

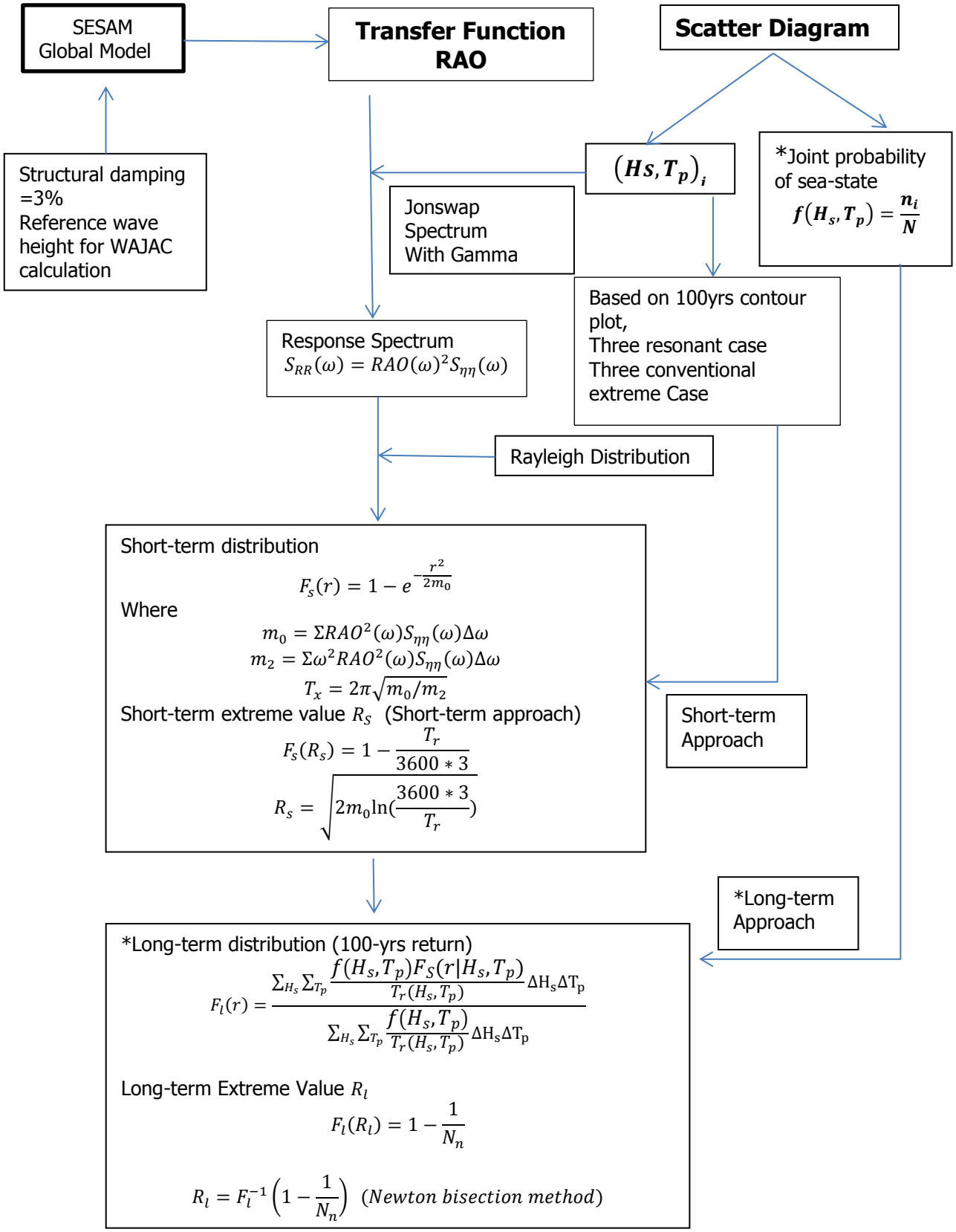

Table II.1 Flow chat for the frequency domain method

II.2. The time domain method

The generalized extreme value (GEV) distribution is adopted for the extreme value prediction. In statistics theory, the generalized extreme value (GEV) distribution is a family of the probability distributions developed for the extreme value prediction to combine the Gumbel, Fréchet and Weibull families.[37] It can be expressed as,

$$GEV:\ F(x;k,\mu,\sigma) = \begin{cases} \exp\left\{-\left(1-\dfrac{k(x-\mu)}{\sigma}\right)^{\frac{1}{k}}\right\}, & if\ k \neq 0 \\ \exp\left\{-\exp\left\{-\dfrac{(x-\mu)}{\sigma}\right\}\right\}, & ifk = 0 \end{cases} \tag{II.14}$$

The Gumbel distribution is a GEV distribution with k=0 and that the Weibull distribution is equal to a reversed GEV distribution with k=1/c, $\sigma = \frac{a}{c}$ and $\mu = -a$.

The studies have shown that the Weibull fitting and Gumbell fitting can be used to predict the most probable extreme value [14]. As a general distribution, the GEV distribution includes Weibull and Gumbell distribution and is thus believed to provide a better fitting.

The WAFO toolbox is used to execute this fitting. This fitting is estimated by the maximum likelihood method (MLE) and the goodness of this fitting is verified by the P-P plot visually [23].

For the extreme value prediction, the mean zero-crossing period T_{mean} is calculated from a specific time point to avoid the transition effect, by using rainflow accounting. The extreme value in 3hrs simulation is calculated by,

$$F(x;k,\mu,\sigma) = 1 - \frac{1}{N} \tag{II.15}$$

Where,

$$N = \frac{3 \times 3600}{T_{mean}} \tag{II.16}$$

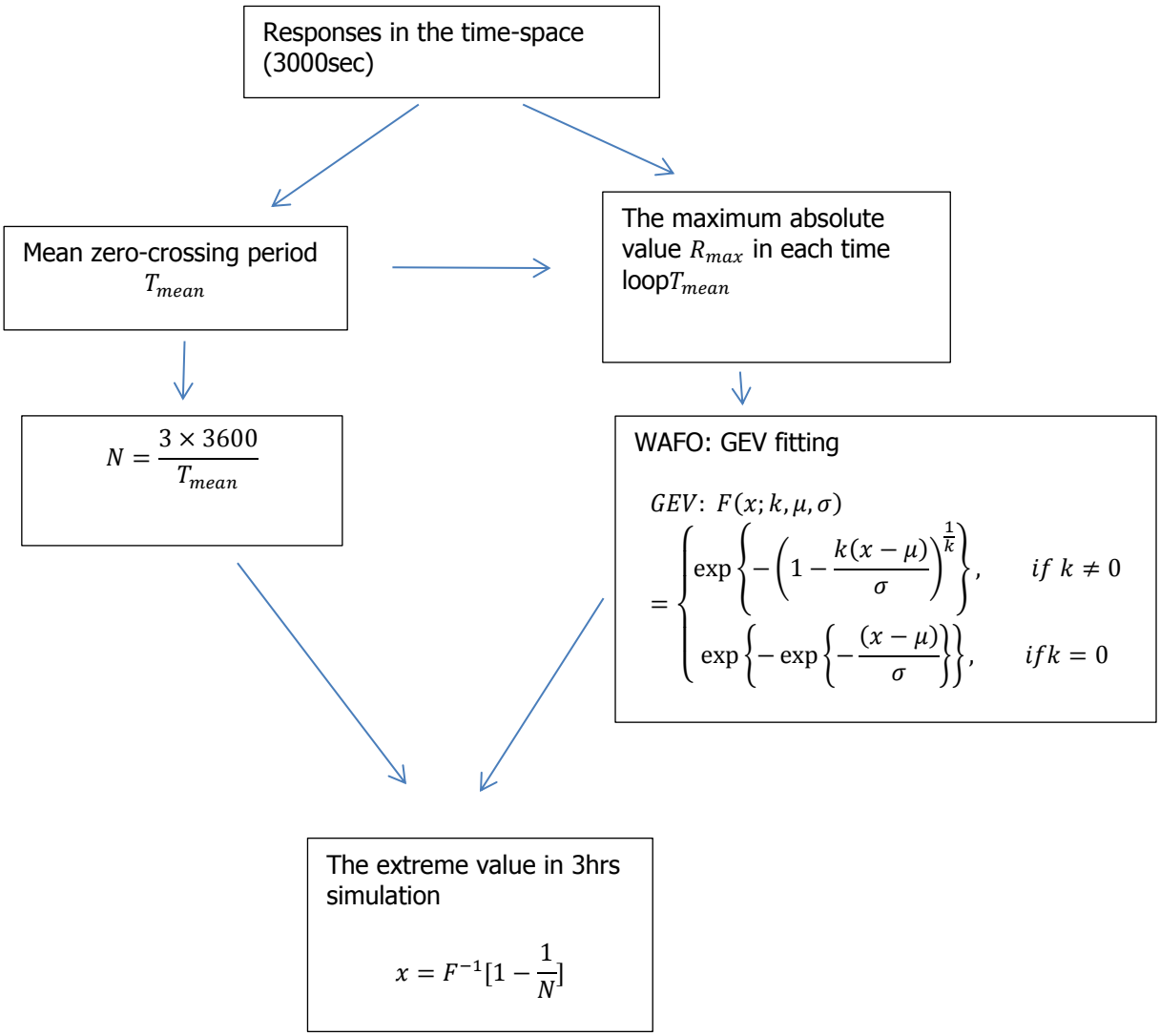

Table II.2 Flow chat for the frequency domain method

APPENDIX III: the Static load conversion method for the frequency domain method

For only segment of response, two methods are proposed to achieve the static load conversion.

The design wave conversion method [24], which is commonly used in the Allseas vessel structure analysis is firstly introduced. The purpose of this method is to replace the stochastic wave excitation with one single regular wave. The statistical extreme response, which is determined in the Appendix II, is approximated to be only excited by the waves with the corresponding peak frequency in the stochastic wave spectrum. The single wave height is then obtained via dividing the statistical extreme response by the corresponding RAO. The statistical extreme value can be obtained from the short-term approach or the long-term approach, of which the largest contributing short-term sea state is used. Table III.1 shows the flow chart of this method.

Alternatively, a new method combining the frequency-domain method and time-domain method is developed for the extreme static load conversion and its flow chart is shown in table.III.2 As indicated previously, a set of stochastic incoming waves can be quantified as,

$$\eta = \Sigma A_i \cos(\omega_i t + \theta_i) \tag{III.1}$$

Where η is the surface elevation at origin, $\eta_{a,i}, \omega_i, \theta_i$ is the amplitude frequency and initial phase angle of airy wave component i.

With its corresponding linear response value r is

$$r = \Sigma \eta_{a,i} |H(\omega_\mathrm{i}, \beta_\mathrm{i})| \cos(\omega_i t + \delta_i + \theta_i) \tag{III.2}$$

Where $|H(\omega_\mathrm{i}, \beta_\mathrm{i})|$, δ_i are the amplitude and phase shift of transfer function for frequency ω_i.

For response type like horizontal displacement, total shear force or total bending moment, a non-linear expression may be assumed. Taking horizontal displacement Δh as an example,

$$\Delta h = \sqrt{\Delta x^2 + \Delta y^2} \tag{III.3}$$

$$\Delta h = \sqrt{\left(\Sigma \eta_{a,i} |H_{Tx}(\omega_\mathrm{i}, \beta_\mathrm{i})| \cos\left(\omega_i t + \delta_{TX_i} + \theta_i\right)\right)^2 + \left(\Sigma \eta_{a,i} \left|H_{Ty}(\omega_\mathrm{i}, \beta_\mathrm{i})\right| \cos\left(\omega_i t + \delta_{Ty_i} + \theta_i\right)\right)^2} \tag{III.4}$$

For typical 3 hours storm waves, at a certain time point T_{max}, response r reaches its maximum value X_{max} where

$$X_{max} = X(T_{max}) = Max\{X(t)\}, \qquad where\ 0 \le t \le 3hrs \tag{III.5}$$

Once the T_{max} is known, its corresponding load case is accessible. The dynamic system for the Yme MOPUstor's global model can be expressed as

$$\boldsymbol{M\ddot{R} + C\dot{R} + KR = F}(\ddot{r}, \dot{r}, t) \tag{III.6}$$

Where $\boldsymbol{\ddot{R}, \dot{R}, R}$ is the acceleration, velocity and displacement vector. $\boldsymbol{F}(\ddot{r}, \dot{r}, t)$ is the external force. For static analysis, only stiffness and external force involved. Thus the expression can be rewritten as

$$kr = F(\ddot{r}, \dot{r}, t) - c\dot{r} - m\ddot{r} \tag{III.7}$$

For simplification, the effect of relative motion and damping can be neglected. First, the calculation of RAO is based on the decoupled model, thus involvement of relative motion after RAO calculation is illogical and may exacerbate the error. Second, the neglecting of damping term may overestimate the result. Considering its relatively small damping ratio (3%) and its corresponding huge conversion task, it is rational to hold this simplification. Thus, the final expression for load conversion can be written as

$$kr \approx F(t) - m\ddot{r} \tag{III.8}$$

It is obvious that the conversed external load consists of static wave load part $F(t)$ and inertia load part $m\ddot{r}$. Static wave load part F(t) can be calculated based on Morrison equation, while inertia load part is calculated by

$$F_{inertia} = -m\ddot{r} = -m\Sigma\eta_{a,i}|H_{\ddot{r}}(\omega_i, \beta_i)|\cos\left(\omega_i t + \delta_{\ddot{r}_i} + \theta_i\right) \tag{III.9}$$

Where $H_{\ddot{r}}(\omega_i, \beta_i)$ is the corresponding transfer function of acceleration on node, e.g. acceleration in x,y,z translation direction.

A disadvantage of this approach is the involvement of uncertainty. The initial phases are generated randomly and thus different result will be obtained for each calculation. To reduce this uncertainty to lowest degree, several cases should been made to perform a comparison study.

In this thesis, codes for both methods have been developed and results for the legs have been developed.

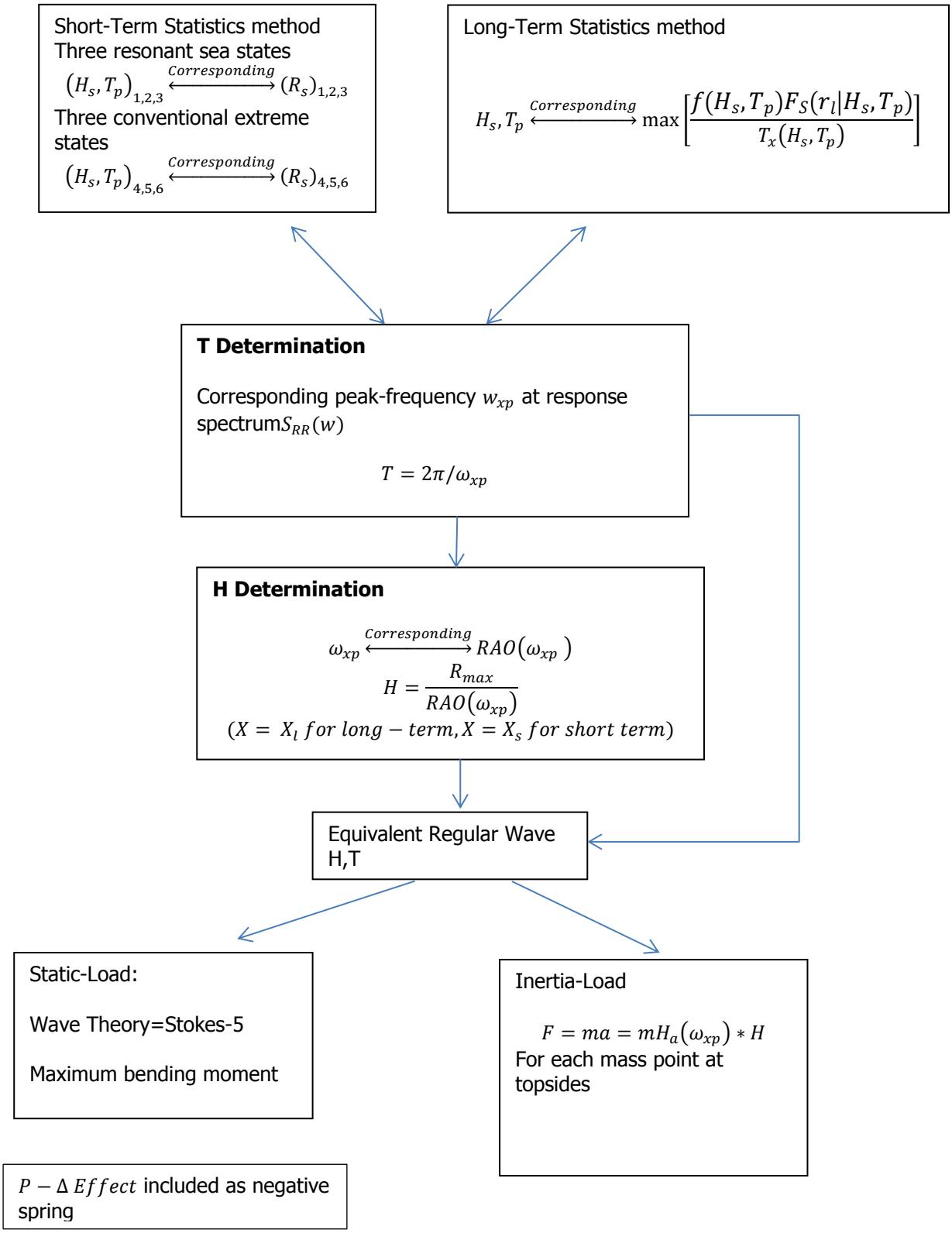

Table.III.1 Flow chart for the regular wave load conversion

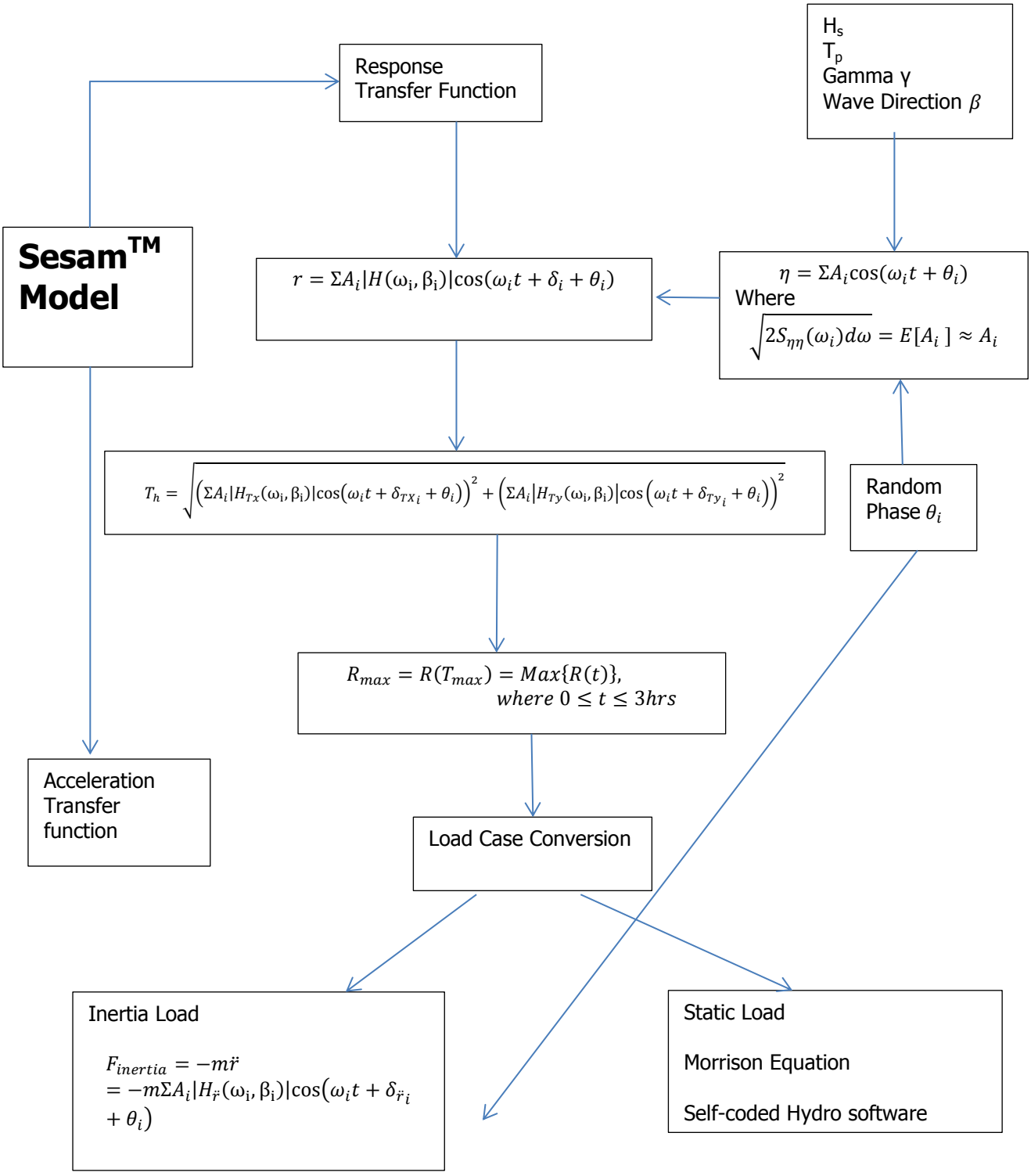

Table.III.2 Flow chart for the linear time-domain load conversion

Appendix IV : The Morison's equation modelling

IV.1. Assumption Spectral Density of ϕ

L.E.Borgman (1965) has proposed an solution for the random hydrodynamic Morrison-type force [21],

$$\phi = cV_0|V_0| + k\frac{\partial V_0}{\partial t} \tag{IV.1}$$

However, his result for wave-current present case is too complex to be used in engineering. Hence, in this paper one extra assumption will be adopted and the expression for the wave-current present case will be significantly simplified.

In his original paper, four assumptions have been made here (Current is assumed in one direction with waves),

1. V(x,y,z,t) and the sample-function derivative,

$$A_0(x,y,z,t) = \frac{\partial V_0(x,y,z,t)}{\partial t} \tag{IV.2}$$

Are two-component Gaussian stochastic process over the parameter space of all vectors of the form (x,y,z,t)

2. The random variable, $V_0(x_0,y_0,z_0,t_0)$ and $A(x_0,y_0,z_0,t_0)$ are independent, and have means $m(x_0,y_0,z_0,t_0)$ and 0 respectively, and variances $\sigma^2(x_0,y_0,z_0,t_0)$and $\rho^2(x_0,y_0,z_0,t_0)$ respectively.

3.
$$-Cov[V_0(x_0,y_0,z_0,t_0),A(x_0,y_0,z_0,t_0)] = Cov[A(x_0,y_0,z_0,t_0),V_0(x_0,y_0,z_0,t_0)] \tag{IV.3}$$

4.
$$V_0(x,y,z,t) = c\frac{\partial V_0(x,y,z,t)}{\partial t} + kA(x_0,y_0,z_0,t_0) \tag{IV.4}$$

In our case, the assumption (4) can be written as in term of the wave and the current separately.

$$\phi = c(V + C_{cur})|V + C_{cur}| + k\frac{\partial(V + C_{cur})}{\partial t}$$

$$\phi = c(V^2 + 2C_{cur}V + C_{cur}^2)sgn(V + C_{cur}) + kA \qquad (IV.5)$$

In which, V presents the velocity of wave, its expectation value E(V)=0, Variance Var(V)=σ^2;
C_{cur} presents the velocity of current, which is assumed to be constant.
A presents the acceleration of fluid.

5. Besides the existing four terms, a new assumption needs to be made. In our case, especially for Ultimate Limit State (ULS), the velocity amplitude of the wave are always much larger than the value of current. Hence, it is reasonable to assume,

$$sgn(V + C_{cur}) \approx sgn(V) \qquad (IV.6)$$

Furthermore, for the ultimate limit state (ULS), this assumption is conservative and reasonable. This assumption defined the upper limit for cases in which current is in the same or opposite direction with waves.

Then, ϕ can be rewritten as,

$$\phi = c(V|V| + 2C_{cur}|V| + C_{cur}^2 sgn(V)) + kA \qquad (IV.7)$$

In which,
The term $V|V|$ presents the non-linear wave-wave interaction in drag term.
The term $2C_{cur}|V|$ presents the non-linear wave-current interaction in drag term.

The term $C_{cur}^2 sgn(V)$ presents the current -current interaction in drag term. In my calculation, this term will be treated as static force and be neglected from dynamic calculation for two reasons: First, the “sgn(V)” will lead to discontinuity in force history and cause a force shift (impulse force), which doesn’t exist in reality (the error induced by assumption (4)). Furthermore, this term is in order of 2 with respect to current’s velocity, which is quite small.

Finally the dynamic part of ϕ can be simplified into

$$\phi = c(V|V| + 2C_{cur}|V|) + kA \qquad (IV.8)$$

Plus static current load.

In the airy wave theory, the velocity and acceleration at position (x,y,z,t) in a wave with phase ϕ, travelling in θ_{wave}- direction can be written as,

$$\begin{cases} V(x,y,t) = a\omega \dfrac{\cosh(kz)}{\sinh(kd)} \cos(kx - \omega t + \phi) \\ A(x,y,t) = a\omega^2 \dfrac{\cosh(kz)}{\sinh(kd)} \cos(kx - \omega t + \phi) \end{cases}$$
$$(2\pi f)^2 = gktanh(kd) \qquad (IV.9)$$

Where ω is the angular frequency and d is the water depth, k is the wave number. The initial phase angle φ is assumed to be a uniform random variable on (0,2π). Then V(x,y,z,t) and A(x,y,z,t) are independent by the orthogonality of the trigonometric functions and have zero expectation. This independence is preserved if the wave train is taken to be the sum of a large number of wavelets of this form, each with its own frequency, amplitude and independent random phase. An application of the central limit theorem, under certain reasonable regularity conditions, gives that V and A, in the limit, are jointly normal and the above properties continues to hold.

IV.2. The covariance of $\varphi_1(x_1,y_1,z_1,t_1)$ and $\varphi_2(x_2,y_2,z_2,t_2)$

Here only the dynamics parts of φ can be considered,

$$\phi = c(V|V| + 2C_{cur}|V|) + kA \qquad (IV.10)$$

Denote φ_1, V_1, A_1 be the force , velocity and acceleration at (x_1,y_1,z_1,t_1) and denote φ_2, V_2, A_2 be the force , velocity and acceleration at (x_2,y_2,z_2,t_2). Hence we have,

$$\phi_1 = c_1\left(V_1|V_1| + 2C_{cur,1}|V_1|\right) + k_1A_1, \qquad at(x_1,y_1,z_1,t_1)$$
$$\phi_2 = c_2\left(V_2|V_2| + 2C_{cur,2}|V_2|\right) + k_2A_2, \qquad at(x_2,y_2,z_2,t_2) \qquad (IV.11)$$

The covariance of φ_1, φ_2, will be,

$$\begin{aligned} Cov(\phi_1,\phi_2) &= E(\phi_1\phi_2) \\ &= E\{[c_1\left(V_1|V_1| + 2C_{cur,1}|V_1|\right) + k_1A_1][c_2\left(V_2|V_2| + 2C_{cur,2}|V_2|\right) + k_2A_2]\} \\ &= 2c_1c_2\left[c_{cur,2}\,E(V_1|V_1V_2|) + c_{cur,1}\,E(V_2|V_1V_2|)\right] \quad (a) \\ &+ 4c_1c_2c_{cur,1}\,c_{cur,2}\,E[|V_1V_2|] \quad (b) \\ &+ 2\left[k_2c_1c_{cur,1}E(A_2|V_1|) + k_1c_2c_{cur,2}E(A_1|V_2|)\right] (c) \\ &+ \{c_1c_2E(V_1V_2|V_1V_2|) + [c_1k_2E(V_1|V_1|A_2) + c_2k_1E(V_2|V_2|A_1)] \\ &+ k_1k_2E(A_1A_2)\} \ (d) \end{aligned} \qquad (IV.12)$$

Term $2c_1c_2\left[c_{cur,2}\,E(V_1|V_1V_2|)+c_{cur,1}\,E(V_2|V_1V_2|)\right]$ (a)

For $E(V_1|V_1V_2|)$

We assumed two joint standard normal distribution function $W_1=V_1/\sigma_1$ $W_2=V_2/\sigma_2$, so have

$$E(V_1|V_1V_2|)=E(W_1|W_1W_2|)\sigma_1^2\sigma_2 \tag{IV.13}$$

Denote,

$$G_1(r_{w_1w_2})=E(W_1|W_1W_2|),\qquad where r_{w_1w_2}=cov(V_1,V_2)/\sigma_1\sigma_2 \tag{IV.14}$$

Applying Price's theorem, We have

$$\frac{\partial}{\partial r_{w_1w_2}}G_1=E\left(\frac{\partial^2(W_1|W_1W_2|)}{\partial W_1\partial W_2}\right)=E(2|W_1|sgnW_2)$$

$$\frac{\partial^2}{\partial r_{w_1w_2}^2}G_1=E\left(\frac{\partial^2(2|W_1|sgnW_2)}{\partial W_1\partial W_2}\right)=E(4sgn(W_1)\delta(W_2)) \tag{IV.15}$$

Hence,

$$\begin{aligned}G_1''&=E\big(4sgn(W_1)\delta(W_2)\big)\\&=\int_{-\infty}^{\infty}\int_{-\infty}^{\infty}4sgn(W_1)\delta(W_2)\frac{1}{2\pi\sqrt{1-r_{w_1w_2}^2}}\exp\left[-\frac{1}{2\big(1-r_{w_1w_2}^2\big)}(W_1^2-2rW_1W_2\right.\\&\qquad\left.+W_2^2)\right]dW_1dW_2\\&=\int_{-\infty}^{\infty}4sgn(W_1)\frac{1}{2\pi\sqrt{1-r_{w_1w_2}^2}}\exp\left[-\frac{1}{2\big(1-r_{w_1w_2}^2\big)}(W_1^2)\right]dW_1\,(AntiSymmetric)=0\end{aligned} \tag{IV.16}$$

To sum up we have,

$$\begin{cases}G_1(0)=0\\G_1(0)'=0\\G_1\big(r_{w_1w_2}\big)''=0\end{cases} \tag{IV.17}$$

Thus, $G_1 = 0$

$$E(V_1|V_1V_2|) = 0 \tag{IV.18}$$

Similarly,

$$E(V_2|V_1V_2|) = 0 \tag{IV.19}$$

The term

$$2c_1c_2\left[c_{cur,2}\,E(V_1|V_1V_2|) + c_{cur,1}\,E(V_2|V_1V_2|)\right] = 0 \tag{IV.20}$$

Term $4c_1c_2c_{cur,1}\,c_{cur,2}\,E[|V_1V_2|]$ (b)

We denote,

$$E[|V_1V_2|] = E[|W_1W_2|]\sigma_1\sigma_2$$

$$where\ W = \frac{V}{\sigma} \tag{IV.21}$$

Then, we assume a function G_2 and denote G_2 be

$$G_2 = E[|W_1W_2|] \tag{IV.22}$$

Applying Price's Theorem

$$\frac{\partial}{\partial r_{w_1w_2}} G_2 = E\left(\frac{\partial^2(|W_1W_2|)}{\partial W_1 \partial W_2}\right) = E[sgn(W_1)sgn(W_2)] \tag{IV.23}$$

$$\frac{\partial^2}{\partial r_{w_1w_2}^2} G_2 = E\left(\frac{\partial^2(sgn(W_1)sgn(W_2))}{\partial W_1 \partial W_2}\right) = E[2\delta(W_1)2\delta(W_2)] \tag{IV.24}$$

$$\begin{aligned}\frac{\partial^2}{\partial r_{w_1w_2}^2} G_2 &= E[2\delta(W_1)2\delta(W_2)] \\ &= \int_{-\infty}^{\infty}\int_{-\infty}^{\infty} 2\delta(W_1)2\delta(W_2)\frac{1}{2\pi\sqrt{1-r_{w_1w_2}^2}}\exp\left[-\frac{1}{2\left(1-r_{w_1w_2}^2\right)}\left(W_1^2\right.\right. \\ &\left.\left. - 2r_{w_1w_2}W_1W_2 + W_2^2\right)\right] dW_1 dW_2 = \frac{4}{2\pi\sqrt{1-r_{w_1w_2}^2}}\end{aligned} \tag{IV.25}$$

In summary, we have

$$\frac{\partial^2}{\partial r_{w_1w_2}^2} G_2 = \frac{4}{2\pi\sqrt{1-r_{w_1w_2}^2}}$$

$$G_2''(o) = 0$$
$$G_2(0) = 2/\pi \qquad (IV.26)$$

It can be solved,

$$G(r_{w_1w_2}) = \frac{2}{\pi} r_{w_1w_2} \arcsin(r_{w_1w_2}) + \frac{2}{\pi}\sqrt{1-r_{w_1w_2}} \qquad (\text{IV}.27)$$

Thus,

$$E[|V_1V_2|] = (\frac{2}{\pi} r_{w_1w_2} \arcsin(r_{w_1w_2}) + \frac{2}{\pi}\sqrt{1-r_{w_1w_2}})\sigma_1\sigma_2$$

$wehre, r_{w_1w_2} = cov(V_1, V_2)/\sigma_1\sigma_2$ (IV. 28)

Term 2$[k_2c_1c_{cur,1}E(A_2|V_1|) + k_1c_2c_{cur,2}E(A_1|V_2|)]$ (c)

For $E(A_2|V_1|)$

$$E(A_2|V_1|) = E[|V_1|E(A_2|V_1)] \qquad (\text{IV}.29)$$

As what we assumed, V_1, A_2 are jointly normal distributed, hence the distribution of $(A_2|V_1)$ will be normal distributed as,

$$A_2|V_1 \sim N[\mu_{A2} + \frac{\sigma_{A2}}{\sigma_{V1}} r_{V_1A_2}(\mu_{V1} - \mu_{A2}), (1 - r_{V_1A_2}^2)\sigma_{V1}^2] \qquad (\text{IV}.30)$$

$$Hence, \qquad E(A_2|V_1) = \left(\frac{\rho_2}{\sigma_1}\right)\rho_{va}, where \rho_{va} = cov(V_1, A_2)/\sigma_1\rho_1$$

(IV.31)

Thus,

$$E(A_2|V_1|) = E[|V_1|E(A_2|V_1)] = E[|V_1|V_1]\left(\frac{\rho_2}{\sigma_1}\right)\rho_{va} \qquad (\text{IV}.32)$$

$$E[|V_1|V_1] = 0\ (Due\ to\ anti\ symmetic) \tag{IV.33}$$

Therefore,

$$2\left[k_2 c_1 c_{cur,1} E(A_2|V_1|) + k_1 c_2 c_{cur,2} E(A_1|V_2|)\right] = 0 \tag{IV.34}$$

Term $\{\boldsymbol{c_1 c_2 E(V_1 V_2|V_1 V_2|)} + [\boldsymbol{c_1 k_2 E(V_1|V_1|A_2)} + \boldsymbol{c_2 k_1 E(V_2|V_2|A_1)}] + \boldsymbol{k_1 k_2 E(A_1 A_2)}\}$ (d)

This term has been already proved by L.E.Brogman(1965). For unconstant coefficients, its original equation should be modified into

$$\{c_1 c_2 E(V_1 V_2|V_1 V_2|) + [c_1 k_2 E(V_1|V_1|A_2) + c_2 k_1 E(V_2|V_2|A_1)] + k_1 k_2 E(A_1 A_2)\} =$$
$$\frac{c_1 c_2 \sigma_1^2 \sigma_2^2}{\pi}\left[(2 + 4{r_{vv}}^2)\, arcsin(r_{vv}) + 6r\sqrt{1 - {r_{vv}}^2}\right] + \sqrt{\frac{8}{\pi}}(c_1 k_2 \rho_2 \sigma_1^2 r_{va} + c_2 k_1 \rho_1 \sigma_2^2 r_{av}) + k^2 \rho_1 \rho_2 r_{aa} \tag{IV.35}$$

Where,

$$r_{vv} = \frac{Cov(V_1, V_2)}{\sigma_1 \sigma_2}$$
$$r_{va} = \frac{Cov(V_1, A_2)}{\sigma_1 \rho_2}$$
$$r_{av} = \frac{Cov(A_1, V_2)}{\sigma_2 \rho_1}$$
$$r_{aa} = \frac{Cov(A_1, A_2)}{\sigma_2 \rho_1}$$

Therefore, in summary, the covariance of $\varphi_1(x_1,y_1,z_1,t_1)$ and $\varphi_2(x_2,y_2,z_2,t_2)$ will be

$$Cov(\phi_1, \phi_2) = E(\phi_1 \phi_2) =$$
$$4c_1 c_2 c_{cur,1}\, c_{cur,2}\left(\frac{2}{\pi} r_{vv} \arcsin(r_{vv}) + \frac{2}{\pi}\sqrt{1 - r_{vv}}\right)\sigma_1 \sigma_2 + \frac{c_1 c_2 \sigma_1^2 \sigma_2^2}{\pi}\left[(2 + 4{r_{vv}}^2)\, arcsin(r_{vv}) + 6r\sqrt{1 - {r_{vv}}^2}\right] + \sqrt{\frac{8}{\pi}}(c_1 k_2 \rho_2 \sigma_1^2 r_{va} + c_2 k_1 \rho_1 \sigma_2^2 r_{av}) + k^2 \rho_1 \rho_2 r_{aa} \tag{IV.36}$$

Applying Taylor expansion into $Cov(\phi_1, \phi_2)$, we obtain

$$Cov(\phi_1, \phi_2) \approx \frac{8}{\pi} c_1 c_2 c_{cur,1}\, c_{cur,2} \left(1 + \frac{{r_{vv}}^2}{2} + \frac{{r_{vv}}^4}{24} + \frac{{r_{vv}}^6}{80} + \dots\right) \sigma_1 \sigma_2 + \frac{c_1 c_2 \sigma_1^2 \sigma_2^2}{\pi} \left[\frac{8 r_{vv}}{1} + \frac{4 r_{vv}^3}{3} + \frac{r_{vv}^5}{15} + ..\right] + \sqrt{\frac{8}{\pi}} (c_1 k_2 \rho_2 \sigma_1^2 r_{va} + c_2 k_1 \rho_1 \sigma_2^2 r_{av}) + k^2 \rho_1 \rho_2 r_{aa} \quad (\text{IV}.37)$$

From term (b), it is clear that the error is related with both the wave and the current. Since $r_{vv} \in [-1,1]$, for worse case (r_{vv}=1) the error of the 4th approximation will be less than 1.7% regardless the ratio between σ and C_{cur}. For our assumption (The velocity of current is quite small compared with wave), a 3rd approximation is accurate enough, with error less than 1.1%.

IV.3. Spectral of $\varphi_1(x_1,y_1,z_1,t_1)$ and $\varphi_2(x_2,y_2,z_2,t_2)$

Form mathematics, auto-covariance $R_{XX}(\tau)$ and spectral density $S_{XX}(f)$ of a function can bilaterally converted via Fourier transformation.

If $\int_{-\infty}^{\infty} |p| dp < \infty$,

- $R_{XX}(\tau) = \int_{-\infty}^{\infty} S_{XX}(f) e^{i2\pi f\tau}\, df$ (Inverse Fourier Transformation)
- $S_{XX}(f) = \int_{-\infty}^{\infty} R_{XX}(\tau) e^{-i2\pi f\tau}\, d\tau$ (Fourier Transformation)

Thus

$$S_{\phi_1,\phi_2}(f) = \int_{-\infty}^{\infty} R_{\phi_1,\phi_2}(\tau) e^{-i2\pi f\tau}\, d\tau = \int_{-\infty}^{\infty} Cov(\phi_1, \phi_2) e^{-i2\pi f\tau}\, d\tau \quad (\text{IV}.38)$$

$$S_{\phi_1,\phi_2}(f) \approx \frac{8}{\pi} c_1 c_2 c_{cur,1}\, c_{cur,2} \left(\delta(f) + \frac{S_{vv}(f)^{*2}}{2\sigma_1^2 \sigma_2^2} + \frac{S_{vv}(f)^{*4}}{24\sigma_1^4 \sigma_2^4} + \frac{S_{vv}(f)^{*6}}{80\sigma_1^6 \sigma_2^6} + \dots\right) \sigma_1 \sigma_2 + \frac{c_1 c_2 \sigma_1^2 \sigma_2^2}{\pi} \left[\frac{8 S_{vv}(f)}{\sigma_1 \sigma_2} + \frac{4 S_{vv}(f)^{*3}}{3\sigma_1^3 \sigma_2^3} + \frac{S_{vv}(f)^{*5}}{15\sigma_1^5 \sigma_2^5} + \dots\right] + \sqrt{\frac{8}{\pi}} \left(c_1 k_2 \sigma_1 S_{v_1 a_2}(f) + c_2 k_1 \sigma_2 S_{A_2 v_1}(f)\right) + k^2 S_{aa}(f) \quad (\text{IV}.39)$$

Where

$$S(f)^{*2} = \int_{-\infty}^{\infty} S(f-g) S(g) dg$$

$$S(f)^{*n} = \int_{-\infty}^{\infty} S(f-g) S(g)^{(n-1)*} dg$$

Here $\delta(f)$ in $S_{\phi_1,\phi_2}(f)$ presents a static value in the time-space.

Therefore, similar to the Method II, a new linearization method can be proposed from the (IV.39), expressed as,

$$|v + c_{cur}|(v + c_{cur}) \approx |c_{cur}|c_{cur} + \sqrt{\frac{8}{\pi}}\sigma c_{cur} + \sigma\sqrt{\frac{8}{\pi}}v$$

$$(IV.40)$$

IV.4. Cross spectral function S_{vv}, S_{VA}, S_{AV} and S_{AA}

According to L.E.Borgman(1965), the covariance between V_1V_2, V_1A_2, V_2A_1 and A_1A_2 are,

$$\begin{aligned}
R_{V_1V_2} &= Cov(V_1, V_2) \\
&= 2\int_0^\infty S_{\eta\eta}(f)(2\pi f)^2 \frac{\cosh(kz_1)\cosh(kz_2)}{\sinh^2(kd)}\cos[k(x_2 - x_1) - 2\pi f\tau]df \\
R_{V_1A_2} &= Cov(V_1, A_2) \\
&= 2\int_0^\infty S_{\eta\eta}(f)(2\pi f)^3 \frac{\cosh(kz_1)\cosh(kz_2)}{\sinh^2(kd)}\sin[k(x_2 - x_1) - 2\pi f\tau]df \\
R_{V_2A_1} &= Cov(V_2, A_1) \\
&= -2\int_0^\infty S_{\eta\eta}(f)(2\pi f)^3 \frac{\cosh(kz_1)\cosh(kz_2)}{\sinh^2(kd)}\sin[k(x_2 - x_1) - 2\pi f\tau]df \\
R_{A_1A_2} &= Cov(A_1, A_2) \\
&= 2\int_0^\infty S_{\eta\eta}(f)(2\pi f)^4 \frac{\cosh(kz_1)\cosh(kz_2)}{\sinh^2(kd)}\cos[k(x_2 - x_1) - 2\pi f\tau]df
\end{aligned}$$

$$(IV.41)$$

It is clear that those “covariance”s have same structure, hence a generalized function can be built. Taking V_1V_2 as an example, we have,

$$R_{V_1V_2} = 2\int_{-\infty}^{\infty} Q(f)\cos[k(x_2 - x_1) - 2\pi f\tau]\,df$$

$$(IV.42)$$

Where,

$$\begin{cases} Q(f) = S_{\eta\eta}(f)(2\pi f)^2 \dfrac{cosh(kz_1)\cosh(kz_2)}{sinh^2(kd)}, if\ f > 0 \\ Q(f) = 0, if\ f < 0 \end{cases}$$

$$(IV.43)$$

$$S_{V_1V_2}(f_c) = 2\int_0^{\infty} Q(f)\cos[k(x_2-x_1)-2\pi f\tau]\,df e^{-i2\pi f_c\tau}d\tau$$
$$= 2\int_{-\infty}^{\infty}\int_{-\infty}^{\infty} Q(f)\cos[k(x_1-x_2)-2\pi f\tau]\,df\cos(2\pi f_c\tau)d\tau$$
$$-\boldsymbol{i}2\int_{-\infty}^{\infty}\int_{-\infty}^{\infty} Q(f)\,cos[k(x_1-x_2)-2\pi f\tau]\,df sin(2\pi f_c\tau)d\tau\,, \qquad f_c>0$$
$$(IV.44)$$

$$2\int_{-\infty}^{\infty}\int_{0}^{\infty} Q(f)\cos[k(x_1-x_2)-2\pi f\tau]\,df\cos(2\pi f_c\tau)d\tau$$
$$= 2\int_{-\infty}^{\infty}\int_{-\infty}^{\infty} Q(f)\,cos[k(x_1-x_2)-2\pi f\tau]\,cos(2\pi f_c\tau)d\tau df$$
$$= 2\int_{-\infty}^{\infty}\int_{-\infty}^{\infty} Q(f)\frac{1}{2}[cos[k(x_1-x_2)-2\pi f\tau+2\pi f_c\tau]$$
$$+cos(k(x_1-x_2)-2\pi f\tau-2\pi f_c\tau)]d\tau df$$
$$= Re\left[\int_{-\infty}^{\infty}\int_{-\infty}^{\infty} Q(f)e^{[k(x_1-x_2)-2\pi f\tau]i}d\tau e^{2\pi f_c\tau i}df\right]$$
$$+Re\left[\int_{-\infty}^{\infty}\int_{-\infty}^{\infty} Q(f)e^{[k(x_1-x_2)-2\pi f\tau]i}d\tau e^{-2\pi f_c\tau i}df\right]$$
$$= Q(f_c)\cos(k(x_1-x_2)) + Q(-f_c)\cos(k(-f)(x_1-x_2))$$
$$= Q(f_c)\cos(k(x_1-x_2))$$
$$(IV.45)$$

$$2\int_{-\infty}^{\infty}\int_{0}^{\infty} Q(f)\cos[k(x_1-x_2)-2\pi f\tau]\,df sin(2\pi f_c\tau)d\tau$$
$$= 2\int_{-\infty}^{\infty}\int_{-\infty}^{\infty} Q(f)\,cos[k(x_1-x_2)-2\pi f\tau]\,sin(2\pi f_c\tau)d\tau df$$
$$= 2\int_{-\infty}^{\infty}\int_{-\infty}^{\infty} Q(f)\frac{1}{2}[sin(k(x_1-x_2)-2\pi f\tau+2\pi f_c\tau)$$
$$-sin(k(x_1-x_2)-2\pi f\tau-2\pi f_c\tau)]d\tau df$$
$$= Im\left[\int_{-\infty}^{\infty}\int_{-\infty}^{\infty} Q(f)e^{[k(x_1-x_2)-2\pi f\tau]i}d\tau e^{2\pi f_c\tau i}df\right]$$
$$-Im\left[\int_{-\infty}^{\infty}\int_{-\infty}^{\infty} Q(f)e^{[k(x_1-x_2)-2\pi f\tau]i}d\tau e^{-2\pi f_c\tau i}df\right]=0$$
$$(IV.46)$$

$$S_{V_1V_2}(f) = Q(f)\cos(k(x_1-x_2)) = S_{\eta\eta}(f)(2\pi f)^2\frac{cosh(kz_1)\cosh(kz_2)}{sinh^2(kd)}\cos(k(x_1-x_2)),$$
$$f>0$$
$$(IV.47)$$